Evaluation of Analytical and Experimental Methods to Predict Constrained Layer Damping Behavior

by

John Francis Schultze

Thesis submitted to the Faculty of the
Virginia Polytechnic Institute and State University
in partial fulfillment of the requirements for the degree of
Master of Science
in
Mechanical Engineering

APPROVED

Dr R. A. Comparin, Chairman

Dr. A. L. Wicks

Dr. H. H. Robertshaw

Dr. C. F. Reinholtz

December, 1992
Blacksburg, Virginia

Evaluation of Analytical and Experimental Methods to Predict Constrained Layer Damping Behavior

by
John Francis Schultze

Dr R.A.Comparin, Chairman

Mechanical Engineering
(ABSTRACT)

Constrained layer damping (CLD) for three layer beams with viscoelastic cores and aluminum or graphite/epoxy composite laminate outer layers was investigated for model comparison, sensitivity to design parameters, and evaluation of experimental loss factor estimation techniques. Model comparison for damping estimation and resonant frequency prediction was performed between finite element analysis (FEA) Ross, Kerwin, and Ungar theory (RKU), developed moment predicted loss factor, and experimental results. Investigated design parameters include; treatment application length and placement, relative thickness of core and constraining layers to base layer, core loss factor, and boundary conditions (free/free, fixed/fixed, and cantilever). Experimental damping estimation techniques evaluated include; frequency response function (FRF) based methods of component analysis, circle-fit method a curve-fit algorithm developed by Han [30] and the time domain of log decrement.

Model comparison of finite elements to experimental results showed good trend prediction correlation. Only fair prediction of absolute loss factors was achieved, possibly due to the difficulty in characterization of viscoelastic properties. Design parameters analysis showed that treatment application length and placement were critical to effective added damping. In one case, for the same amount of damping material, the effective added damping of a well designed application was seven times greater than that of a poorly considered one. The effectiveness of treatment on a region appears to be strongly related to the magnitude on the moment acting on that region. Parameter analysis also showed that although a symmetric beam realizes the highest damping, in most cases near optimal damping can be obtained with constraining layer one half as thick as the base layer. Experimental methods for damping estimation showed the simple FRF component analysis to be consistent with the other methods (experimental and FEA) and the most computationally efficient.

Dedication

This thesis is dedicated to my family and friends for their support and encouragement throughout my life. I know I have a small part of them in me, so this is their work also.

Acknowledgements

I would first like to thank Dr. Charles Reinholtz for his help throughout my time at Virginia Tech through classes, technical questions, and for his friendship. I would like to thank Dr. Harry Robertshaw also for his help in my class with him and many outside endeavors and always encouraging me to try some idea out. Thanks also to Dr. John Kosmatka, with his help and direction I was able to complete this research. I was able to pursue many different theories and models that, while they all did not end up in the thesis, taught me many things about engineering. His help with the Finite Element Analysis was critical to resolving many problems that came up with the modelling process and his experience with viscoelastics was integral to any development here. Lastly, my thanks to Dr. Al Wicks who was of immeasurable help in the lab and the many hours I spent in his office discussing everything form complex modal vectors to the Baltimore Orioles. Also his help with administrative problems and just as a sounding board to whatever was going on was essential in completion of this effort. Without his help with acting as a second major professor this would have been a much more difficult time. I would also like to thank Dr R. A. Comparin for chairing my committee and reviewing this document. Finally I would like to thank my entire committee for their review of this thesis and the comments that only make it a better technical product.

Table of Contents

List of Figures

Nomenclature

a,b	end-points of treatment for loss factor integrals
A	area (m^2)
A_i	area, layer, i = 1,2,3 (m^2)
B	bending stiffness, EI
B_i	bending stiffness, EI, layer i = 1,2,3
B^*	bending stiffness of composite beam
B'	normalized bending stiffness, B^*/B_1
c	viscous damping constant (kg/s)
$[C]$	viscous damping matrix
d	diameter of acceleration Nyquist plot (1/kg)
D	neutral plane offset (m)
D_{sym}	neutral plane offset for symmetric beams (m)
D_{tape}	neutral plane offset for thin application (m)
$[D]$	laminate bending stiffness matrix
$[D^*]$	developed laminate bending stiffness matrix, [36]
DOF	degree-of-freedom
dx	differential element length
E_i	Young's modulus, layer i = 1,2,3 (kPa.)
E	Young's modulus (kPa.)
E_v	Young's modulus of viscoelastic (kPa.)
f	forcing function
F	shear force on viscoelastic core
g	shear parameter
G	shear modulus (kPa.)
G_i	shear modulus, layer i = 1,2,3 (kPa.)
G^*	complex shear modulus (kPa.)
h_{total}	total thickness composite beam (m)
h_{i1}	distance from midplane of layer i to layer 1, i=1,2,3 (m)

h_i	thickness of layer i=1,2,3 (m)
h_i'	normalized thickness of layer i=1,2,3
I	area moment of inertia (m^4)
I_i	area moment of inertia about a layer, i=1,2,3
j	$\sqrt{(-1)}$
k	stiffness
k_i	normalized stiffness of layer i=1,2,3
K	extensional stiffness (EA)(N)
K_i	extensional stiffness, $(EA)_i$ i=1,2,3
$[K]$	stiffness matrix
$[K^*]$	element stiffness matrix
$[K^{**}]$	global stiffness matrix
$[K_{imaginary}]$	imaginary component of the stiffness matrix $[K^{**}]$
$[K_{real}]$	real component of the stiffness matrix $[K^{**}]$
L	length (m)
l_i	treatment or element length (m)
m	mass (kg)
M	moment on cross-section (N-m)
$[M]$	mass matrix
n	number of degrees of freedom
p	wave number
$p(x)$	loading function
r	ω_n/ω
s_i	generalized coordinate coefficients
t	time (s)
T	kinetic energy
u,v,w	displacement in cartesian coordinates
u_i	lateral displacement, cycle i
U	potential strain energy
V	shear on cross-section (N)
w_i	z-direction displacement, node i
W_{eta}	work done by internal damping forces

W_{ext}	work done by external forces
x,y,z	cartesian coordinates
X	displacement vector
$\frac{\ddot{X}}{F}$	accelerance FRF
Y	geometric parameter
Y_{RKU}	geometric parameter, RKU approximation

Greek Letters

α_M	scale factor for moment developed loss factors
α_V	scale factor for shear developed loss factors
γ	shear strain
ε	extensional strain
ζ	viscous damping ratio
η	structural loss factor
η'	normalized structural loss factor
η_i	viscoelastic structural loss factor of layer i=1,2,3
η_c	composite loss factor
η_M	moment predicted loss factor
η_v	viscoelastic structural loss factor
η_V	shear predicted loss factor
θ	ply angle (degrees)
$(\theta_{x,y,z})_i$	rotational degree of freedom, x,y,z, node i
λ	eigenvalue
λ_n	eigenvalue of mode n
ν	Poisson's ratio
π	3.141592654
Π	Potential energy
ρ	mass density per unit length (kg/m^2)
ρ'	normalized three-layer beam mass density
ρ_i	mass density of layer i=1,2,3
τ	time for n cycles (s)

τ_d	damped period of oscillation (s)
ϕ	beam slope (flexural angle)
Φ_i	eigenvector vector, mode i
ψ	central layer slope (flexural angle)
ω	circular frequency (cycles/s)
ω'	normalized resonant frequency
ω_{cross}	frequency of zero crossing in real FRF
$(\omega_d)_n$	damped resonant frequency, mode n (cycles/s)
ω_n	natural frequency (cycles/s)
ω_r	resonant frequency (cycles/s)
ω_{min}	frequency of minimum response in real FRF
ω_{max}	frequency of maximum response in real FRF
ω_{peak}	frequency of largest response in imaginary FRF
ω_1	frequency of lower half power point
ω_2	frequency of higher half power point

Superscripts

'	normalized
.	derivative with respect to time

Subscripts

c	composite beam property
d	damped
i	layer or cycle increment
M	moment
n	mode
r	resonant
v	viscoelastic
V	shear

1 Introduction

Control of structural vibration is a recurring problem in such diverse ranging fields from machinery silencing in mining equipment to attenuating response in composite aerospace structures. Vibrations, which can cause cyclic loading of a structure, considerably reduce fatigue life resulting in increased failure rate. One of the most common ways to decrease vibration levels in a structure is through the addition of damping. Damping is the property of a material or structure that describes the amount of energy that is dissipated due to vibration, generally referenced to a per cycle dissipation or percent of 'critical damping'.

Damping is generally characterized as being viscous or structural in nature. Viscous damping models assume that the damping is a function of the deformation time rate of change of the structure (similar to velocity). A simple example of this is the viscous damping that occurs in a dashpot. Structural damping models damping is presumed to be a function of the body's state of deformation. An example of structural damping is the audible decay of vibration in a tuning fork.

In current aerospace design, use of advanced materials allows the engineer to tailor materials to meet application requirements of mass and stiffness, but often acceptable levels of damping can not be achieved. Damping inherent in these constitutive materials of systems are normally the primary mechanisms for attenuation of structural vibration. When the unmodified level of attenuation is unacceptable, alternative methods for control must be employed. Techniques for vibration control can be active, passive, or combinations of the two.

Active controllers can be designed to adapt to changes in operating environment. This adaptability allows for a wider range of frequencies for which the controller can be used. Active control generally involves

actuators imbedded within the structure. These actuators are often constructed using piezo-electric materials. Use of actuators involves an increase of mechanical hardware in addition to derivation of a problem-specific 'static' (non-updating) control law or implementation of an adaptive algorithm. Adaptive Infinite Impulse Response (IIR) algorithms used in feedback control of strutures can be unstable and add poles to the system. Due to the complexity of design, active controllers can have a potential mechanical and electrical reliability concern. Often, to achieve a suitable controller, the actuator system must be made very responsive, resulting in a very expensive design and often unstable system. For simple tonal dominated response applications, hybrid or passive systmes are the more prqatical solution.

Passive control of vibration is incorporated through the addition of damping material to inherently dissipate more vibration related energy. Alternately, designing a structure with relatively high damping is a commonly chosen technique. This increases the dissipated energy per cycle, thus reducing the response. Another technique which uncouples the forcing frequencies from the resonant frequencies (moving *natural* frequencies out of the operating range) can be accomplished through altering the mass and/or stiffness properties of the materials, the geometry, and/or the boundary conditions (attachments/joints). Passive damping has the advantages of relatively high mechanical reliability, design and manufacturing ease, and low cost. However, if the device is operated near a resonance, the energy to drive it increases dramatically due to the increased damping. Another practical concern is that viscoelastic damping materials are often highly frequency and temperature dependent in their structural properties of loss factor (η_v) and shear modulus (G). These nonlinear properties result in difficulty in analysis or design in anything but a small frequency and temperature range where the behavior can be assumed pseudo-linear.

The last method employed is a combination of the two previously described techniques. By moderately increasing the damping values through passive damping, and adding a less sophisticated active

controller/actuator than used in full active implementations, satisfactory attenuation can be obtained. The creation of more hysteresis of the structure by passive damping reduces the need for a fast controller. Optimization techniques can be readily applied to reduce cost and sophistication of design since this process involves both types of control. The main active controller problems still exist, (control law, mechanical reliability, cost), but are reduced.

Passive damping seems the most effective method for structures that have a limited number of modes of concern. One prevalent technique is Constrained Layer Damping (CLD). This method involves sandwiching a viscoelastic medium between two stiff outer layers. The viscoelastic material (core layer), a rubber-like compound, dissipates energy via shear deformation. The two outer layers undergo the significant bending and extensional loads while the central layer withstands the majority of the shear forces (see Figure 1.)

The principle objectives of this research are to evaluate and verify analytical and numerical models of viscoelastic imbedded beams and investigate different experimental methods to extract damping values for these beams with simple boundary conditions. This investigation will also quantify the effectiveness of partial coverage treatments vs. full treatments, the effectiveness of CLD in symmetric composite beams, and the optimal location of damping treatment and its thickness. A simple model to predict damping effectiveness will also be developed. This survey will be particularly useful to designers and analysts of advanced aerospace structures where fatigue is a significant problem. The three boundary conditions considered are (1) a fixed/fixed (spar-like) beam, (2) a cantilever member (similar to wings and other rotary wing structures) for treatment application analysis, and (3) free/free specimen for geometric parameter investigation (ref Figure 2). The closed form solutions and finite element models are compared with experimental results for the specific test cases of partial coverage.

This thesis is subsequently divided into seven chapters. Chapter Two presents a review of research in the science of viscoelastic damping (modeling and experimentation). Chapters Three and Four review in detail the analytical models and experimental methods, respectively, utilized in this research. Chapter Five presents design analysis of critical Ross, Kerwin, and Ungar parameters. Chapter Six presents numerical results and experimental studies. Chapter Seven presents conclusions and recommendations for future research. Chapter Eight lists references.

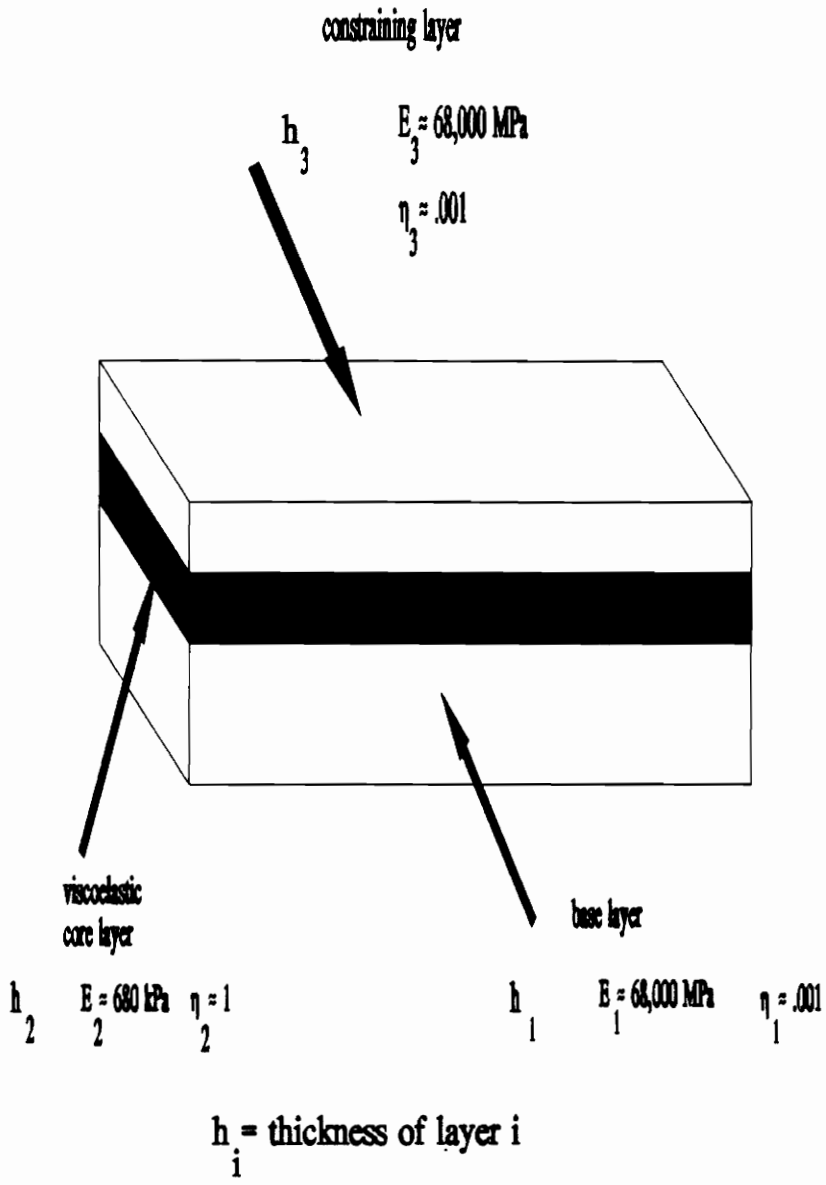

Figure 1 Constrained Layer Beam Element

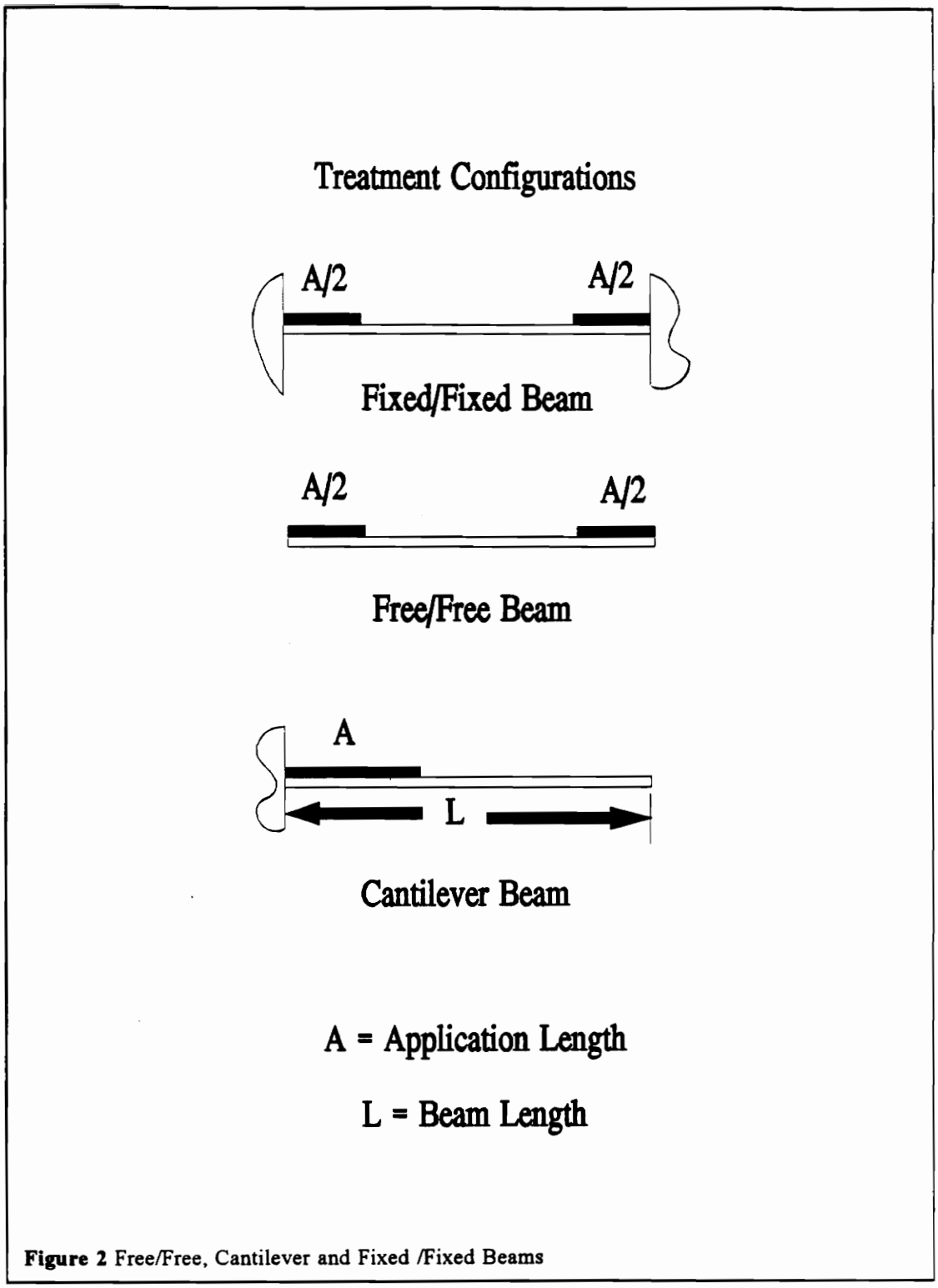

Figure 2 Free/Free, Cantilever and Fixed /Fixed Beams

2 Literature Review

Presently there are many areas of research associated with constrained layer damping. These can be divided into two main classes - analytical and experimental investigations. Analytical studies to examine the internal shear energy dissipation have been based on elasticity based solutions (closed form) or approximate methods based on energy principles. Experimental research to estimate the damping present in a structure has been conducted primarily using time and frequency domain techniques.

Passive attenuation, through the use of viscoelastic materials which increase the composite damping of a structure, has gained wide acceptance in recent years. Discussions on uses of viscoelastics are presented by Mar [1]. Techniques to incorporate viscoelastics into design are presented by Drake [2]. This overview is accompanied by an unique approach in treatment design optimization. This technique involves varying the material properties (G and η) as opposed to the geometric parameters of thickness and length. An illustration of how viscoelastics are used in reducing fatigue induced damage in aircraft wings is shown by Hogan [3]. Another passive vibration reduction technique is the addition of a heat generating device in the structure such as a capstan spring, McCarty [4].

Hagood [5], presents a model of viscoelastic damping using complex impedance and Rayleigh approximations for a circuit. He also presents a comparison of attenuation with viscoelastics versus piezoelectric materials. Bland [6] presents basic linear viscoelastic theory, for characterizing viscoelastic behavior, enhanced by many analytical models (spring/dashpot combinations and circuit analogies) and experimental data fitting techniques to determine the complex modulus of the viscoelastic material. Nashif et al. [7] review vibration damping with specific reference to viscoelastics.

2.1 Analytical Methods

Analytical methods can readily be divided into two categories. First, closed form elasticity solutions used in relatively simple structural analysis. Second, approximate solutions, such as Finite Element Analysis (FEA), are applied to structures too complex to readily handle with closed-form solution methods.

2.1.1 Elasticity Solutions

Analytical elasticity solutions for viscoelasticly damped structures can be traced to the fundamental work by Oberst [8]. He developed a theory that utilized the extension/compression energy dissipation characteristics of viscoelastics. A single layer of damping material is applied to the surface of a structure in his model, (see Figure 3). This theory showed effective ('composite') damping, η_c, to be a factor of viscoelastic extensional stiffness and loss factor (E_v, η_v). He showed that for low viscoelastic layer loss factors ($\eta_v < .3$), the composite loss factor was linear in treatment thickness and loss factor. His theory showed a maximum composite loss factor limited to forty percent of the treatment loss factor ($\eta_c < .4\eta_v$) and with the additional constraint of soft viscoelastic (low EA, effective elastic stiffness) that this maximum was governed by the square of the relative thickness of treatment (treatment thickness, h_2, divided by the base beam thickness, h_1 refer to Figure 1).

A more efficient method, with respect to added material and treatment thickness, was developed by Ross, Kerwin, and Ungar, (RKU), [9]. This work is generally considered by many to be the substantive work in Constrained Layer Damping (CLD) as they where the first to fully investigate the behavior of three layer beams. In their configuration, a third stiff 'constraining' layer was added to the composite beam (see Figure 3). Thus, the outer layers carried the main extension and bending loads, while the constrained layer had a relatively high shear gradient across its thickness. The resulting shear strain energy was dissipated through heating of the viscoelastic core, which would be then dissipated. It should be noted at this point

that viscoelastics, as a general characteristic, have comparatively high structural loss factors, η_v, (.5 to 1.5) and low shear moduli, G, (700 to 70000 kPa.) with respect to common isotropic engineering structural materials ($\eta < .01$ and $G < 7*10^7$ Kpa). In their development, RKU assumed linear vibrations applied to infinitely long or simply supported beams. This eliminated the consideration of end conditions in the analysis. They also introduced the concept of a complex shear modulus, G^*, for the viscoelastic. Their theory also dealt with considerations of neutral plane offset, D, (a measure of neutral plane displacement for the center of the original beam) and the ratio of added bending to extensional stiffness, Y. The physical significance of these parameters is covered in more detail in Chapter 5.

DiTaranto and Blasingame [10-12] developed a sixth order differential equation to model the mode shapes of a symmetric three layer beam with a thin viscoelastic core ($h_2 << h_1$). This theory was developed assuming that the outer layers were of equal stiffness and carried *all* of the extensional and bending loads. Their model, as with Ross, Kerwin, and Ungar [9], was also based on longitudinal displacements only and utilized the no slip condition at the interface between the stiff outer layers and the viscoelastic core. The resulting differential equations of motion extended the RKU beam fourth order differential equation to sixth order. This higher order equation was required to include relative shearing (and accompanying longitudinal relative slip between outer layers) in the developed composite moment equation (eq no. 18, [11]). Also the relation between composite loss factor and natural frequency was shown to be independent of *non-dissipative* boundary conditions but dependent upon the geometry and the physical properties of the materials. This model also demonstrated good correlation with experimental results for the cases of free/free unbolted, free/free with shear bolts, and fixed/fixed boundary conditions. 'Shear bolts' were bolts used to restrain all layers from relative translation at the free ends of the beam. This is done to show independence from non-dissipative end conditions.

Mead and Markus [13-15] also developed a sixth order differential equation of motion for encastre' (sandwich) beams. Their development was similar in form to DiTaranto and Blasingame but used

transverse, not longitudinal displacements. They also demonstrated orthogonality of the damped modes of vibration. This implied that these complex modes could be treated as uncoupled.

Abdulhadi [16] developed a sixth order differential equation for three layer plates. This equation allowed for any of the layers to be elastic or viscoelastic in character. These relations did not allow for extensional stiffness in central layer but did compensate for the viscoelastic weight. The resulting bending stiffness of this model reduces to that of RKU theory [9] for the case of Poisson's ratio equal to zero (ν=0, beam) and a soft viscoelastic core.

Kerwin's [17] preliminary three layer beam theory differed from RKU [9] in two assumptions. First, the central layer loss factor was restricted to be much less than one (1). Additionally, the relative bending stiffness of the constraining layer (layer 3) to the base layer (layer 1) be less than one-tenth (.1). The restriction of low central layer loss factor resulted in his elimination of the ***relative slip*** in the computation of bending stiffness, resulting in a slightly stiffer structure and higher estimate of composite loss factor and natural frequency. The restriction of weak constraining layers did not allow for symmetric beams, one of the more efficient designs.

Plunkett and Lee [18] examined increasing effective damping by cutting applied constrain layer treatments at specific intervals (segments) to induce higher shear in the viscoelastic. When this optimal segment length procedure was used the composite loss factor, η_c, was strongly dependent on stiffness of the constraining layer (backing) and the loss factor of the viscoelastic core (η_v), while being weakly linked to the shear modulus of the viscoelastic (G_v). This optimal segment length was dependent on the geometry and frequency of the mode of interest. Their research experimentally verified this optimal cutting length.

Rao [19] developed a sixth order, energy based, differential equation of motion for three layer sandwich beams. The potential energy due to extension and bending was restricted to the stiff outer layers, potential

energy due to shear strain was restricted to the central layer and kinetic (inertial) energy included all three layers' lateral acceleration. He demonstrated, as RKU [9], the existence of optimal loss factors, dependent of the treatment characteristics. He also showed that after an optimum thickness was reached, the composite loss factor was only dependent on the central layer loss factor, η_v. This model correlated well with experimental results.

2.1.2 Approximate Solutions (Finite Element Analysis)

The aforementioned elasticity solutions, while closed form and exact in nature, can not be easily applied to complex structures. This leads the analyst to develop approximate solutions. Finite Element Analysis (FEA) is perhaps the most widely used and accepted approximate solution technique in engineering. FEA approaches problems from a boundary value method. (Boundary value methods are distinct from initial value methods in that they use the value of parameters at particular regions in the structure and interpolate between them to develop a line, field, or volume of solution, where an initial value solution takes the value at a specific instant in time and extrapolates how the media will respond.) FEA uses the principle of minimum potential energy to transform the partial differential equations that define the structure to a set of linear algebraic equations.

Carne initiated application of FEA to the research of Constrained Layer Damping (CLD) [20]. His model of CLD beams consisted of two beam elements and an intermediate shear panel element, with the motion restricted to in-plane translation and rotation. Carne showed good correlation of his beam model with identical end constraints on the outer layers. When one layer's end conditions were left free and the other fixed, a model error on the order of fifty percent was evident, as compared with experimental results. This enlightened analysts to the limitations on the analytical models, with particular emphasis on dissipative end conditions and their correlation in experimental modelling.

Holman and Tanner [21] developed finite element analysis for prediction of dynamic response of integrally damped structures, primarily three layer constrain sandwich beams and plates. They present two 'new' elements; a 16 degree of freedom (DOF) beam element which combines a 12 DOF planar beam bending element with a 4 DOF beam element for torsion and beam extension, and a 28 DOF plate element which combines a 20 DOF quadrilateral plate element and an 8 DOF plate membrane element. They demonstrated correlation with previous analysts' work [9,20] for the case of low central layer loss factor (η_v = .01).

Roussos et al. [22] examined the FEA of non-proportional structural damping. They accommodated for the nonlinear response via a pseudo-Newmark Method by adding an additional matrix that accounted for the non-proportional damping in the structure in their analysis. This resulted in matrices for mass, stiffness, proportional viscous damping and non-proportional structural damping. Due to the nonlinear response of a structure that is not proportionally damped, iteration techniques were necessary in solution.

Kluesener [23] investigated aspect ratio problems in the modelling of viscoelasticly damped structures in FEA using three dimensional (3-D) solids and degree-of-freedom reduction techniques. He demonstrated that aspect ratios (of the element characteristic lengths) as high as 1000 were acceptable. (This is in excess of the recommended limit of 100 for thick shells and solids.) Also included in his research is the use of membrane elements to model constraining layers as a reduction in model complexity without significant decrease in accuracy.

Liguore and Kosmatka [24] used the FEA based technique of Modal Strain Energy (MSE) to characterize constrained layer damping in isotropic plates and symmetric sandwich beams. This method is a weighted sum computation of composite loss factor. It sums the product of each element's strain energy and loss factor and normalizes this sum to the total stain energy in the model. These results compared well with analytical closed form solutions.

2.2 Experimental Methods

Experimental investigation of any analysis is imperative for verification of the model. In this light, many techniques are used to determine the composite damping and stiffness of constrained layer beams. There are two main classes of experimental verification methods; time domain and frequency domain analysis. Briefly, time domain techniques look at the decay rate of a structure's response or cyclic response to a given input to extract these parameters. Examples of this type extend from the log decrement method, to damped complex exponential analysis, to auto-regressive/moving average (ARMA) methods, finally to polyreference techniques. Classic log decrement analysis merely involved measuring the amplitude and frequency of the peaks of a decaying time history to deduce damping present in the structure. Damped complex exponential is a least squares matrix extension of this principle that involves more of the time history and typically is used to examine many modes simultaneously. Poly-reference techniques are used to extract repeated roots and to study multiple input systems. Alternately, frequency domain methods investigate the response function of a structure to a varying frequency input. From this the parameters of dynamic stiffness, receptance, natural frequency and damping factor are extracted. Examples of this approach (frequency domain) are the Frequency Response Function (FRF),and least squares frequency domain solutions. Circle Fit techniques and other real and imaginary component analysis of the FRF are commonly employed.

The log decrement method, perhaps the most fundamental and easily applied technique, is described in many texts [25,26]. This method extracts damping values by analyzing the decaying amplitude of vibration of a structure as a measure of the energy dissipated per cycle. This method assumes linear damping, but is not restricted to viscous damping, in fact if interpreted properly, it can give insight to the damping mechanism of investigation (viscous, Coulomb, or, structural).

Plunkett [27] reviews experimental methods for single degree of freedom system estimations. Limitations and inherent errors are discussed for decay rate (log decrement), bandwidth (FRF), steady state phase angle (normal mode excitation) and impedance methods. He concluded that the simple decay rate (log-decrement) was reliable for most applications.

Luk and Mitchell [28] developed an experimental method for determining system parameters of natural frequency and damping factor (structural or viscous) using a single degree of freedom system. The model assumes proportional lightly damped systems. They showed that Nyquist plots were only truly circular for the cases of mobility (velocity/force) for viscous damping models and dynamic compliance (displacement/force) for structural damping models. They also demonstrated the least squares fit approach to these particular functions to a be circle. (This process is sometimes called a 'circle-fit'.) For the case of light damping (less than one percent, <1%) the two fits are complementary (i.e. $\eta = 2\ \zeta$). For more moderate damping care must be taken in examination of damping mechanism, viscous or structural and accompanying results.

Hyer et al. [29] observed modes of the outer layers of a symmetric beam when exciting a three layer beam at one half the natural lateral vibration frequency (sub-harmonic). They also documented nonlinearities in large amplitude response. (These were in addition to the inherent nonlinearities of viscoelastics of temperature and frequency dependent mechanical properties.)

Liguore and Kosmatka [24] used modal analysis techniques to quantify optimal thickness of the viscoelastic layer in three layer beams and plates. These simple structures were supported using a soft elastic cord to simulate free boundary conditions along the edges and were excited by a roving hammer (impact) approach.

Han and Wicks [30] present an algorithm utilizing orthogonal Forsythe polynomials to determine modal parameters for experimental data. Utilizing this class of functions (orthogonal polynomials) allows for

uneven frequency spacing and weighting. This is contrasted to typical multi-degree-of-freedom (MDOF) Prony based (time domain) and other non-linear least squares frequency domain models. The curve-fitter performed well (damping ratio relative error was less than four percent when data had coherence above .90). This method can use information about the coherence in the construction of pole estimates. It can be also applied to multiple FRF's simultaneously due to the nature of the chosen polynomials.

In their next paper [31] Han and Wicks extend the work presented in [30] through application of weighting functions. The variance weighting function used is based on the coherence of the data and the particular model used, H_1 or H_2. The poles estimates were dramatically improved using this weighting. Improvements of an order of magnitude reduction in standard deviation of damping estimate were typical, (this parameter is normally the most difficult to estimate.)

An alternate method to standard polynomial methods is derivatives of the Auto-Regressive Moving-Average (ARMA) technique. Gersch and Sharpe [32] developed an estimation technique for finite order ARMA models. This implementation of finite order is necessary to readily handle data. The fully general ARMA involves all the past input (up to the present time index) and all the past output (up to last index) in formulation of the model. Model order must be iterated upon for satisfactory fit.

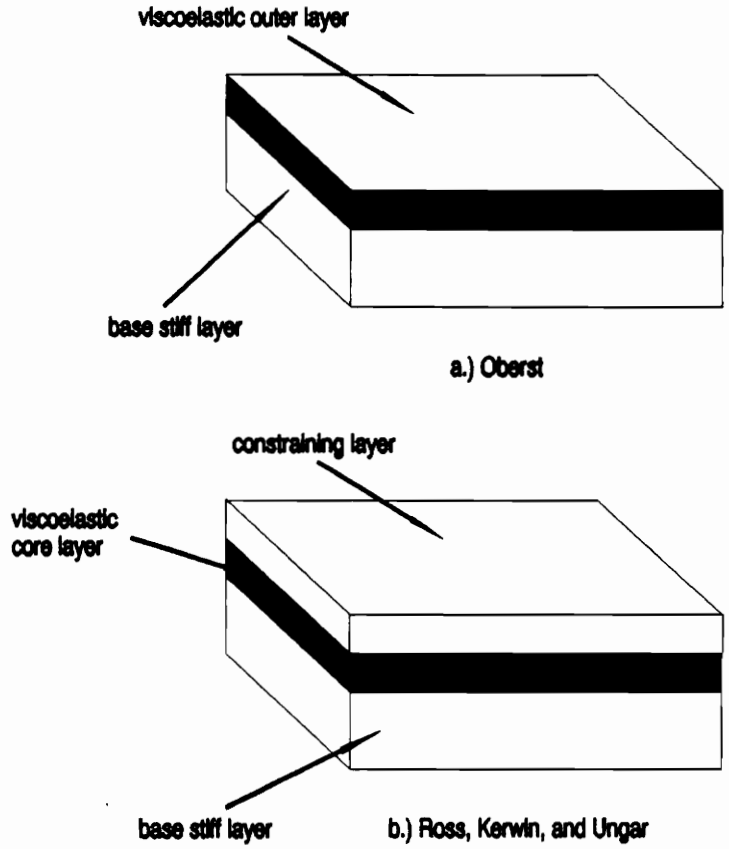

Figure 3 Representation of viscoelastic layered beams studied a.) Oberst and b.) Ross, Kerwin and Ungar.

3. Analytical Methods

Analytical models for studying the vibration behavior of beams with imbedded damping have been developed by numerous researchers. These are based on either elasticity solutions or approximate solutions (derived from variational energy principles). In addition, a moment based development for predicting treatment effectiveness is presented.

The main goal of this research was to quantify damping efficiency, in terms of application length, for the cases of partial and full coverage treatment of constrain layer beams. Sensitivity of the modal parameters of natural frequency, ω_n and 'composite' loss factor, η_c, due to changes in treatment geometric parameters (relative thickness of the layers and partial coverage treatments) and boundary conditions were also examined. 'Composite' loss factor is the effective loss factor of the treatment and base structure for a particular application, mode and boundary conditions. Finite element analysis was the numerical technique chosen to study design parameter sensitivities of these beams.

3.1 Beam Theory

Theories for describing the dynamic behavior of beams generally treat lateral, torsional and longitudinal modes as uncoupled. This assumption requires the centroidal and elastic axes (or neutral plane) are coincident and the beam is long and slender. Euler isotropic beam theory is the idealized model for closed-form elasticity based solutions for linear vibrations of slender beams. (This development is reviewed in Appendix A). Several extensions have been developed for general multi-layer beams. The three-layer viscoelastic core beams used in constrained layer damping are a special case of these multi-layer theories. Ross, Kerwin, and Ungar [9] developed the fundamental work in constrained layer damped beams.

Restrictions common to most theories include small linear vibration and wavelengths of propagation at least one order of magnitude higher than the characteristic dimension (thickness in the case of lateral vibration). Approximate methods are normally derivative forms of the classic Rayleigh-Ritz technique.

3.1.1 Three Layer Beam Theory (Ross, Kerwin, and Ungar)

Ross, Kerwin and Ungar's model was based on a differential length element as shown in Figure 4 and Figure 5. The development of this model starts with the Euler beam relation for forced vibration;

$$B\frac{\partial^4 w}{\partial x^4}+m\frac{\partial^2 w}{\partial t^2}=f(x,t) \tag{3.1}$$

where B is the ratio of the moment applied to the element curvature, m is the mass per unit length, x is the direction of wave propagation (for beams, longitudinal direction), w is the displacement normal to wave propagation (for beams, lateral direction), f is the forcing function, and t is time. While this equation is true for linear vibration of isotropic beams, modification is required to accommodate multi-layer beams. The first consideration is the neutral plane displacement, D. The neutral plane is the plane in which there is zero shear stress. This plane originally lies in the center of the base layer orthogonal to the lateral-longitudinal plane (x-z plane) and is shifted up toward the new center to compensate for the added layers. Another consideration is the relative shear (longitudinal displacement) between the two outer-layers, $h_2\,\partial\psi/\partial\phi$, (where h_i is the thickness of layer i , ψ is the shear angle of the viscoelastic core and ϕ is the shear angle of the outer layers). To make use of these developed relationships it is necessary to first determine how ψ and ϕ vary with respect to each other and to define the dimensionless shear parameter, g (again refer to Figure 5).

The relation for the shear of the central layer can be developed by recognizing that shear angle, ψ, is proportional to the change in force over the element length;

missing page

contact arthur

$$h_2\frac{\partial\psi}{\partial\phi}=\frac{K_1h_{21}+K_2(h_{31}-h_{21})}{K_1+\frac{K_2}{2}+g(K_1+K_2+K_3)} \tag{3.6}$$

where h_{i1} is the distance between the center of layer i and layer one (1). Details of the complete development can be found in [9]. An expression for the flexural rigidity may now be formulated as;

$$B=\sum_{i=1}^{3}\frac{K_ih_i^2}{12}-K_2\frac{h_2^2}{12}\frac{\partial\psi}{\partial\phi}+\sum_{i=1}^{3}K_i(h_{i1}-D)^2-\sum_{i=2}^{3}\frac{K_i}{2}(h_{i1}-D)h_2\frac{\partial\psi}{\partial\phi} \tag{3.7}$$

These relations 3.2-3.7 constitute the general solution for three layer beams. The composite loss factor, η_c, can then be approximated as;

$$\eta_c\approx\frac{g\eta_vY(1+\frac{K_3}{K_1})}{1+g(2+Y)(1+\frac{K_3}{K_1})+g^2(1+Y)(1+\eta_v^2)(1+\frac{K_3}{K_1})^2} \tag{3.8}$$

where η_v is the loss factor of the viscoelastic core and Y is a geometric parameter based on the relative treatment stiffness. Approximate solutions for a number of ordinarily encountered geometries are examined in Chapter 5 and [9].

Other theories exist for modelling the vibrations of three layer composite beams, such as DiTaranto and Blasingame [10-12] and Mead and Markus [13-15] sixth order differential equation formulations, but RKU was the most readily verified since many published results and comparisons exists for validation.

3.2 Moment Predicted Loss Factor

The governing assumption in this model is the same as the that RKU, specifically, the shearing of the central layer is the main component of energy dissipation in the beam-like structures. This model assumes the shear of the viscoelastic layer is determined by the moment on the section. This shear results in relative longitudinal motion of the two outer layers. Assuming that energy dissipation is proportional to the magnitude of the moment on the section (hence relative motion) a relation was formulated as;

$$\eta_M = \alpha_M \int_a^b |M(x)|\,dx \tag{3.9}$$

where η_M is the moment predicted loss factor, M is the moment, α_M is a mode and treatment dependent scale factor, and x is the longitudinal coordinate of the beam. The end points of the definite integral, a and b, are used to model treatment sections. The exact solution for the moment of an **Euler** beam was used as the approximation to the composite beam behavior (no shear beam effects), and was evaluated only over the treatment section. This last restriction neglects the step change in the bending stiffness of the beam, while the moment change must be continuous and therefore lags this change. This error is assumed to be small since the physical step was also small (for thin treatments).

The moment predicted loss factor, η_M, developed in this section is superior to a similarly developed shear based loss factor, η_V. Specifically defining η_V as;

$$\eta_V = \alpha_V \int_a^b |V(x)|\,dx \tag{3.10}$$

where V is the shear function of a mode shape and α_V is the shear function scale factor. It may appear that this loss factor, η_M, is simply the slope of the beam, but unfortunately it is not that elegant. The

absolute magnitude of the moment is the critical component not its sign. Again since damping is an energy based concept this should not be confusing.

3.3 Finite Element Analysis (Approximate Solutions)

The development of the Finite Element Analysis (FEA) was spawned from the need to handle complex structures and loading situations in a reliable alternate manner to closed-form solutions. This need is a function of the complexity and scale of structures in addition to the laborious, if available, closed-form solutions.

Except in the simplest of cases, these closed-form solutions can not be solved analytically. Structures that are more complex require an approximate method to the closed form relations for the system (model) governing partial differential equations (PDE's). This induces the scientist to develop a numerical approximation technique, among these the Rayleigh-Ritz method is very popular and readily applied to Finite Element Analysis (FEA). In this application of Rayleigh-Ritz, the total energy of the system, Π_{total}, is minimized with respect to the coefficients of an assumed displacement field s_i,

$$\frac{\partial \Pi}{\partial s_i}=0 \qquad i=1,2,3,\ldots,n \tag{3.11}$$

The displacement field must be an admissible solution, that is it must not violate internal compatibility at the nodes within the model or at geometric boundaries. In order to guarantee convergence the assumed displacement field must be complete. Completeness implies that if more terms are added to the field the exact displacement solution and its derivatives (strain, stress, etc) must be matched arbitrarily close. The Rayleigh-Ritz approach, as implemented in FEA, differs from the classical method in that it incorporates many lower order (third order or less) polynomials over sections of the model as opposed to a single

function to fit the entire model. These polynomials are often sufficient to assure piece-wise continuity and completeness through the derivation of stress. Rayleigh-Ritz minimizes the square of the errors in stress computation in solving these PDE's.

By applying Hamilton's Principle to the model and separating the total energy of the system into U, T, W_η and W_{ext}; the strain energy, kinetic energy, work of internal damping (non-conservative) and external forces, respectively, Π_{total} can be expressed as;

$$\Pi_{total} = U - T + W_\eta + W_{ext} \tag{3.12}$$

The separation of the work term into W_{ext} and the term, W_η, allows for internal damping forces in the system and is analogous to the integral over the displacement field of the Rayleigh dissipation function [33,34].

The minimum total energy condition (Equation 3.11) forces the differential equations of equilibrium to be satisfied within the body and boundary equilibrium equations to be satisfied where displacement is not specified (i.e. loading specified on boundaries). Therefore when using the Rayleigh-Ritz method, equations of equilibrium are not satisfied everywhere in the element, only at the nodes where piece-wise continuity is enforced, with errors generally reduced with mesh refinement. Since most finite element analysis is based on displacement solutions, the force continuity, directly based on displacement, is better than the stress approximations which are functions of the second derivative of the displacement field. Through inspection of the Rayleigh-Ritz procedure, Cook [35], it can be shown that results from this analysis form an upper bound for the actual stiffness. If the model is exact, then the Rayleigh-Ritz/FEA approach should give the closed form solution. From the Calculus of Variations approach it can be shown that if the displacement solution is somewhere other than the minimum state (i.e. equilibrium), then the structure is

at a higher strain energy level. This approach results in consistently low displacement approximations, overestimates of natural frequency, and generally high estimates of the stress levels.

Two finite element models were developed for this research. The first model was constructed with isotropic outer layers simulated by standard Bernoulli-Euler beam elements (2 nodes, 6 DOF per node) sandwiching a viscoelastic core modelled as a quadrilateral shear panel (4 nodes, 2 in-plane translation DOF per node). (See Figure 6 and Figure 7)

A shear panel is a derivative of the quadrilateral shell element (4 node, 5 DOF per node) which resists only the action of tangential forces on its element boundary. Briefly, nodal forces are resolved into forces tangent to the element edges. The element's shear stiffness is constructed from the product of its shear modulus and the shear flow area of its geometry. This development leads to the element having no extensional or out of plane stiffness. The development is covered in detail in [36]. This element is well suited to model the viscoelastic core of a three layer beam since it was developed to be applied between two relatively stiff layers, which in this research are the constraining and base layers. This model was used to study the effect of geometric and material parameters on the modal damping and frequency, in addition to quantification of vendor supplied material properties and experimental model correlation.

The second finite element model consisted of quadrilateral plate elements (4 Node, 5 DOF per node) sandwiching solid brick elements (8 node, 3 DOF per node). The plate elements modeled graphite-epoxy composite laminate outer layers, while the brick elements represented the viscoelastic central layer. (See Figure 6 and Figure 7). Within the FEA, material matrices are developed from the laminate ply information (stack-up and lamina mechanical properties) to form an equivalent anisotropic material matrix.

The motion in both models was restricted to lateral displacement. The beam and the plate element which both use third order displacement functions and have rotational degrees of freedom must be made compatible with the linear (translation only) displacement functions of the shear panel and the solid brick. This is done through the use of multi-point constraints, discussed later in this chapter (Refer to figure 6 and 7).

The beam elements and the plate elements were offset from their defining node by one half their thickness to properly model the stiffness of the outer layers while giving the shear panels and the solid elements the proper dimensions. The material properties of the shear modulus and the loss factor for the viscoelastic core and the loss factor of the aluminum beams were determined by correlating finite element results to experimentation after initial experimental comparison demonstrated the provided nomograms where inappropriate. The complement of the material properties were selected from available material handbooks.

3.3.1 Multi-Point Constraints

Multi-Point Constraints (MPC) are equations used to constrain degrees of freedom (DOF) to have a specific interrelation within a finite element model, [36]. These relations can be used to model rigid connections, provide for element compatibility, or other intrinsic relation that need to be described explicitly in the model. An appropriate example of their application is the compatibility requirements of a quadrilateral plate element to the surface of a solid linear brick element. The quadrilateral element was developed to have 6 DOF/node (3 rotations and 3 translations) where as the solid element is developed with only 3 translation DOF/node. Thus one must use MPC's to assure that the plate elements do not pass through the solid layer.

The inclusion of MPCs in this model, see Figure 6 and Figure 7, was necessary because of two problems in modelling of the viscoelastic material with shear panels [37]. The shear panels have only 2 DOF/node (u, w) and are 'sandwiched' between two beam elements having 6 DOF/node. These beam elements were restricted to in-plane behavior (3 DOF: u, w, θ_y), but the rotation still needed to be made compatible with the DOF shear panel. The rotation was then approximated by applying the central difference theorem to the lateral translations of the beam. The central difference theorem, applied to this model, has the form of;

$$(\theta_y)_i = -\frac{1}{2}\left(\frac{w_{i+1}-w_i}{l_i}+\frac{w_i-w_{i-1}}{l_{i-1}}\right) \tag{3.13}$$

where w_i, l_i, and $(\theta_y)_i$ are the lateral translation of node i, longitudinal distance from node i to node $i+1$, and the in-plane rotation of node i, respectively. This approximation forces the beam to have the same slope as the shear panel at the constrained nodes. Thus creating a series of linear approximations of the third order nature of the element (refer to Figure 7).

The model, without more MPC's, allowed for almost total decoupling of the two stiff layers. This was due to the relatively soft viscoelastic stiffness, several orders of magnitude less than the outer layers. MPC's were added to enforce that no relative lateral translation of the layers occurred between nodes at the same (undeformed) longitudinal location and to properly couple the bending stiffness of the base and constraining layer. This resulted in computational modes where the constraining layer passes through the base layer. This restriction to equal lateral translation does not invalidate the model since the two layers are still allowed to translate longitudinally, causing shear in the central layer (the primary energy dissipation mechanism in this structure).

When the rotational constraints are applied separately the mode shapes are continuous and well behaved, but to assure that the constraining layer did not pass through the base layer, the translational restraints were also applied.

3.3.2 Eigenvalue Solution

The primary goal of this research was to extract natural frequencies and modal damping factors from the finite element model. This required solution of the model's equations of motion. The general form of these equations can be written as;

$$[M]\{\ddot{X}\}+[C]\{\dot{X}\}+[K]\{X\}=f(x,t) \tag{3.14}$$

where $[M]$, $[C]$, and $[K]$ are the mass, damping, and stiffness matrices, respectively and $\{X\}$, $\{f\}$, and t are the longitudinal spatial coordinate, forcing function and time, respectively. The equations of motion can be derived from Equation 3.12 by differentiating the different terms of the equation; U, strain energy yields the stiffness matrix; T, kinetic energy yields the mass matrix; W_η yields the damping matrix; and W_{ext} yields the forcing functions. Assuming harmonic free vibration ($f = 0$), eq 3.14 reduces to;

$$[-\lambda^2[M]+j\lambda[C]+[K]]\{X\}=0 \quad . \tag{3.15}$$

Solution of this equation for practical application requires use of an Eigenvalue solver in addition to insight into the development of the component matrices.

The mass matrix, $[M]$, is n by n, where n is the number of DOF in the model. It normally takes one of two forms. The first is a diagonal lumped mass matrix which only associates the mass of adjoining nodes with a degree of freedom. This matrix will consistently yield a low estimate of the natural frequency, but will converge to the exact solution with mesh refinement. The second general type of mass matrix is the

consistent mass matrix, which uses the same shape functions that are used for interpolation and integration of element fields (in the construction of the stiffness matrix) to allocate the mass to the appropriate degrees of freedom. This results in a matrix that more realistically links the degrees of freedom, which is no longer diagonal but is banded like the stiffness matrix [K]. Although it is not generally a fully populated matrix, computational and assembly effort is greatly increased. Though this matrix formulation, nominally, overestimates the natural frequency(ies), its error in frequency estimation is normally much less than the lumped mass matrix, and it converges to the exact solution more rapidly. The consistent mass matrix formulation was chosen after test case comparison showed it to be a better model for this analysis.

The damping matrix, [C], is often used to model equivalent viscous damping, but since damping in this analysis is assumed to be structural in nature, it was decided to use a complex stiffness approach and neglect the effects of viscous damping. The most significant difference between the viscous (ζ) and structural (η) damping models in this analysis is whether the dissipative term is associated with the velocity or displacement fields. Previous experimental analysis has consistently shown that viscoelastic behavior is more closed modelled by structural damping theory. The relation of between the two damping terms, ($\eta \approx 2\ \zeta$) , is examined in the next chapter on experimental methods.

The complex stiffness matrix used in this analysis, [K^*], is developed from scaling the component of each element symmetric stiffness matrix by the appropriate element loss factor (η_i);

$$[K^*]_i = (1 + j\,\eta_i)\ [K]_i \qquad (3.16)$$

where j is $\sqrt{-1}$. The model stiffness matrix, $[K^{**}]_i$ is then assembled from the element stiffness matrices resulting a complex global matrix [K**]. While this matrix is symmetric, it represents a non-proportionally damped system. This is evident from the different loss factors for the aluminum

(η=.005) and the viscoelastic (η=1). This non-proportionality is almost always present in nonhomogeneous systems.. Due to the complex nature of the stiffness matrix the general solution to this model becomes;

$$[M]\{\ddot{X}\}+[K^{**}]\{X\}=\{0\} \tag{3.17}$$

where $[K^{**}]$ is separated into real and imaginary components and $\{\ddot{X}\}$ represents the second time derivative of $\{X\}$. While the solution to this system of equations results in complex mode shapes and eigenvalues the complexity for a realist case can be show to be negligible. If, for instance the viscoelastic medium has a loss factor on the order of one (1) and a shear modulus several orders of magnitude lower than the aluminum (or alternative outer layer) with essentially no relative damping; then, the system behaves as a real weakly coupled system. All matrices are now n by n, and the resulting eigenvalue solution will have n complex conjugate pairs of eigenvalues. These are in the form;

$$\lambda_r = \eta_r(\omega_d)_r \pm j(\omega_d)_r \tag{3.18}$$

where $(\omega_d)_r$ is the damped natural frequency and η_r is the structural damping factor for mode r .

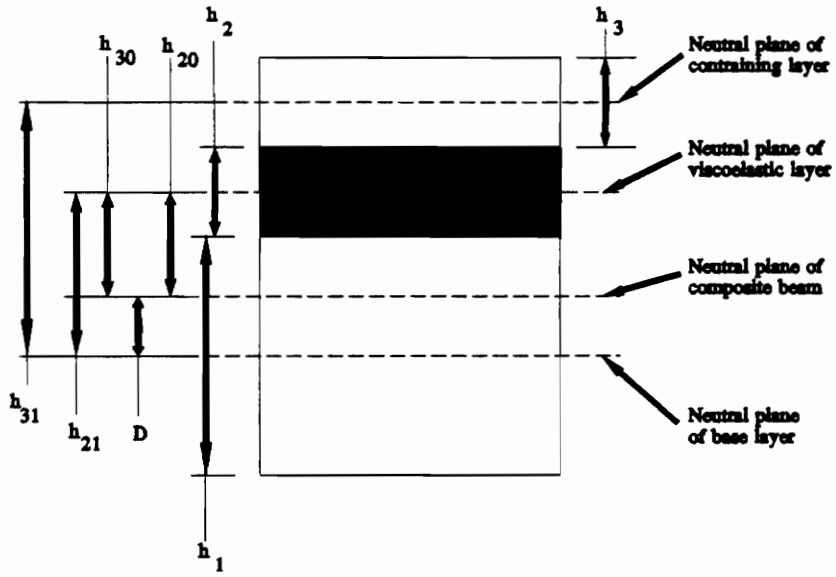

Figure 4. Geometric Parameters, Three Layer Differential Beam Element

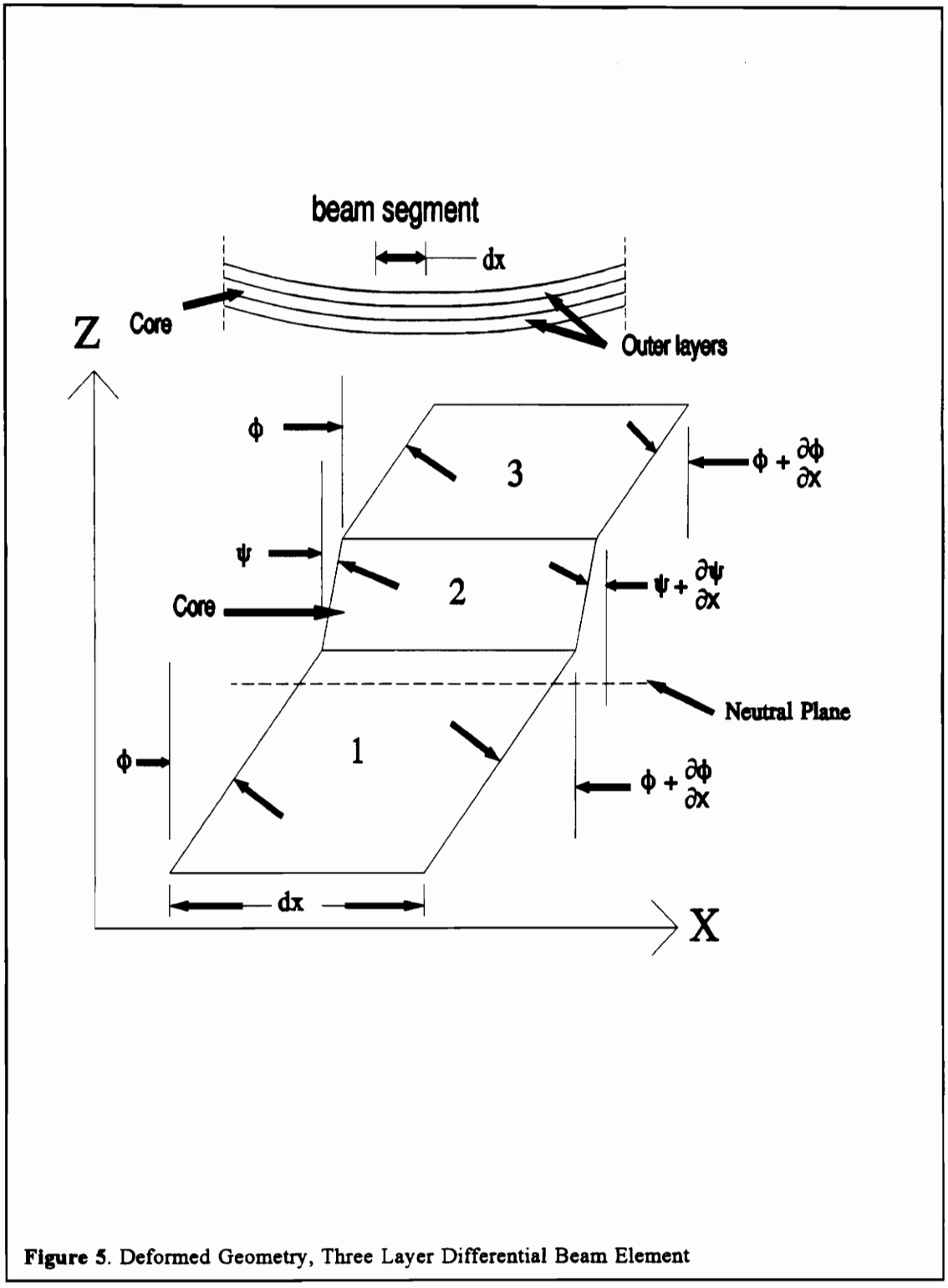

Figure 5. Deformed Geometry, Three Layer Differential Beam Element

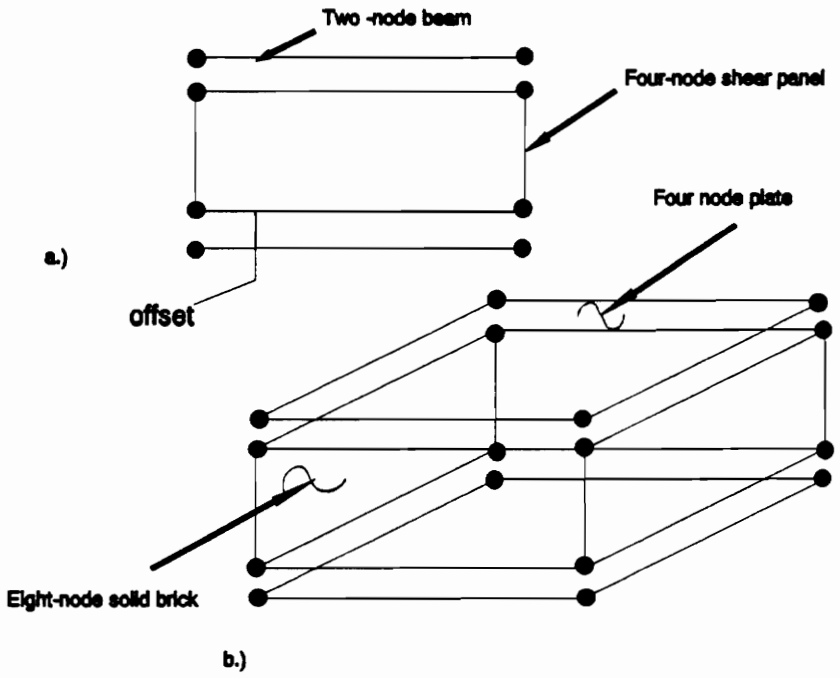

Figure 6. Finite Element Analysis Models: a.) Isotropic Beam Model b.) Laminate Beam Model

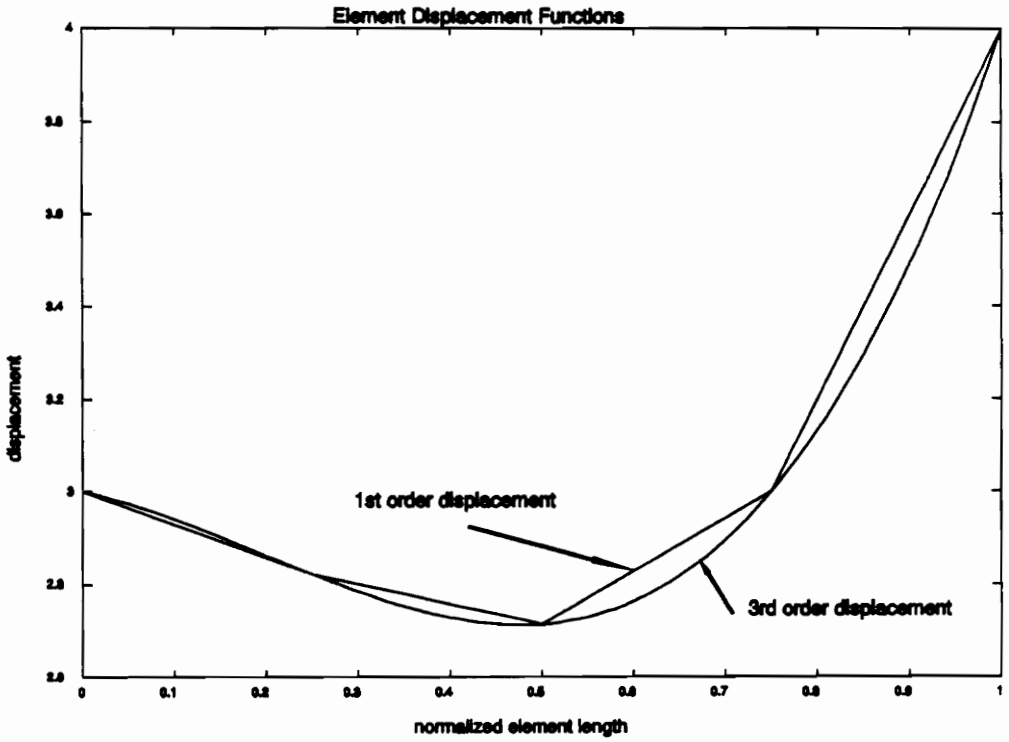

Figure 7. Comparison of First and Third Order Displacement Approximations

4 Experimental Methods

Experimental verification of any model is essential to validate its assumptions and inherent theory. The specific tests performed here involved both time domain and frequency domain analysis of random burst excitation and impulse response generated data records. The objective of this research was to quantify the parameter sensitivity of natural frequency (ω_n) and modal damping factor (η_n) to changes in boundary conditions, application length and location of additive viscoelastic treatment(s), and data extraction technique. The specific beams were chosen because they had slender geometric characteristics and could readily be modeled as Euler beams for the undamped cases. The beams were designed to be moderately flexible so that several of the lower modes would see relatively high damping with the particular low frequency viscoelastic material that was available. (see Figure 8 and Figure 9)

4.1 Excitation Methods

The two basic testing excitation methods were hammer impulse and random burst. Impulse testing is distinct from a plucking type because the system is initially at rest and has no pre-imposed displacement, only an instantaneous step in velocity, (imparted from the transfer of momentum from the hammer head to structure). Plucking, on the other hand, imparts an displacement, requiring a different analysis procedure involving this initial condition. Impact, or impulse, testing has obvious advantages over other testing methods in setup, hardware required, ability to easily shape input function power spectra (through hammer head selection and mass), and resonance detection when used in log decrement analysis. It has the disadvantages of double hits, pushing (the tip contact duration is too long and the hammer imparts displacement as well as velocity on the specimen), excitation to the nonlinear vibration levels, data clipping, saturation of the filter without overload, and repeatability. These problems can all be detected through

inspection of the data records. Double hits have twin peaks in response; pushing has initial DC offset; nonlinearities can be seen from non-proportional change in the level of response or signature for changes in forcing function level or applied boundary conditions; filter saturation can be seen from flattened peaks in the data record, repeatability simply comes with experience and avoiding all the previous problems.

A random burst signal is created by sending a synthetic random signal (white noise) through a low pass filter set above the frequency range of interest. (The low pass filter is employed above the frequency range of interest to ensure significant roll-off does not occur in the frequency band. Additionally, the filter reduces aliasing of high frequency content, a function of the burst signal content, hence, this filter is sometimes referred to as an anti-aliasing filter). The amplitude of the signal is then adjusted to assure no filter/data acquisition saturation. Then the signal is converted to a forcing function via an electro-mechanical shaker which is attached to the structure. Appendix B lists the equipment and the test(s) on which they were used.

4.2 Parameter Extraction Methods

Two main techniques, time and frequency domain methods, were used in the extraction of the modal parameters of damping and resonant frequency from the specimens. Time domain techniques were used for the isotropic based and laminate composite based beams to extract first mode information (loss factor and resonant frequency). The isotropic beams based were also studied using frequency response techniques to estimate modal parameters.

4.2.1 Time Domain Techniques

The time domain approach(s) used two setups. In the first, the isotropic beams were excited with an impact hammer and response was measured for the dominant first mode characteristics. The other impulse-based method employed with the composite beams used an eddy current probe to record their response. An eddy current probe produces a voltage proportional to the relative displacement of the metallic specimen (over a small range from its static equilibrium position) by measuring relative changes in the local magnetic field. Secondly, this type of transducer does not require physical contact, therefore there is no significant mass loading, which is essential when dealing with the light composite beam specimens chosen. (Some negligible mass loading and localized stiffening did occur because a metallic strip had to be bonded to the composite beams.) (see Figure 10) For the isotropic beams the ratio of the accelerometer mass to the beam mass was very small and was therefore neglected.

The time domain techniques used here were limited to applications of the log decrement method to extract damping ratios, frequencies and damping characteristics. This method was selected because it does not assume linear damping and is relatively simple to perform and interpret. This method entails recording a time varying signal (acceleration or displacement) within an envelope (time period) in which the signal decays significantly. The time period chosen for the isotopic beams was approximately 1 second (this allowed for almost complete attenuation of signal, 50 cycles, for damped beams) while the some of composite beams required significantly longer time periods (from .5 to 14 seconds) because of their lower resonant frequency. Resonant frequency was extracted with the following relation;

$$\omega_d = \frac{1}{\tau_d} \quad \textit{where} \quad \tau_d = \frac{\tau}{n} \tag{4.1}$$

where τ is the time for n cycles of response oscillation, and τ_d is the damped period of oscillation. Structural loss factor is developed from the relative amplitude of successive peaks in the response record by the relation [25, pp. 81-83] ;

$$\eta = \frac{1}{n\,\pi}\,\ln\left(\frac{w_i}{w_{i+n}}\right) \tag{4.2}$$

where w_i is the peak amplitude of cycle i of the lateral (z-direction) response. The signal, to be of practical use in this method, should be dominated by one frequency only. To accommodate this, placement of transducer and signal filters must be carefully chosen. Obviously, placement at the free end of a cantilever beam is a poor location since it is an anti-node for all modes, while slightly in from the free end, (approximately one fifth the total beam length), motion is dominated by the first mode and it is very close to the nodes for the second and third modes. Analogous situations exist for the other setups investigated. A band-pass filter can also be used to separate the higher modes from the more dominate lower modes.

4.2.2 Frequency Response Methods

Frequency domain techniques are used to investigate the relationship between variables (input vs. output) with respect to changing frequency, (normally referred to as Frequency Response Functions (FRF's)). Since data is normally taken in the time domain, transform methods must be employed to decipher the frequency content of the signal. The most common of these methods are the Discrete Fourier Transform (DFT) and the Fast Fourier Transform (FFT). The transformed data is then referred to as a frequency record.

With respect to vibration analysis, when the output channel (generally displacement or acceleration) is related to the input channel (generally force) the resulting FRF can be used to develop the modal parameters of resonant and natural frequencies, mode shape and modal damping factor.

Presented here are methods used to extract frequency and modal damping from the real and imaginary portions of the acceleration FRF. These parts of the function can also be used separately or as a set such as in the Nyquist plot circle fits and other curve fit algorithms.

The frequency response function methods chosen were based on separating random burst generated data records into real and imaginary components. Through assumption of a single degree of freedom (SDOF) model of a vibrating system, for these well separated modes, investigation of the components separately can yield direct extraction of the modal parameters of loss factor and resonance frequency. (Damping is relatively high for some of these cases, $\eta \approx .05$ but the influence of adjacent modes did not appear significant and therefore the SDOF model appeared acceptable.) The model for the basic equation for SDOF system separated into real and imaginary components as follows (see Figure 11). Assuming harmonic force and response and equivalent viscous damping;

$$\frac{X}{F} = \frac{1}{k - m\omega^2 + jc_{eq}\,\omega} = \frac{1/k}{1-(\frac{\omega}{\omega_n})^2 + j2\,\zeta_{eq}(\frac{\omega}{\omega_n})} = \frac{1/k}{1-(\frac{\omega}{\omega_n})^2 + j\,\eta} \qquad (4.3)$$

where m, c, k are the mass damping and stiffness of the system. Letting $r = \omega/\omega_n$ and separating into real and imaginary components the relation becomes;

$$\frac{kX}{F} = \frac{1-r^2}{(1-r^2)^2+(\eta)^2} - j\frac{\eta}{(1-r^2)^2+(\eta)^2} \qquad (4.4)$$

Examination of the *real* component shows that the natural frequency occurs when this function crosses zero response, independent of damping level. In addition, the damping can be estimated using the frequencies that produce the maximum and minimum response (refer to Figure 11.);

$$2\eta = (\frac{\omega_{max}}{\omega_n})^2 - (\frac{\omega_{min}}{\omega_n})^2 \qquad (4.5)$$

The *imaginary* components yield;

$$(\frac{\omega_r}{\omega_n})^2 \approx 1 - \frac{\eta^2}{6} \approx 1 \qquad (\eta \le .2) \qquad (4.6)$$

and the half power points yield;

$$Im: \qquad |\frac{\omega_2 - \omega_1}{\omega_n}| \approx \frac{2\eta}{3} \qquad (4.7)$$

where ω_1 and ω_2 represent the half power points below and above the peak response ω_n, respectively. A half power point is a point whose amplitude is $1/\sqrt{2}$ of the peak amplitude, the name 'half power' is because the power is related to the square of the amplitude.

A short discussion of the viscous and structural damping models is appropriate at this time. Briefly the development of the viscous model is as follows;

$$\frac{X}{F} = \frac{1}{-m\omega^2 + k + j\omega c}$$

$$= \frac{1/m}{-\omega^2 + \omega_n^2 + 2j\zeta\omega\omega_n}$$

$$= \frac{1/(m\omega_n^2)}{-r^2 + 1 + 2j\zeta r} \qquad (4.8)$$

at resonance

$$= \frac{1/m}{2j\zeta\omega_n^2}$$

The structural damping model is developed similarly;

$$\frac{X}{F} = \frac{1}{-m\omega^2 + (1+j\eta)k}$$

$$= \frac{-1/m}{\omega^2 - \omega_n^2 - j\eta\omega_n^2} \qquad (4.9)$$

at resonance

$$= \frac{1/m}{j\eta\omega_n^2}$$

The following models were based on viscous damping assumption and then converted to equivalent structural loss factor. It is often cited that this approximation $\eta \approx 2\,\zeta$ is only truly valid at resonance, but as shown in Figure 12 and Figure 13, this approximation is valid for light to moderate damping for a broad range (r=.8 to 1.2) of frequencies near the resonance. These plots where constructed with two systems, the first had viscous damping ratios (solid lines) that varied from .005 to .05 and the second system (dotted lines) had equivalent loss factors which varied from .01 to .1 . In first of these figures the deviations are essentially undetectable until the highest level of damping. The second of theses figures shows the Nyquist plot of the same functions. It is clear that for the lightly damped cases the difference is negligible though it is discernable for the higher damped cases. It should be noted here again that the Nyquist plot is only truly a circle for the viscous damping case of displacement FRF's and for the structural loss factor cases of mobility.

Also, the curve fitting techniques of Han [38] were applied to the function. Generally fitting is done over some sub-range (for most cases forming a band about the resonant frequency of ±25% ω_r) of the total record with a finite number of poles (most cases 2 or 3). Iteration on the number of poles and frequency range is then continued until some preset fit tolerance (in this case less than 5% change in η and 1% change in ω_r) is reached. These equations estimate loss factors well for SDOF systems and multiple degree of freedom (MDOF) systems with well separated modes, but for closely spaced modes additional terms must be included in the model to compensate for the residual stiffness and mass from nearby modes outside the sub-range of the interest.

When using a Nyquist plot, the damping ratio can be extracted from a circle fit of the real component vs. the imaginary component of the displacement FRF, (as cited earlier this is not truly a circle for the structural case here and is fit as an equivalent viscous model) and due to the fact [31] that the diameter

is inversely proportional to the damping ratio. Specifically;

$$\eta = \frac{1}{d\omega_r} \tag{4.10}$$

where d is the diameter of the circle and ω_r is the resonant frequency of the mode. Typically, for each mode, most points on the Nyquist plot are near the origin but with as few as 8 points, spaced about the determinant part of the circle (20 to 340 degrees) sufficient accuracy is predicted. Problems arise when the damping is high, resulting in small imaginary components and data near the noise floor, or with low resolution data where the frequency spectra are spaced too far apart and only have a few points on the majority of the perimeter of the circle. The tests here were conducted with resolution such that at least 8 points where on the determinant part of the circle.

Experimental 'windows' are functions which are multiplied by the data time record in a specific way called convolution (discussed in many texts [37]) to weight the data to reduce leakage and amplitude errors when the data is transformed to the frequency domain. (Leakage is the phenomena of energy associated with a frequency not at a spectral line being smeared or leaked into neighboring spectra. When this occurs at a resonant frequency peak amplitude is underestimated and damping is overestimated.) Many windows exists, such as Hanning, Hamming, Box-car, Exponential and Force, all with specific attributes. The most common of these are the Hanning, Hamming, and Exponential; the Hanning and Hamming use similar functions to reduce leakage through a moving weighted average approach while the Exponential window simply applies a decaying exponential to the time history to reduce the signal to the noise floor by the end of the observation period (resulting in a fully observed signal). If windows used on the data are applied equally to the channels (force and acceleration) they should not add noticeable damping since the FRF is based on the ratio of these channels. Exponential windows were not used in the analysis because of problems in their implementation on the hardware used in testing. This windowing can corrupt the data,

and qualitative inspection of data records without it show very good correlation throughout the frequency spectra of interest. Hanning and Hamming windows were not applied because they degrade amplitude estimates and when applied did not appreciably improve correlation or general data quality.

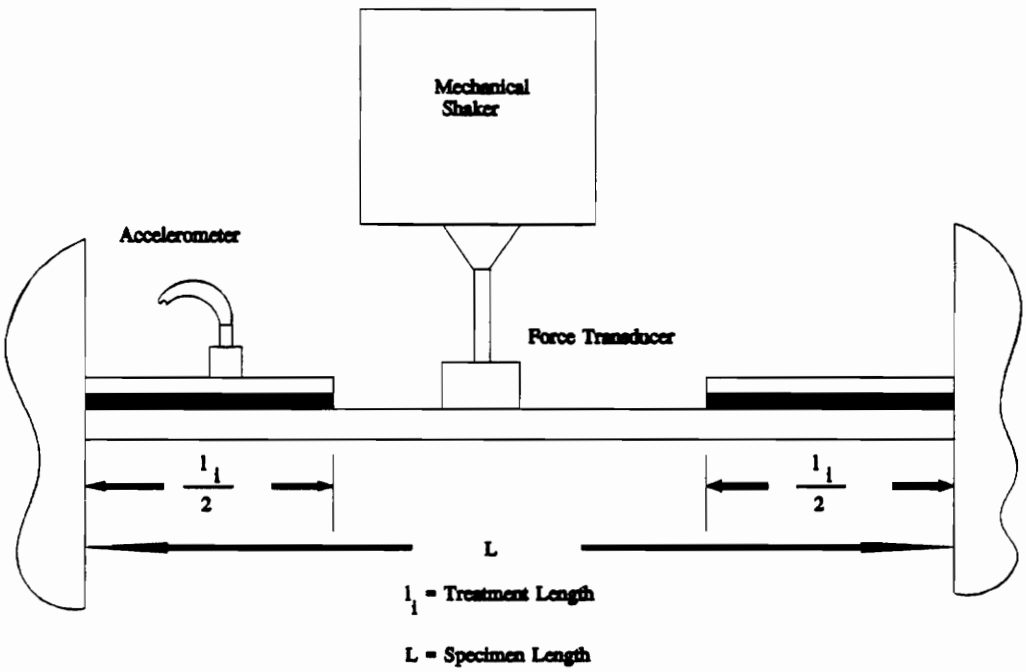

Figure 8. Fixed/Fixed Beam Set-up, Random Burst Tests

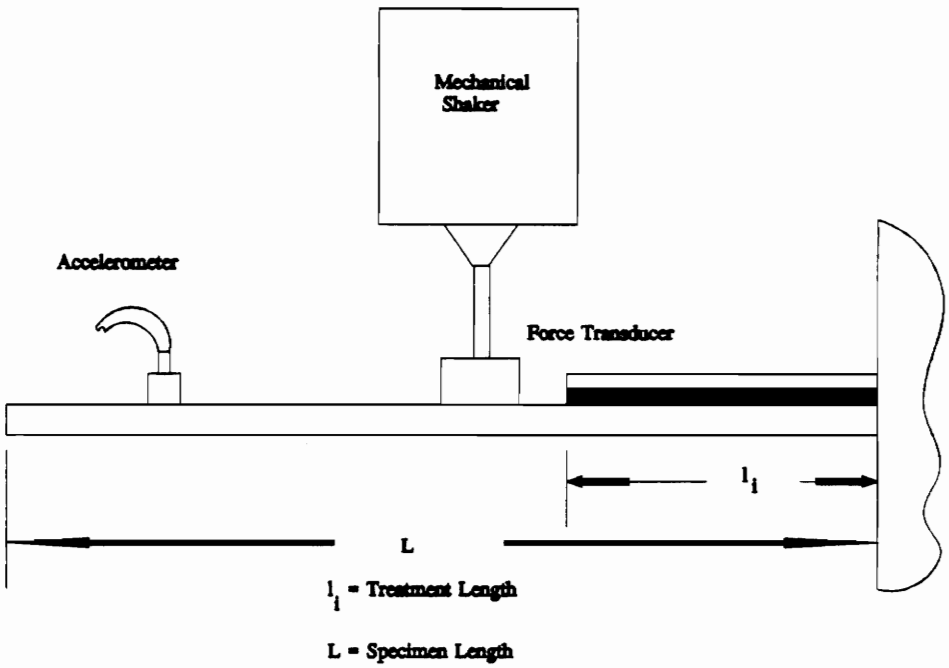

Figure 9. Cantilever Beam Set-up, Random Burst Tests

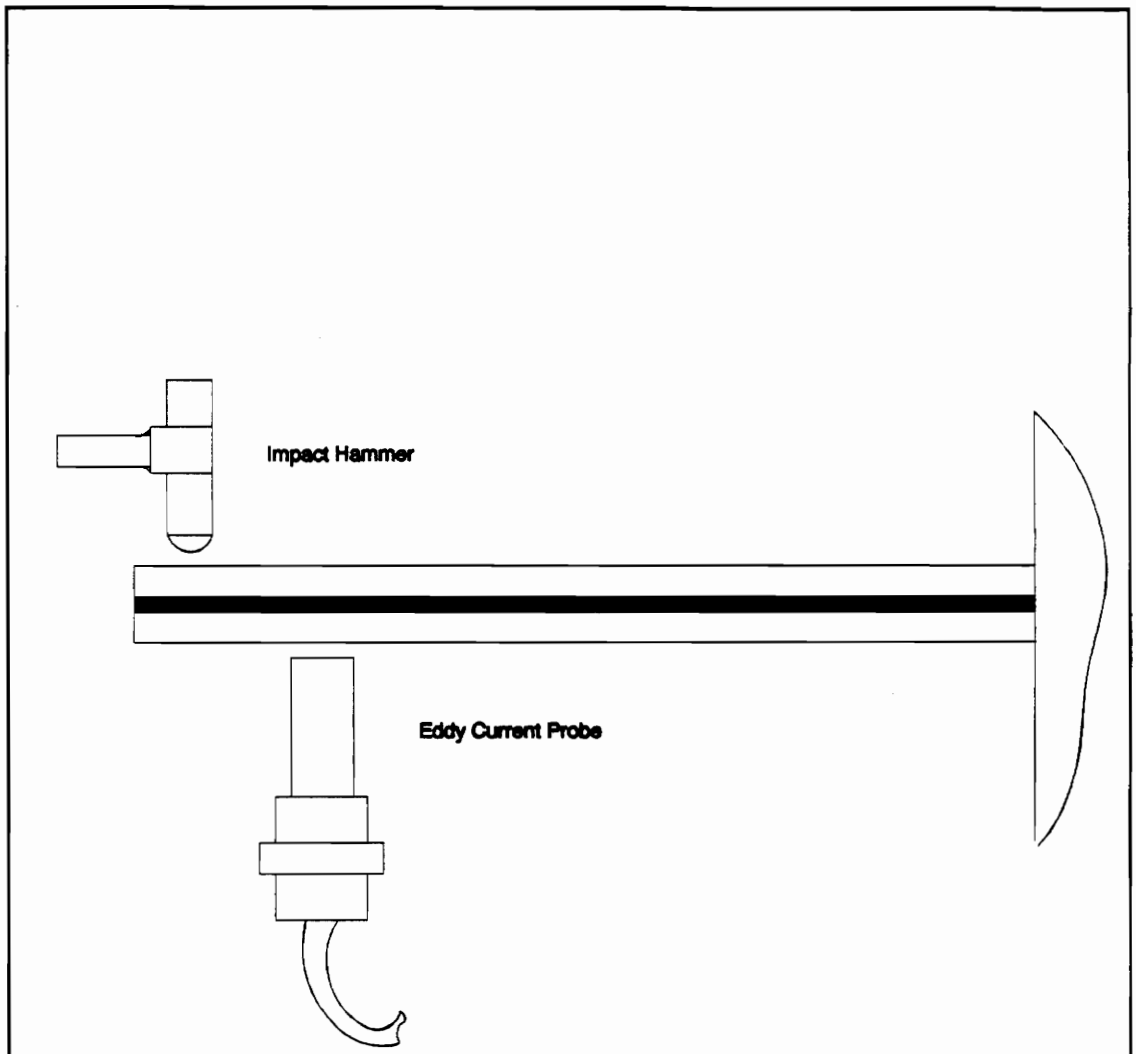

Figure 10. Eddy Current Probe, Laminate Beam Set-up

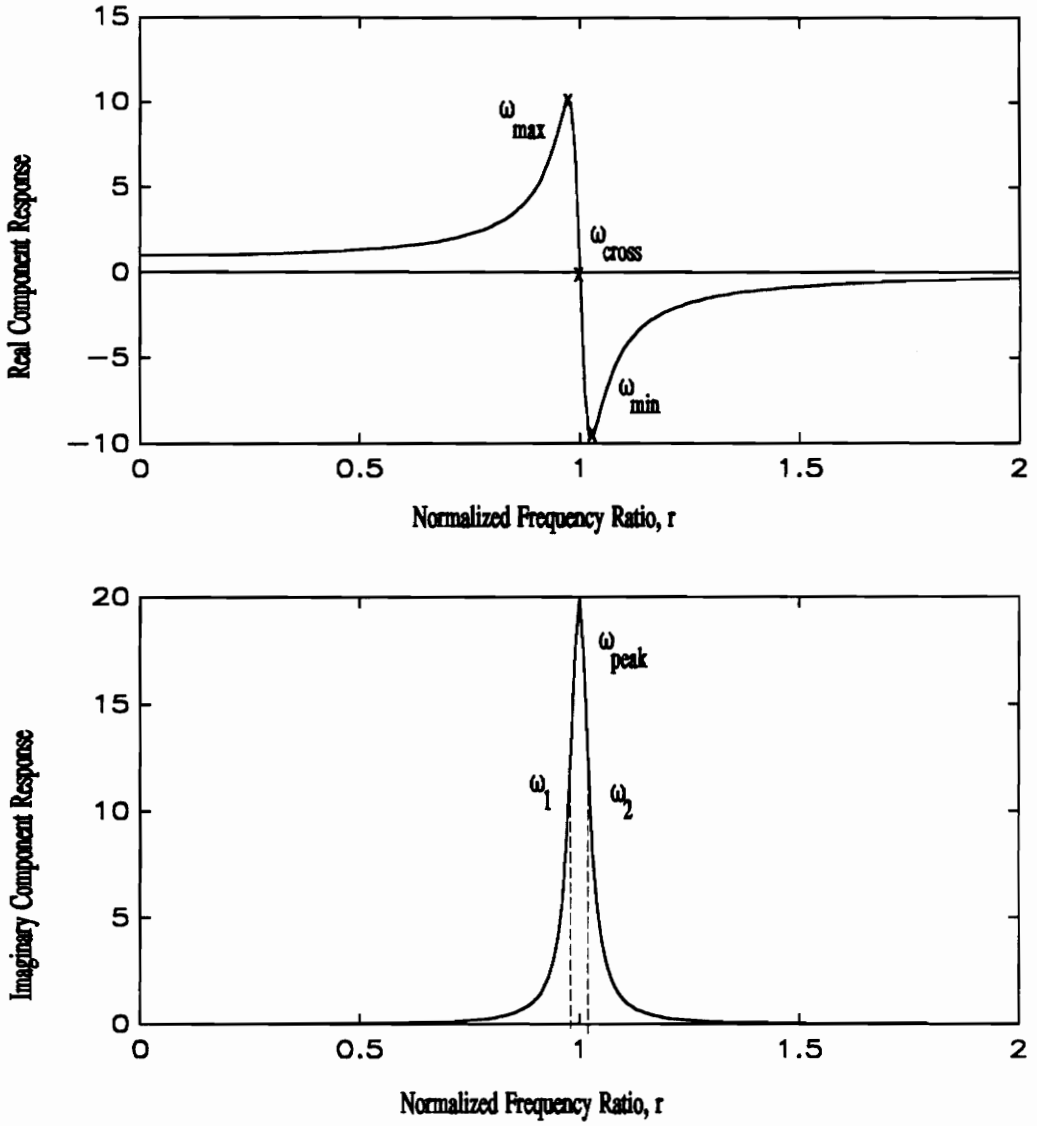

Figure 11. Real and Imaginary Components of SDOF FRF

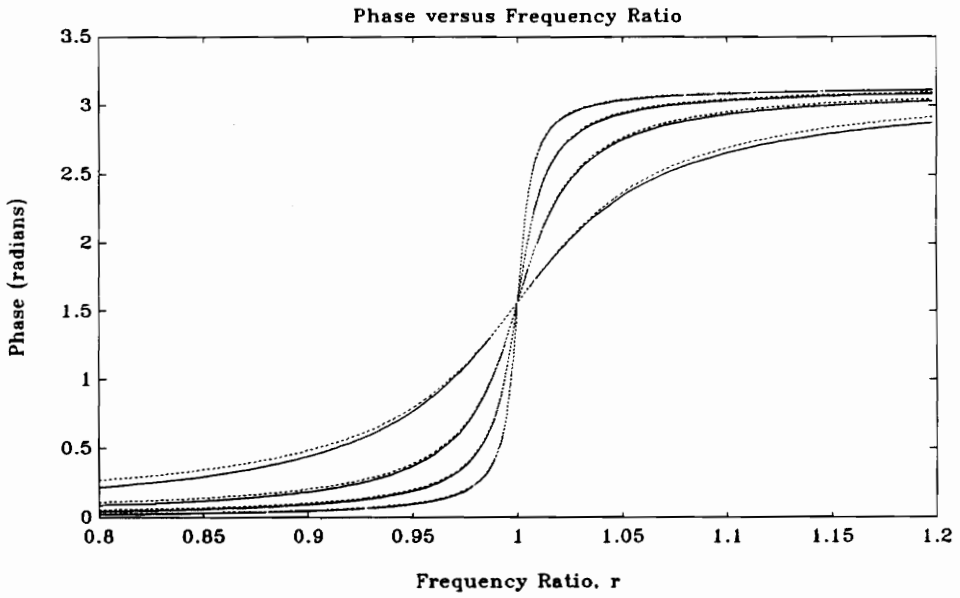

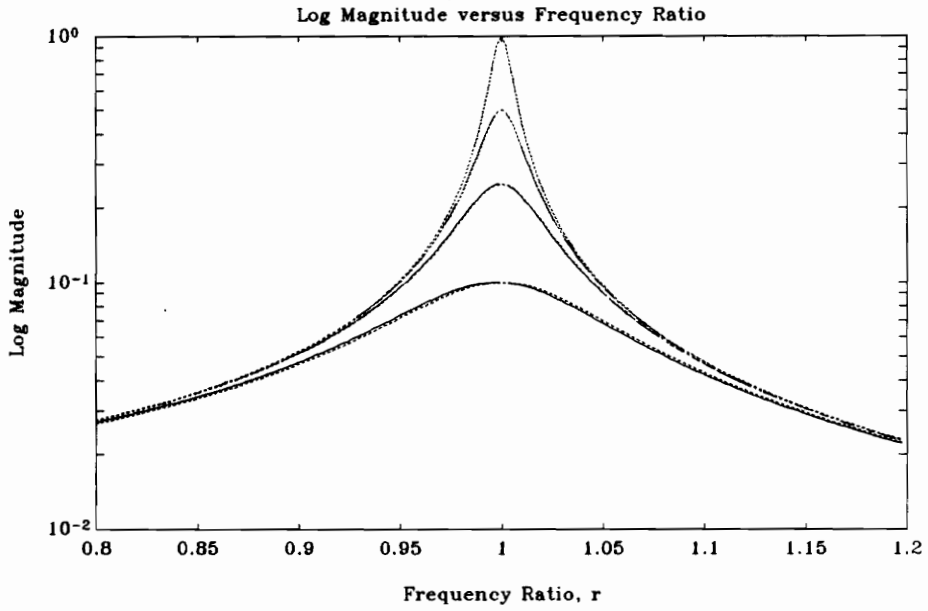

Figure 12. Phase and Magnitude displacement FRF for viscous (solid lines) and structural (dotted) damping models .

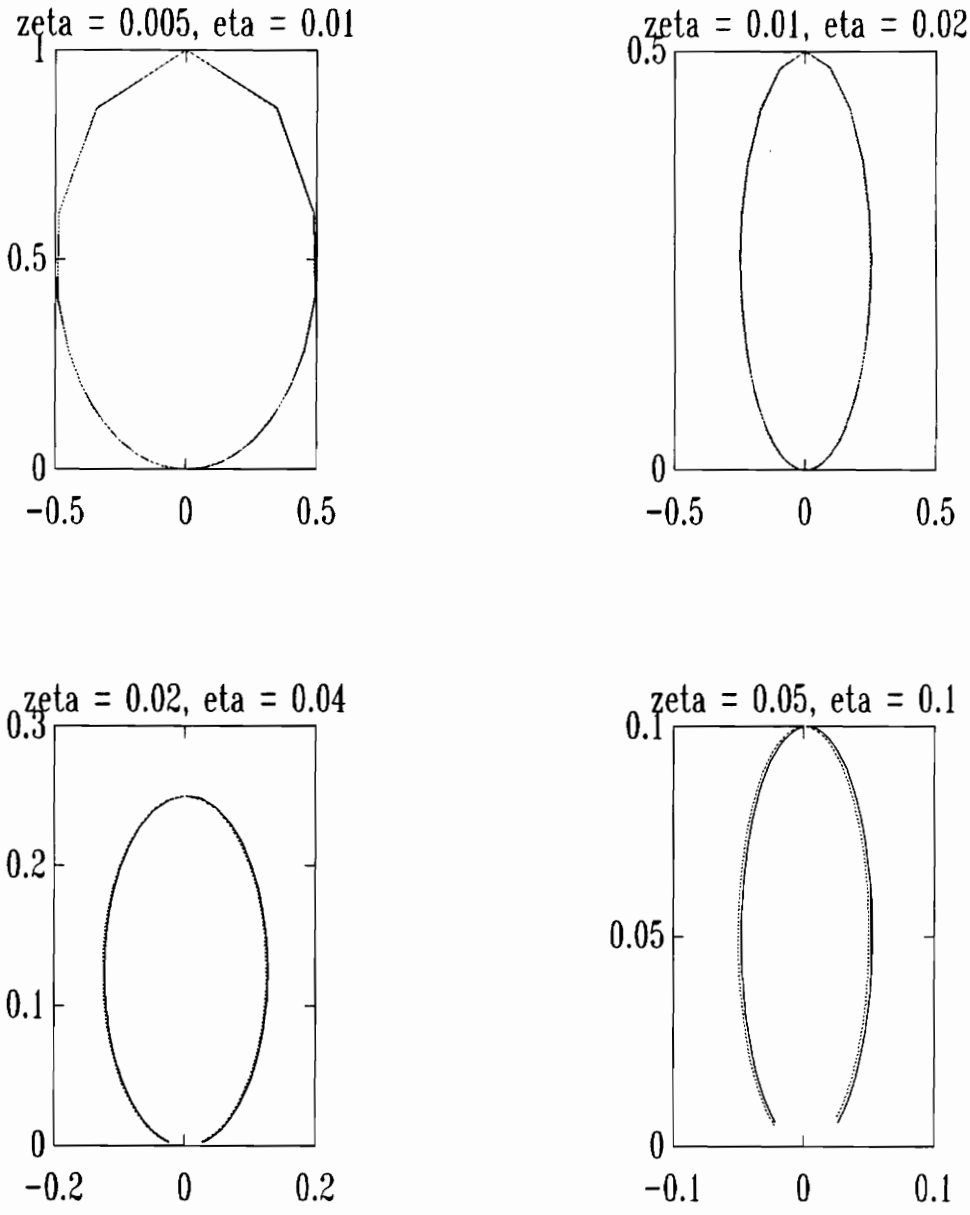

Figure 13. 'Nyquist' plot displacement FRF for viscous (solid lines) and structural (dotted) damping models .

5 Effects of RKU Parameters on the Flexural Rigidity and Damping of Constrain Layer Beams

The development of this section will proceed from the basic postulations and assumptions of Ross, Kerwin and Ungar, (RKU), to their fundamental parameters and finally to the effect of these parameters on the flexural rigidity, B, and composite structural loss factor, η_c. The basic premise of this RKU-based analysis is that by constraining the viscoelastic damping material with stiff outer layers, it effectiveness can be improved over the free layer (or unconstrained) treatment previously used. The addition of this constraining layer dramatically improves the treatment's net material effectiveness, or the increase of damping per unit weight or volume perspectives. The basic assumptions made by RKU were linear vibration, low viscoelastic stiffness, infinitely long or simply supported boundary conditions and the majority of the extensional loading carried by outer layers, (predominantly the original base layer).

The first parameter to be investigated is the geometric parameter, Y. This parameter quantifies the relative increase, provided by the constraining layer, to the overall bending stiffness based on a geometric development. This relationship for beams using the same material for the constraining layer and the base layer ($E_1 = E_3 = E$) with a thin soft viscoelastic core ($E_2 < E$; h_1, $h_3 > h_2$) (this will be the beam parameters investigated throughout this chapter) can be simplified using Equation 28 of [9] in the following form;

$$Y = \frac{12\frac{h_3}{h_1}\left(\frac{h_{31}}{h_1}\right)^2}{\left(1+\frac{h_3}{h_1}\right)\left(1+\left(\frac{h_3}{h_1}\right)^2\right)} \tag{5.1}$$

where h_i is the layer thickness and h_{ij} is the distance from the center of layer i to center of layer j. For the cases of thin damping tape ($h_3 < h_1$, $h_{31} \equiv h_1/2 = h_{21}$) or symmetric beams ($h_3 = h_1$, $h_{31} = 2\ h_{21} \equiv h_1$) this parameter, Y, can be approximated by (both cases);

$$Y_{RKU} = 3.5\frac{h_3}{h_1} \tag{5.2}$$

As can be seen, (see Figure 14), the relation developed by Ross et. al., Y_{RKU} , underestimates the actual value for most cases ($h_3/h_1 < .9$), but is a good approximation for Y at the end regions(h_3/h_1 >= .10 and .8 < h_3/h_1 <= 1.0). This approximation, Y_{RKU}, accommodates h_2 taking on small values, (Y_{RKU} : 0.05 < $2h_2 + h_3 < 0.15\ h_1$). **Note** that this parameter, Y, is **not**, explicitly or implicitly, a function of η_v, the central layer loss factor.

From this derivation the next parameter to be investigated is $h_2(\partial\psi/\partial\phi)$. This term can be thought of as the relative slip of the outside layers in the longitudinal direction. The basic relation is;

$$h_2\frac{\partial\psi}{\partial\phi} = \frac{k_1h_{31} + k_2(h_{31} - h_{21})}{k_1 + \frac{k_2}{2} + g(k_1 + k_2 + k_3)} \tag{5.3}$$

where; $k_i = E_i/h_i$, and $g = G_2/k_3h_2p^2$, p^2 is proportionally related to the driving frequency, ω. Figure 14 shows the effect of varying h_3/h_1 and g on this relative slip. As can be deduced from the formula (Eq 5.3) and the graph (Figure 12), the effect of h_3/h_1 is greatly reduced as g increases. It is also evident that this value follows the relation (for high g);

$$\frac{h_2}{h_1}\frac{\partial\psi}{\partial\phi} = \frac{1}{2g} \tag{5.4}$$

For the special cases of damping tape and symmetric beams, respectively, this relation can be simplified to;

$$\frac{h_2}{h_1}\frac{\partial\psi}{\partial\phi} \approx \frac{1}{2(1+g)} \quad , \quad \frac{1}{1+2g} \tag{5.5}$$

The next fundamental parameter to be investigated is the neutral layer offset, D. This parameter is used to adjust the effective bending moment of inertia to reflect the shift in neutral plane from the center of the base layer. This parameter is described by the relation;

$$D = \frac{k_2(h_{21} - \frac{h_{31}}{2}) + (k_2 h_{21} + k_3 h_{31})g}{k_1 + \frac{k_2}{2} + (k_1 + k_2 + k_3)g} \tag{5.6}$$

For the case of $k_1 = k_3$ and $k_2 = 0$, it is evident that this relation will under estimate D for the symmetric

$$\frac{D_{sym}}{h_1} \approx \frac{g}{1+2g} \tag{5.7}$$

beam in an inversely proportional manner with respect to shear parameter g . (It is intuitively obvious that this should be equal to .5 for any symmetric viscoelastic core beam.) Note that the relation for symmetric beams does not depend on the central layer stiffness k_2 at all. For the case of damping tape, D can be approximated by;

$$\frac{D_{tape}}{h_1} \approx \frac{h_3 g}{h_1(2+2g)} \tag{5.8}$$

D, if k_2 is small, is roughly linear in h_3/h_1 for $.01 < g < .5$, (Figure 15.). D also behaves in an asymptotic manner for a given h_3/h_1 with increasing g, (with limited return for $g > 1.$), (see Figure 15.). Note that D is shown normalized, in all figures, to h_1 and is not a function of central layer loss factor. For the wide range of applications where $E_2 < E_1, E_3$ *and* $E_1 = E_3$, a relation can be drawn between the neutral plane offset, D, and the relative slip between layers 1 and 3, $h_2(\partial\psi/\partial\phi)$;

$$D_{sym} = g h_2 \frac{\partial\psi}{\partial\phi} \tag{5.9}$$

Now that the constitutive parameters have been investigated it is appropriate to investigate the composite beam structural loss factor, η_c . The relation for this parameter is described by;

$$\eta_c=\frac{\eta_v Y(1-\epsilon)g(1+(k_3/k_1))}{1+[2+Y(1-\epsilon)]g(1+(k_3/k_1))+[1+Y(1-\epsilon)](1+\beta^2)g^2(1+(k_3/k_1))} \tag{5.10}$$

where;

$$\epsilon=(\frac{k_2}{gk_3})\frac{h_{21}}{2h_{31}} \tag{5.11}$$

For the case of soft viscoelastic center layer, $\varepsilon \equiv 0$ ($k_1, k_3 > k_2$) . If again the constraining layer and the base layer are of the same material, ($k_3/k_1 = h_3/h_1$). For thin damping tapes, the relation for composite loss factor can be simplified to;

$$\eta_c=\frac{\eta_v Yg}{1+[2+Y]g+[1+Y](1+\beta^2)g^2} \tag{5.12}$$

For symmetric beams, η_c is simplified to;

$$\eta_c=\frac{2\eta_v Yg}{1+[2+Y](2g)+[1+Y](1+\beta^2)4g^2} \tag{5.13}$$

As can be seen in Figure 16, the composite loss factor for the practical range of central layer loss factor (.5 to 1.5) is fairly linear in η_v with its slope and offset functions of g . The relation between η_c and g is much more complex and follows the basic form of;

$$\eta_c=\frac{q_1 g}{1+q_2 g+q_3 g^2} \tag{5.14}$$

where q_1, q_2, and q_3 are functions of geometry and central layer structural loss factor. Clearly, this function is linear in g for low g, constant over a range, and inversely proportional to g for high shear parameter values. The relation between η_c and g, η_v and h_3/h_1 has optimal g value ($.3 < g_{opt} < .75$) that is that is not strongly dependent on the other factors (η_v and h_3/h_1). For a beam with constant central layer thickness

and loss factor, (h_2/h_1 = .05 and η_v = .5) the effect of constraining layer thickness and shear parameter on composite loss factor is illustrated in Figure 17. There exists an optimal shear parameter value, between .2 and .5, which is inversely related to the constraining layer thickness. These Figures also show that there exists an optimal value of constrain layer thickness, (around .5 for this case), where increasing the thickness does not appreciably increase the loss factor (this is true for all levels of shear parameter, g , studied).

The flexural rigidity, B , of the composite beam is expressed as;

$$B=k_1\left(\frac{h_1^2}{12}+D^2\right)+k_2\left(\frac{h_2^2}{12}+(h_{21}-D)^2\right)+k_3\left(\frac{h_3^2}{12}+(h_{31}-D)^2\right)-\left[\frac{k_2}{2}\left(\frac{h_2}{12}+h_{21}-D\right)+k_3(h_{31}-D)\right]h_2\frac{\partial\psi}{\partial\phi} \qquad (5.15)$$

If the beam again has a soft thin central layer, $k_2 << k_1$, k_3 and $h_2/h_1 < .05$, then the relation can be approximated by;

$$B\approx k_1\left(\frac{h_1^2}{12}+D^2\right)+k_3\left(\frac{h_3^2}{12}+(h_{31}-D)^2\right)-k_3(h_{31}-D)h_2\frac{\partial\psi}{\partial\phi} \qquad (5.16)$$

This relation can then be normalized to base layer rigidity;

$$B'=\frac{B}{k_1\frac{h_1^2}{12}}\approx 1+12\frac{D^2}{h_1^2}+\left(\frac{h_3}{h_1}\right)^2+12\frac{h_3}{h_1}\frac{(h_{31}-D)^2}{h_1^2}-12\frac{h_3}{h_1}\frac{(h_{31}-D)h_2}{h_1^2}\frac{\partial\psi}{\partial\phi} \qquad (5.17)$$

The effect of shear parameter, g , and treatment thickness on flexural rigidity can then be investigated (Figure 18). This shows that increasing g yields a consistent, yet diminishing, increase in the flexural rigidity from its coupling effect on the outer layers. Increasing h_2/h_1 also yields an increase in B′ that appears to be related to the cube of constraining layer thickness. For higher g, strong coupling, the flexural rigidity reaches near the values expected for an isotropic beam of the same stiff material and thickness ($h_1 + h_3$, excluding the damping material).

The next proposed parameter is the normalized natural frequency, ω'. This parameter will be defined as

$$\omega' = \sqrt{\frac{\beta'}{\rho'}} \quad \textit{where} \quad \rho' = 1 + \frac{\rho_2}{\rho_1}\frac{h_2}{h_1} + \frac{\rho_3}{\rho_1}\frac{h_3}{h_1} \tag{5.18}$$

and ρ_i is the linear mass density of layer i. (This is not an RKU parameter but was developed by the author using previously mentioned parameters and Euler theory.) In Figure 19 there is initial dip in ω' as constrain layer thickness is increased (for low g applications). This reduction appears to be inversely related to the coupling in magnitude and duration. An indication that while the density is being increased the stiffness has not been substantially increased. The effect of increasing g is consistently positive, as would be expected, since this increases the coupling, therefore the strain energy, hence the frequency of natural oscillation.

A short example of the design procedure utilizing these graphs can now be examined. Briefly, assume that there exist a large flexible structure, such as a space station or antenna, that has an rectangular appendage that is made of aluminum (E = 70 GPa, ρ = 2710 kg/m^3) and .75 m in length, .1 m in breadth and .02 m in thickness. This platform is to be redesigned as a symmetric three layer damped beam to alleviate resonance problems at the second mode of cantilever vibration (245 Hz). This construction results in highest shearing forces applied to viscoelastic and has been shown to be the superior design prior to manufacture. (Add-on treatments must typically be made very thin and are used almost exclusively in an ad-hoc fashion.) The beam with have treatment along the its total length to ease manufacture.

Since the beam outer layer characteristics are already known, the wave number, p, and stiff layer elastic constant K_3 are fixed. Therefore the shear parameter, g, (refer to Eq. 3.4) can only be effected by the viscoelastic core shear modulus (G_2) and thickness (h_2). From Figure 14, it is clear that the shear gradient, hence relative slip, is inversely proportional to the shear parameter g. This is an indicator that as the structure becomes more coupled, (higher G_2) , the gradient is reduced. From Figure 14, the Geometric

parameter Y is approximately 3, which would be the homogeneous result, it is slightly higher to reflect the increase in moment of inertia produced by the offset due to the core layer.

Assuming that the viscoelastic material has a loss factor (η_v) of 1.0 at 250 Hz, then from Figure 16 the maximum composite beam loss factor is approximately .053 with a shear parameter value of .55. Using these results and Figure 18 the estimated normalized flexural rigidity is 5.5. This number is reference to a single beam of thickness equal to one of the outer layers in this construction, hence the homogeneous beam parameter would be 8 ($((h_1+h_3)/h_1)^3$). This reduction is a reflection of the decoupling effect of the core layer and is also evident in Figure 19 , where the normalized resonant frequency is 1.6 compared to an isotropic specimen's equivalent result of 2.0. Since the shear modulus of the viscoelastic are typically very low, (G ≈ 500 kPa) the shear parameter is typically adjusted by choosing an appropriate thickness, h_2. The platform with this design would be somewhat weaker in bending and have a shifted resonance, but is damping would be dramatically improved. Iterations on this design could then be performed until an acceptable tradeoff between stiffness and damping was reached.

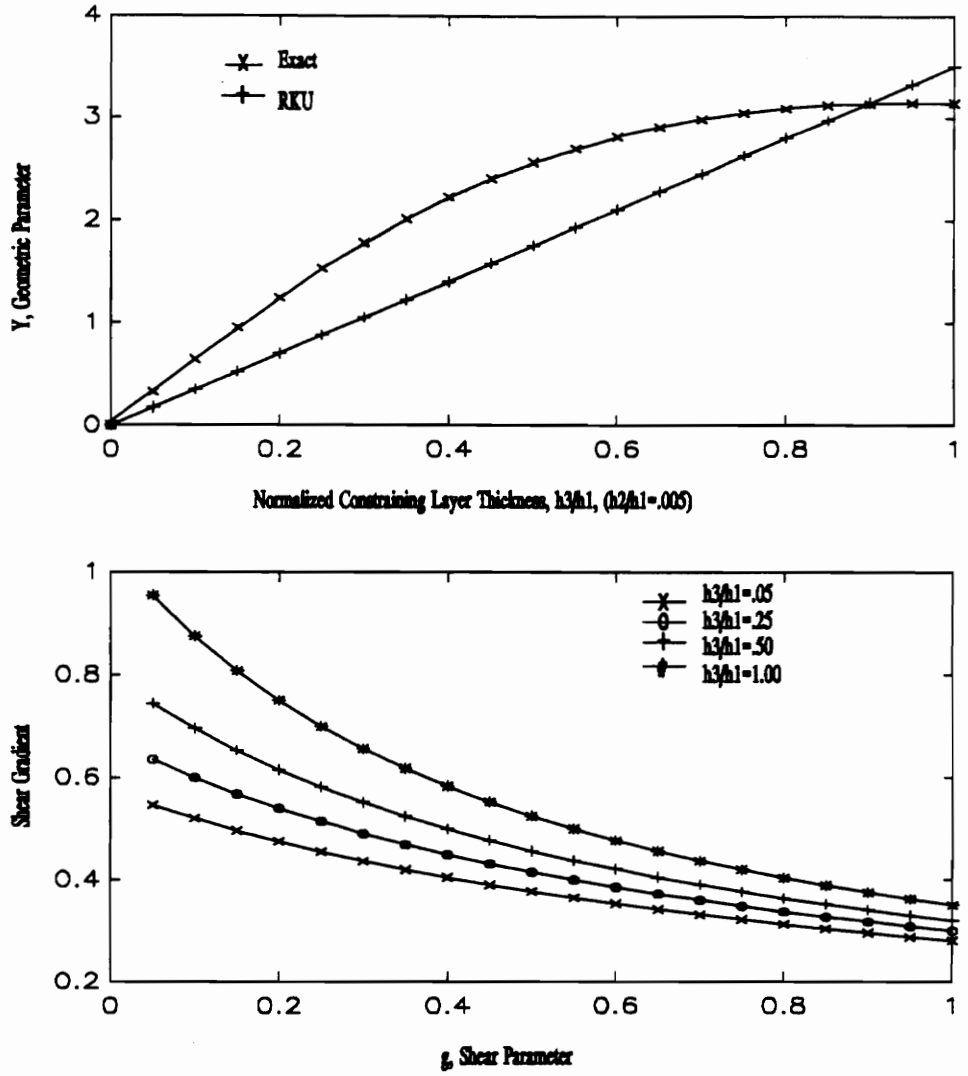

Figure 14. Effect of Constraining Layer Thickness on Geometric Parameter, Y (Eq 5.1, 5.2) and Effect Shear Parameter, g, on Viscoelastic Core Shear Gradient (Eq 5.3).

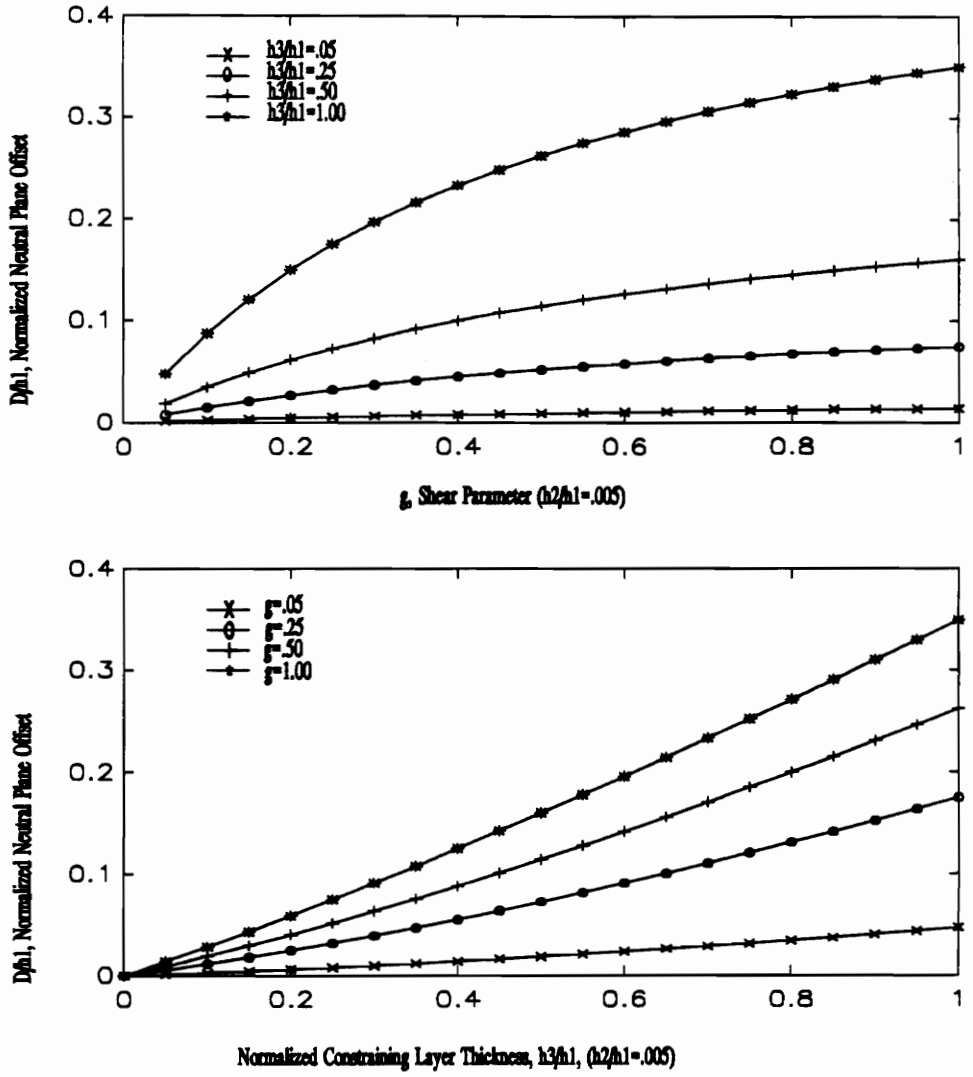

Figure 15. Effect of Shear Parameter g, and Constraining Layer Thickness, h_3 on Neutral Plane Offset, D (Eq. 5.6).

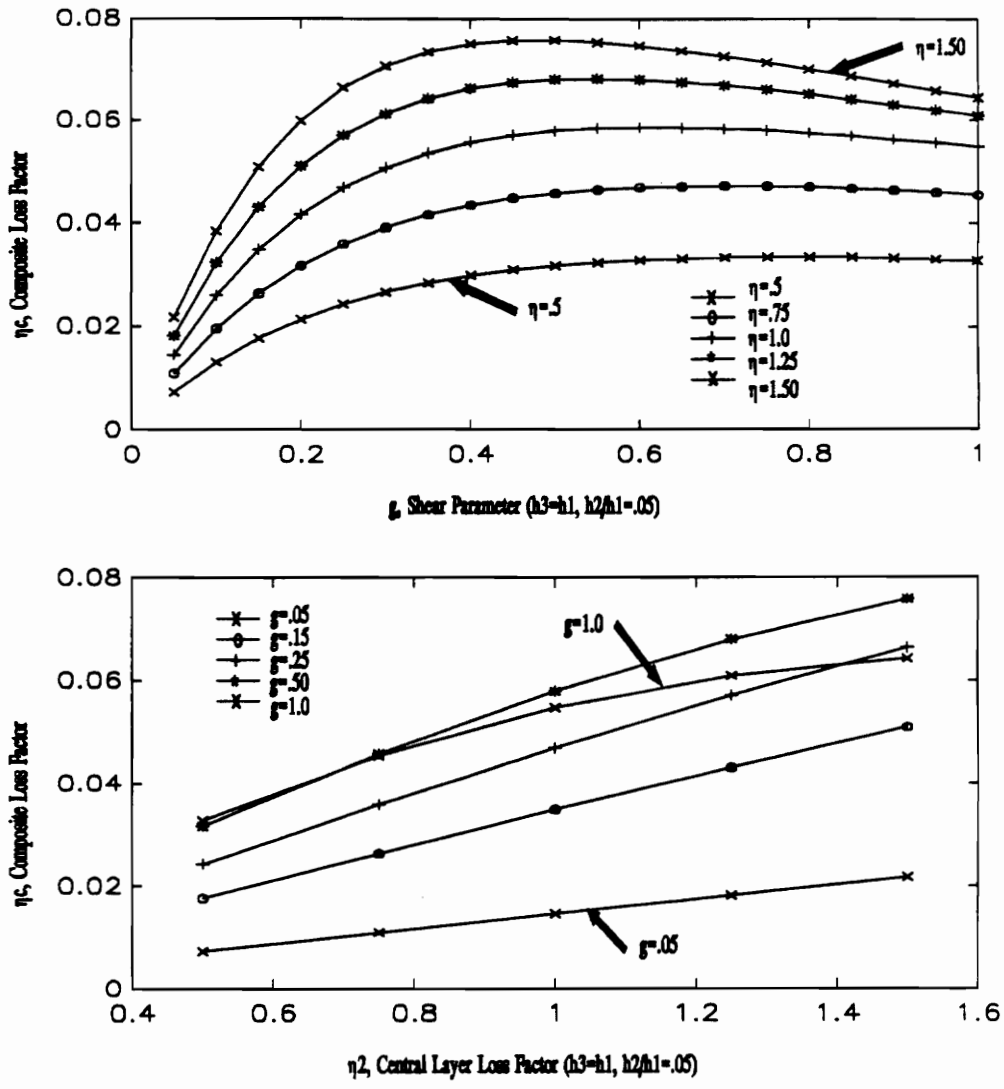

Figure 16. Effect of Shear Parameter, g, and Central Layer Loss Factor, η_2 on Composite Loss Factor η_c (Eq 5.12).

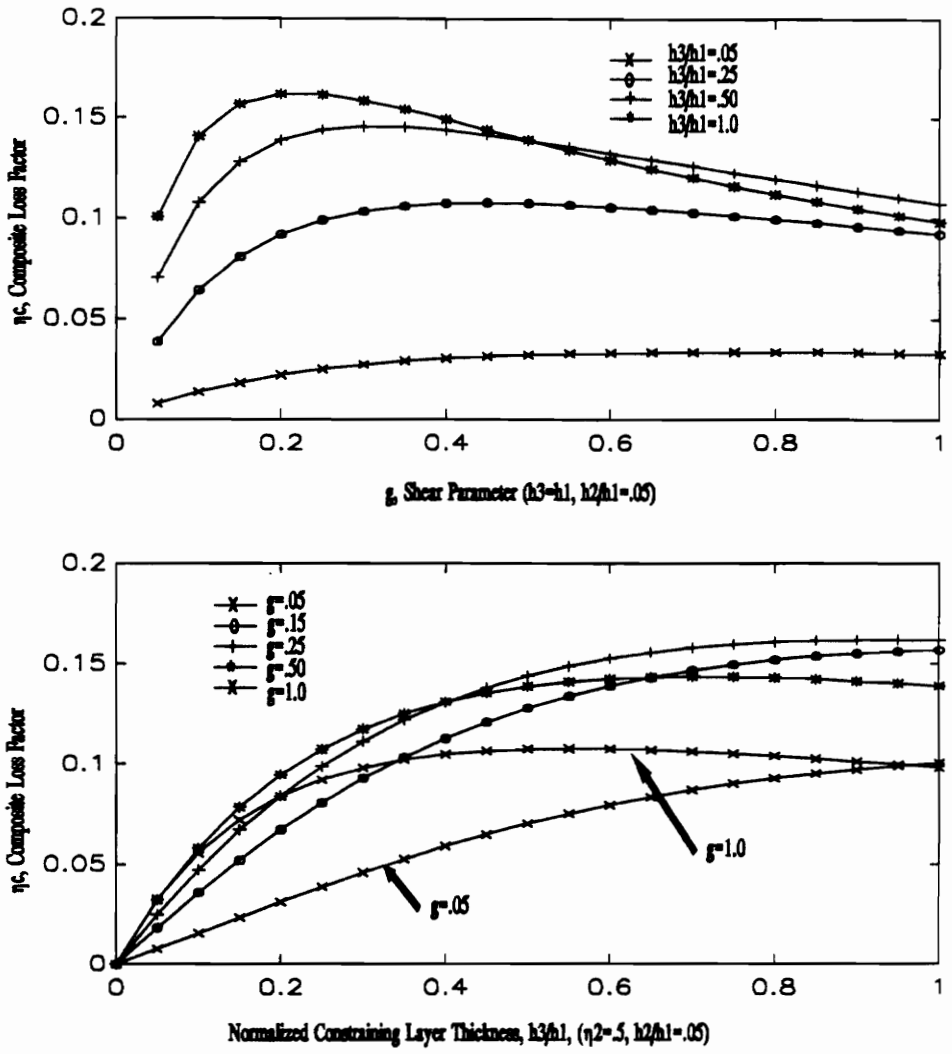

Figure 17. Effect of Shear Parameter, g, and Constraining Layer Thickness, h_3 on Composite Loss Factor, η_c (Eq 5.12).

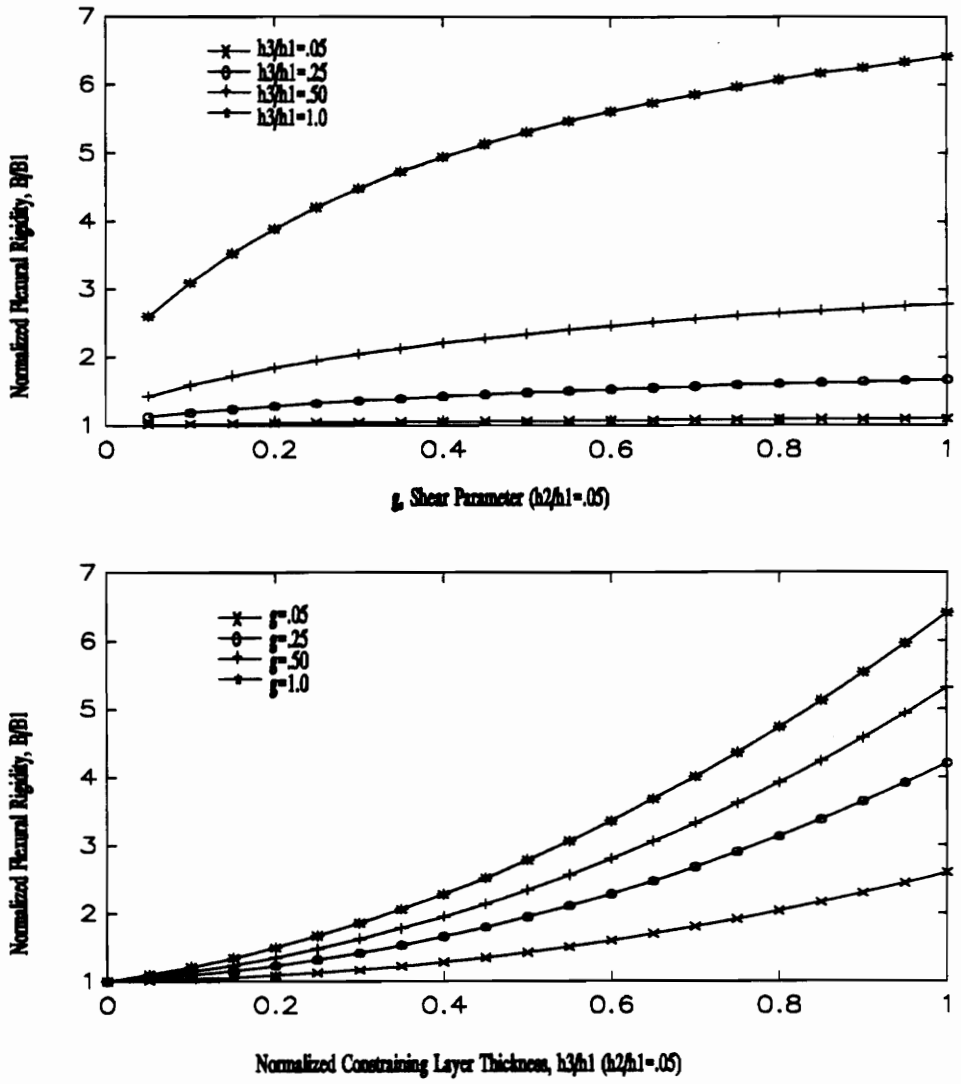

Figure 18. Effect of Shear Parameter, g, and Constraining Layer Thickness, h_3 on Flexural Rigidity, B (Eq 5.17).

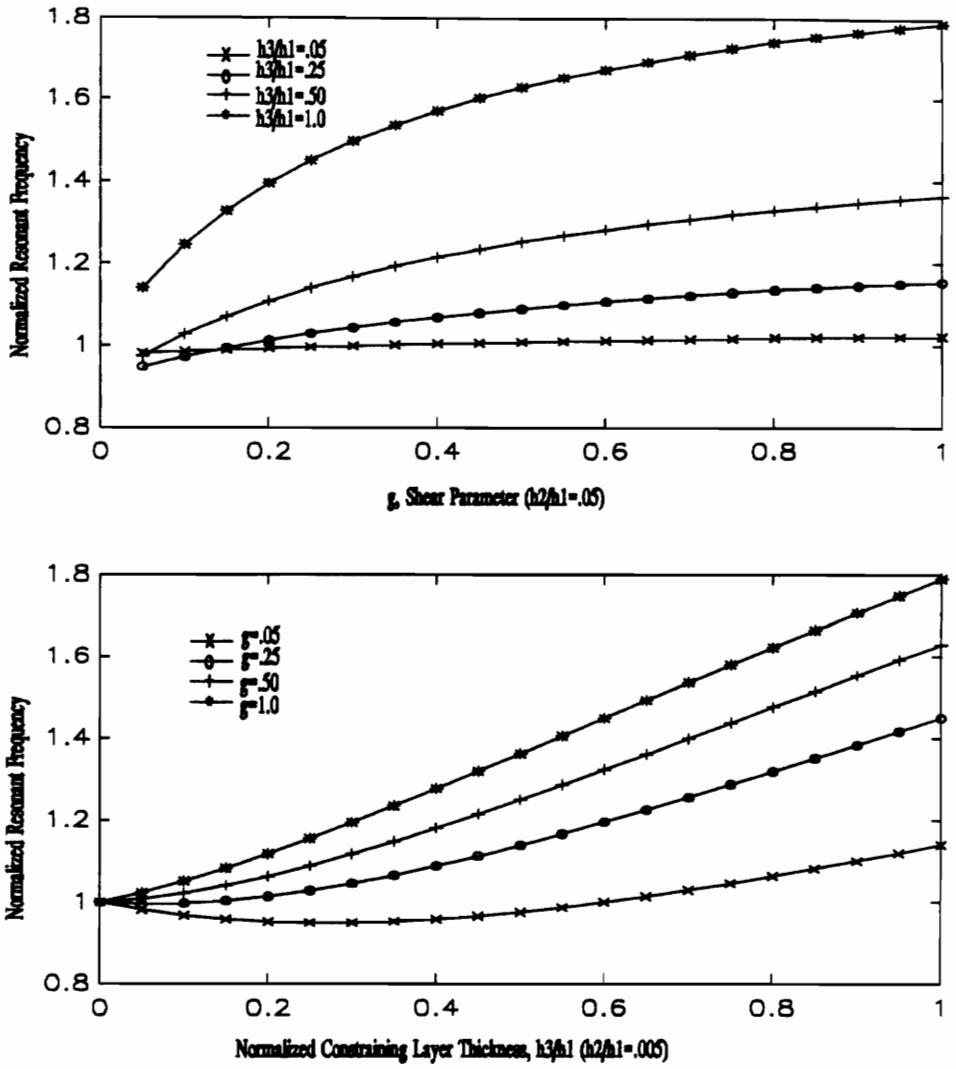

Figure 19. Effect of Shear Parameter, g, and Constraining Layer Thickness, h_3 on Resonant Frequency Shift, ω' (Eq. 5.18).

6 Numerical and Experimental Studies

This chapter is divided into three subsections. First, NASTRAN results are presented to investigate damping properties as a function of various treatment design parameters for isotropic and composite beams. Secondly, the moment predicted loss factor theory is examined for an isotropic beam with several sets of boundary conditions, (free/free, fixed/fixed, cantilever, and simply supported). Finally, experimental studies of damping extraction algorithms and model verification are presented. Within each subsection particular parameters are discussed and inter-study comparisons are made as appropriate.

6.1 Finite Element Analysis

Finite element analysis was performed using MSC/NASTRAN to investigate how several design parameters (constraining layer thickness; core layer thickness, boundary conditions, application location sensitivity) effected the damping treatment performance.

6.1.1 Multi-Point Constraints

The inclusion of Multi-Point Constraints (MPCs) in these models was required because of two difficulties with the models discussed in Chapter 3. Essentially these constraints were added to enforce that no relative lateral translation of the layers occurred and to properly couple the bending stiffness of the base and constraining layer.

The effect of these impressed multi-point constraints is illustrated in Figure 20. This case studied the effect of the relative thickness of the constraining layer (h_3/h_1) on the loss factor of a three layer beam with isotropic material (aluminum) outer layers and thin viscoelastic core (h_2/h_1 = .008). This analysis shows the effect of the in-plane rotational constraints (to assure element compatibility) and equal lateral

displacement constraints (to assure physically valid mode shapes), separately and combined compared to a beam with no multi-point constraints. The 'base' three-layer beam, or the beam with no multi-point constraints, shows a unrealistic discontinuity in response to increasing constraining layer thickness (from h_3/h_1 = .15 to .30). The addition of the lateral displacement constraint does not significantly alter the behavior but is required to assure realistic modes. When the rotational constraints are applied separately the response is continuous and well behaved, but to assure that the constraining layer did not pass through the base layer, the translational restraints were also applied.

6.1.2 Varying the Viscoelastic Core and Constraining Layer Thicknesses

The thickness of the viscoelastic core effects both the 'composite' (or effective three layer beam) damping and the natural frequency. Two limiting cases were investigated, the first case had a very thin foil constraining layer (h_3/h_1 = .08, h_3 = 10 mils (.0254 cm)). The second case involved a symmetric beam where both the constraining and the base layers are of equal thickness ($h_3 = h_1$). In both cases, the viscoelastic core thickness is varied while the constraining layer thickness is held constant. The boundary conditions for the composite beam structure were defined as free/free. The finite element model consisted of ten beam-type elements for the base and constraining layers and ten shear panels to model the viscoelastic core. The material properties for the three layers are defined in Appendix B.

The loss factor for these beams is related to the viscoelastic core thickness (damping tape, h_3/h_1 = .08, and symmetric beam $h_3/h_1 = 1$, L = 9 in., and width = .875 in configurations) as shown in Figure 21. The core thickness was normalized by dividing it by the total beam thickness ($h_2' = h_2/h_{total}$), where the total beam thickness is represented by h_{total}, ($h_{total} = h_1 + h_2 + h_3$). For mode 1, of a free/free beam, the loss factor, η_e, shows a strong increase for a thin central layer ($h_2 < .2h_{total}$) from .005 at $h_2' = 0$ to .05 at h_2'=.2 , with only a limited return (less than 30 % additional) for increasing the viscoelastic core thickness to that of

the base layer ($h_2 = h_1$). This clearly indicates that unless additional damping is critical to design, the weight and compliance penalty is not readily justified. For the second bending mode, of the same beam, the loss factor, η_c, shows significant increase from ,006 at $h_2 = 0$ to a level of .10 at normalized thickness (h_2/h_{total}) of .35 and little payoff after that.

For symmetric beams ($h_2/h_{total} \cong .50$), the maximum loss factor $\eta_{max} = .075$ occurs at the lowest normalized constrain layer thickness, (Figure 21). For the second mode the loss factor has a maximum of .155 at the lowest normalized core thickness and a final value of .065. This is due to the fact that the layer is at the geometric and stress mid-plane where shear is the highest. The additional material placed between the layers does increase the moment, but the damping layer is so compliant that shear is concentrated at the top and bottom interfaces as they move relative to the soft, fairly low shear gradient core, thus reducing the energy dissipation potential. The gradient is lowered through two mechanisms, one because the distance over which the net shear force acts is increased and this also increases the thickness in which it can be accommodated, and secondly it appears the core will have a higher shear gradient at the interfaces. This is evident if the symmetric beam is considered to be two separate beams on elastic foundations. Clearly, there would be less stress and relative shear between the base layer and a static foundation, than that of a equivalent beam that is moving synchronously in the opposite (longitudinal) direction.

The resonant frequency of vibration is inherently influenced by these changes in geometry and composite effective stiffness. For the cases of tape and symmetric beam applications (Figure 21), the resonant frequency is reduced with increased normalized viscoelastic core thickness. Resonant frequency is normalized by dividing it with the resonant frequency for the thinnest core beam ($h_2/h_1 = .004$) investigated ($\omega' = \omega/\omega_{thinnest}$). This implies that the stiffness increase gained by offsetting the two stiff layers is not as

great as the weight penalty and the decoupling nature of the treatment. The behavior of the first and second mode symmetric cases are similar in pattern with a large initial decline to .82 and .92, respectively, and then a gradual near linear decline to .75 and .86 . The tape applications show a slower near linear decline but the lower frequency mode is less effected than the second mode. The first tape mode goes from 1 to .85 while the second mode reaches a final value of .78. It should also be pointed out that the difference between normalized frequencies of the tape and symmetric beam configurations for the second mode is less than the first mode with opposite tendency. This shows that for certain configurations (between tape and symmetric) of the boundary conditions, there may be a point where the normalized frequencies for tape and symmetric may coalesce.

The effect of increasing the constraining layer thickness (h_3) while holding the viscoelastic core thickness constant (h_2/h_1 = .008) is seen in Figure 22. The composite loss factor shows a fairly consistent increase for both modes up to .08 for mode 1 and .14 for mode 2 at a normalized constraining layer thickness of h_3/h_{total} = .38. The slope of these curves is constantly decreasing with increased thickness. Mode 1 reaches 80 percent of total gain at h_3/h_{total} = .33 and mode 2 reaches 80 percent at h_3/h_{total} = .27 . Clearly illustrating that again a conservative application is more than satisfactory in most cases.

In the examination of the effect of increasing normalized constraining layer thickness, h_3/h_{total}, the normalized natural frequency, $\omega' = \omega/\omega_{(h3 = .01)}$, undergoes significant changes. For the first mode of a free/free beam the natural frequency shows a consistent, near second order, increase to 1.24 with increasing thickness of the constraining layer as in comparison with the linear relation of an isotropic beam (with the same thickness of stiff material). This illustrates that the first mode is more sensitive to the change for this level of viscoelastic layer thickness (h_2 = .08 h_1). The natural frequency never reaches the expected increase of a comparative isotropic beam , ω' = 1.5, (same thickness of stiff material) due to the de-

coupling of the two stiff layers by the viscoelastic. This de-coupling effect increases with increase in constraining layer thickness as the offset between the elastic center and the viscoelastic core center decrease. The second mode is even more strongly decoupled by the viscoelastic and attains a final ω' = 1.1 with an initial dip from h_3' = 1. to ,4 .

6.1.3 Boundary Conditions and Treatment Designs

Boundary conditions investigated here include free/free, clamped/clamped, and cantilever isotropic beams with viscoelastic central layers. The treatment designs investigated were applications either from clamped ends or from the center for the cases with symmetric boundary conditions. In addition to these studies, some specialized segmented treatments were also analyzed.

The effect of different boundary conditions on the potential total increase in loss factor ($\eta_{100} - \eta_0$) and the relation of added treatment to normalized gain is of considerable concern to the analyst. Total potential, or absolute loss factor, is the loss factor realized at 100 percent application length for a specific set of boundary conditions and mode. Normalized loss factor is the realized loss factor for a specific application treatment, mode, and boundary conditions less the inherent structural damping of the stiff material divided by the total potential increase loss factor of that mode. Defining η_0 as the inherent or no coverage structural loss factor, η' as the normalized loss factor, η_{100} as the loss factor for 100 percent coverage, and η_l as the loss factor for a specific application, then

$$\eta' = \frac{\eta_l - \eta_0}{\eta_{100} - \eta_0} \tag{6.1}$$

Both of these terms, total potential and normalized loss factors, are needed for thorough analysis of any treatment. The total potential gives a reference level for the treatment, to determine if the any treatment modification will provide sufficient energy dissipation or attenuation for a particular application. The

normalized term illustrates how much treatment is required and the best location to apply it on the beam. The boundary conditions effect both the total potential and normalized loss factors dramatically. The mode of interest and the treatment placement are also concerns of the analyst when investigating the different treatment applications.

The modes of vibration were studied for free/free and fixed/fixed (symmetric) and cantilever (asymmetric) boundary conditions. There were also two basic treatment schemes investigated, root-end application and center application.

Root-end application for the free/free and fixed/fixed boundary conditions cases involved applying treatment in equal length segments at each end of the beam and using the sum of two segments as the effective treatment length for comparison. For the cantilever beam, the root-end application lengths were measured from the fixed end out. For the cantilever and fixed/fixed cases with root-end application, the base and constraining layer endpoints were grounded or built-in. Center applications were only used with the free/free and fixed/fixed boundary conditions, as they could be readily compared as the converse of the root-end, with one segment treatment centered along the length of the beam.

For the root-end application (Figure 23), the maximum normalized loss factor for the cantilever mode exceeded all the others and in addition to having the rare property of exceeding one (1.0) (η'_{max}=1 .5). The curve has a low initial region followed by a sharp increase to its maximum value at 60 percent application and then it slopes down to the full coverage level. This is because the first mode cantilever has a peak moment at the fixed end and is constantly decreasing in magnitude over the length with a sharp decline at the free end. This results in low shear near the free end while, the weight penalty is constant, creating a lower rate of added damping per unit length or treatment efficiency. Because this efficiency is degraded so severely after the initial region of high moment we see a peak value present prior to complete

or 100 percent coverage. This single peak moment also is the cause for the cantilever having higher normalized damping at the beginning as this is the only place where there is sufficient moment to utilize the material to its potential. The fixed end case shows moderate increase to .6 until it reaches .9 treatment coverage percentage where it has a sharp increase to 1.0. at 100 percent coverage. This discontinuous behavior is more pronounced for the free end case where the loss factor does not exceed .2 until 100 percent coverage.

Note that the fixed/fixed and the free/free mode shapes have the unique property that the displacement for one is the moment function for the other (free/free displacement is the moment function for fixed/fixed). From observation of this property it is clear to understand that the fixed/fixed beam which has high moment at the ends (mode shapes of the free/free beam) is more effective with the root-end applications than the free/free cases.

Second mode root-end application (Figure 23), also demonstrates the same behavior as the first with respect to the fixed/fixed being consistently higher than the free/free case. It is important to note that the superiority is less dominant as the fixed/fixed application goes through a zero moment region soon after 40 percent application creating a plateau ($\eta' = .4$) in the relation. The free/free beam on the other hand goes through a constantly increasing moment until the mid-length but the beam has a very low moment at the root-end region. The cantilever curve also has a plateau ($\eta' = .25$) in its region of zero moment around 40 percent, attributable to the same treatment efficiency phenomena. Thus, for either cantilever or fixed/fixed beams, large increases of second mode damping can be gained in the 30 to 40 percent treatments or and the 50 percent to 70 percent treatments, respectively.

For the first mode center application (Figure 24) both the fixed/fixed and free/free have significant moments at the center and follow the same basic trend of consistent increase until the fixed gets near its zero moment

region and falls off (η' =.6 at A/L=.6). The fixed/fixed beam has a discontinuity in the response to increase treatments as it switches from one long segment which has no shear at the end to one where the ends are fixed and the moment is very high creating a large increase in damping. This phenomena is discontinuous in nature and occurs when the segment reaches the clamp end (treatment length = 100 %).

In the second mode of vibration, for the center application cases, again the free/free boundary condition is slightly better than the fixed end boundary condition. While both have zero moment at the center for second mode bending the moment is more evenly applied over the fixed beam. The curves again very similar and only differ in the last 25 percent of application percentage. The discontinuity in the fixed/fixed is not as severe in this case, due in part to the lower (relative) moment at the end and the fairly even nature of the moment curve.

Designed treatments are applications designed to damp out a particular mode or set of modes of vibration based on knowledge of the damping mechanism and its potential effectiveness. They are normally characterized by several short treatments placed over particular regions of a structure. In this investigation, treatment was placed in regions of high moment. These regions are highly effective because they induce large relative motion between the two stiff layers. It is this large relative motion which causes shearing in the core and hence increased damping in the structure as a whole. This is well supported by the preceding application studies performed on the three sets of boundary conditions and root-end versus center treatments. The effect of a moment on the section is dealt with in more detail in the next section (Moment Predicted Loss Factor).

The reasons for choosing regions of high moment are threefold. First, the dissipative nature of this treatment is governed by relative longitudinal displacement of the outer layers, which itself is directly related to the 'local' or differential moment on the section of the beam. Second, integration of the absolute

value of the moment over the body indicates the highest potential for damping (as shown by the slope of the change in potential damping per increase application length) is in these regions. (Further discussion on moment derivations are presented in section 6.2.) Finally, the initial finite element studies of the three boundary conditions and continuous treatment designs show the maximum damping gain per increase in application length generally in these regions, leading the analyst to predict that optimization, albeit crude here, is definitely possible. Based on these observations, treatments were designed for the three boundary conditions investigated here (cantilever, free/free and fixed/fixed).

Cantilever Segmented Treatment

The treatment designs, refer to Figure 28 and Figure 25 for the cantilever beam all used a total application length of 40 percent of the beam's length. The first application had two equal segments from .2L to .4L and from .6L to .8L measured from the clamped end, where L is the beam total beam length. The second treatment had one long segment from .1L to .5L, again measured from the clamped end. The third treatment had two unequal treatment lengths covering from the clamped end to .1L and the second from .4L to .7L. Again all treatments that begin or end at a clamped are restrained with the base layer from any motion.

All three designs (refer to Figure 31) were less effective than the root-end application coverage with the second design being the most effective of the three. The second design achieved the highest return (η_2 = .018) of 50 percent of the composite damping (40 percent of the added damping) of the equivalent continuous root-end coverage. The second mode showed that the first two designs(η_1 = .008 and η_2 = .010) were less effective than the third (η_3 = .016) and the root-end coverage (η_{root} = .0125) . The third design had 29 percent higher composite damping (55 percent higher added damping) than the clamped-end continuous segment of root-end application. The results show that the root-end application appears to be the superior for the first mode, as would be expected from a moment driven analysis,

(Figure 28) and the root-end while good is not the best design for higher modes as it places coverage at regions where the magnitude of moment is low or zero. Following this line of reasoning, the first treatment would seem to have potential for third mode application. Analysis for the specific case of 40 percent coverage root-end treatment this design has almost twice as much added damping (.00545 versus .00287) as the equivalent root end treatment.

Free Ends Segmented Treatment

Based on moment functions of free/free modes and displacements of fixed/fixed modes, it is clear that the center application would be the superior treatment for the first mode, therefore treatments were designed for the second mode (Figure 29 and Figure 26). Conversely, root-end applications would be the least efficient of designs for any mode, therefore treatment designs for second mode avoided placement in that region. For the second mode the moment has a low magnitude region in the center so treatment was restricted from there also. The two treatment designs both had two equal length segments offset from the ends. The first treatment had segment lengths of .2L and offset from one end equal to .2L. The second treatment had segment lengths of .3L and offset of .1L.

For the first mode both treatments ($\eta'_1 = .010$, $\eta'_2 = .013$) had less than one-third the added damping of the center application ($\eta'_{c40} = .018$, $\eta'_{c60} = .032$), though both were better than the root-end application ($\eta'_{r40} = .006$, $\eta'_{r60} = .006$) for the same amount of damping material, (Figure 33). For the second mode both treatments ($\eta'_1 = .0125$, $\eta'_2 = .021$) far exceeded the equivalent center application ($\eta'_{c40} = .008$, $\eta'_{c60} = .012$) by significant margins; treatment 1 had almost five times the added damping, while treatment 2 had more than two times the added damping. The root end application ($\eta'_{r40} = .0072$, $\eta'_{r60} = .009$) were inferior to the designed treatments and center treatments.

Fixed Ends Segmented Treatment

There were four designs investigated for the beam with fixed ends. The first treatment was the same design as the first cantilever with two short segments, of .2L length, offset from either end of the beam (Figure 26). The second treatment was also two equal length segments offset from either end, with length of .3L and offset of .1L. (Figure 27). The third treatment had four segments, two very short, .1L length, segments at each clamped end, and two longer, .2L, segments offset from the ends by .2L. The final treatment was designed with three segments, two very short, .1L length, at the clamped ends and one .2L treatment centered on the beam.

For the first mode, no treatment ($\eta'_1 = .007$, $\eta'_2 = .0075$, $\eta'_3 = .011$, $\eta'_4 = .012$) exceeded the root-end application design ($\eta'_{r40} = .014$, $\eta'_{r60} = .019$) (Figure 32). Only treatment 4 exceeded the center application design ($\eta'_{c40} = .0115$, $\eta'_{c60} = .017$) for equivalent amount of damping material. To better illustrate the sensitivity to placement of treatment, designs 1 and 4 have the same amount of damping material, but treatment 4 realizes increased loss factor of .0062 compared with .00093 or greater than six times as much. Another example of the location sensitivity is seen when comparing the designs of 2 and 3, which have equivalent damping material, treatment 3 produces five times the added damping of treatment 2. While 3 is far superior to 2, neither is as effective as either center or root-end applications for this mode, which has high moment at the end and moderate moment in the center, where these treatments have no coverage (Figure 30).

The second mode treatment interrelation ($\eta'_1 = .011$, $\eta'_2 = .015$, $\eta'_3 = .014$, $\eta'_4 = 09$) is almost totally the reverse of the first mode. Note that the moment for this mode is maximum at the ends and has a fairly long region of moderate magnitude from .15L to .4L from either side and nodes at the center and at .11L from either side. The worst performing, as expected based on the moment behavior, of the specialized treatments is treatment 4. This design is still better than the center application design where the material

is placed primarily in a region of low moment. Treatment 1, the other 40 percent application, is very effective and superior to even the root-end application by 35 percent added loss factor. The sixty percent segmented designs, 2 and 3, both exceed center and root-end applications. Treatment 3 in this case is not as effective as treatment 2, which has 13 percent more added damping. Indicating that there is more damping potential from .1L to .2L than from the clamped end to .1L region. Also since it takes some finite distance for the moment to be redistributed over the viscoelastic layer at the points of application the .1L length segments may not be experiencing the full expected moment.

A few summary points in designing treatment should be clear at this point. First, location is of primary importance in the application of constrain layer damping. This was shown by some treatments being six times more effective than there equivalent continuous treatments, or one-forth or less effective if poorly designed. The magnitude of the moment on a region appears to be strongly related to the effectiveness of a treatment. It can be easily seen that this is not true of displacement, where the root-end sees no displacement but high moment for clamped end conditions and for center application of the fixed beam where displacement is greatest but effectiveness is minimal. The slope is also not a good indication as the slope is also zero at fixed ends where effectiveness is high and in fixed/fixed modes where slope is high at about .15L from the ends but the effectiveness is low.

6.1.4 NASTRAN Composite Laminate Results

A composite laminate sandwich beam was modelled using two three-ply laminate composite plate elements to enclose a viscoelastic layer defined as a solid brick element (Figure 6). The laminae was defined using graphite epoxy material with varying ply angle orientation. The properties for the viscoelastic core (solid element) were determined based on modal testing and vendor supplied nomograms. The solid element was near the limit of an acceptable aspect ratios of 100, but refinement of the model, to lower aspect ratios, showed no significant (less than .1 %) change in frequency or damping. Each composite laminate had a

total thickness of .018 inch (.046 cm, or 3 layers at .006 inch) and the viscoelastic core and a thickness of .010 inch (.025 cm). The mechanical properties for the graphite/epoxy laminae and the viscoelastic material are presented in Appendix B.

To review, additive damping is that damping above the structural damping that is inherent in the stiff material. It can be readily described in absolute or relative (with respect to viscoelastic loss factor) terms. The resonant frequency is examined of a mode of free vibration and is normalized to the frequency at either 0 degrees or minimal thickness response, dependent on test variable.

Multi-point constraints were used to assure compatibility between the linear displacements elements (solid brick) and cubic displacement elements (composite plate). The central difference method was used to approximate the rotation at interface nodes. Restricting the two layers to equal lateral translation was not necessary in this case and was not included. (Testing with and with out this restriction revealed sufficient coupling of the lateral translation through the central layer.)

Laminae Ply Angle Effect

The basic model consisted of a stack-up [θ/-θ/θ/viscoelastic core/-θ/θ/-θ], where θ varied from 0 to 90 degrees in 10 degree increments. This was stacking sequence chosen to maximize shearing of the central layer. The beam was again modelled by two layers of quadrilateral shell elements (composite plates) sandwiching a row of solid brick elements (viscoelastic core) (Figure 6). The free/free boundary conditions were chosen to simplify the analysis comparisons. (Refer to Figure 34.)

The effect of ply angle on the resonant frequency is reasonably well predicted by Whitney's [38] method, which uses the (D_{11}^*) term for estimation of longitudinal bending stiffness of a composite beam,

neglecting the effect of structural damping on effective stiffness, (Figure 35). The D^* matrix is defined roughly as the reciprocal of the inverse bending matrix D. Whitney's model appears to be a lower bound for the Finite Element Analysis (FEA) method used here. By using the D_{11} term from Jones [39] as an estimate of the equivalent bending stiffness, and again neglecting the effect of structural damping on effective stiffness, the resonant frequency is overestimated significantly ($\approx$ 25 %) in the ply angle range of 30 to 60 degrees. The dominant ply angle effect is the contribution of fiber stiffness, a function of $\cos^4(\theta)$, to the equivalent stiffness. Since both closed form solutions [38,39] have the same terms at the end-points of this analysis (0 and 90 degrees) they agree exactly at those points. The first mode from the FEA study an small apparent overestimate of the resonant frequency in the lower ply angle orientations, this could be due to the restriction of analysis to lateral degrees of freedom which result in artificial cross ply stiffness and exclusion of longitudinal translation in direct computation. This same phenomena is exhibited to a smaller degree in the second mode case. This reduction can be expected because higher energy modes are more dependent on mass characteristics and less dependent on the structural stiffness.

The relation between ply angle, total mode strain energy, percent strain energy in viscoelastic elements, and composite loss factor is supported well by the modal strain energy (MSE) approach [24] as shown in Figure 36. First, the fraction of the total strain energy (from MSE theory) in the viscoelastic elements follows closely the additive composite damping in response to the changing ply angle. This relation is present in both modes of vibration. The first mode, which has higher damping, approaches its maximum much faster and then levels off, while the second is almost linear in its response. Both curves appear to be functions of sine of the ply angle to some order.

Viscoelastic Core Thickness Effect (Composite Laminate Beams)

The basic model stack-up for this analysis was [90/0/90/viscoelastic core/90/0/90] with .006 inch thick (.015 cm) thick laminae and varying viscoelastic thickness (.00125 to .030 inches, .0032 to 076 cm). The results are illustrated in Figure 37 and Figure 38. The beam was modelled with free/free and cantilever boundary conditions and with the vibrations calculated for flapping motion only.

Generally, the lower the resonant frequency of the mode, the higher the additive damping. All modes studied approach a maximum loss factor predicted by RKU [9], for this analysis the maximum value appears to be about .50. Also while the absolute values tend to differ from mode to mode, the trends appear to be independent of boundary conditions as DiTaranto and Blasingame stated [11]. Specifically, modes 1 and 2 of the free/free beam and mode 2 of the cantilever all have a seven to one ratio from h_2 = .00125 to h_2 = .030, while the first mode cantilever exhibits less relative growth since it approaches its asymptote earlier. The additive damping does not exhibit this close of a match due to the subtraction of the inherent structural damping in the laminae, though the trend is still present.

The effect of increasing viscoelastic layer thickness on the normalized resonant frequency requires somewhat more subtle inferences. Normalized resonant frequency is here defined as the ratio resonant frequency for a specific thickness divided by the resonant frequency for the thinnest application investigated (h_2 = .00125 inches) for the same mode. ($\omega' = \omega_{h_2}/\omega_{thinnest}$) The dominant characteristic appears to be that increasing energy level required for a mode shape negatively effects the resonant frequency for that mode. In other words, as cantilever modes 1 and 2 are lower energy modes (lower base frequency), the effect of increasing thickness on resonant frequency is positive. while somewhat less for the second mode (for mode 1 from 1 to 1.55 and for mode 2 from 1 to 1.15). Consistent with this trend, the first mode of the free/free case, about the same energy level as second cantilever, has a small increase (from 1 to 1.07).

While the effect of central layer thickness increases on the second mode of free/free beam is somewhat negative, (from 1 to .95) .

6.2 Moment Predicted Loss Factor

The shear based loss factor,η_V, was calculated for the cases of root-end application for the boundary conditions of free/free, fixed/fixed, and cantilever for modes 1 and 2 (Figure 41). (In all the cases studied except for the asymmetric cantilever mode shapes the function was modeled over only half of the beam and scaled appropriately.) The shear based loss factor has points of inflection later in response to increased treatment length (as would be expected from inspection of shear diagrams) and compares less favorably for trend prediction when compared with finite element analysis results (Figure 23). The moment predicted loss factor, η_M follows trends from previous FEA results much more closely than η_V. It may appear that this loss factor, η_M, is simply a the slope of the member, but it is the absolute value of the moment that is considered, realizing that positive and negative slopes have the same shear effect on the core layer. If the absolute value was not utilized the loss factor would cancel out positive and negative slope contributions and result in a zero net effect, an impractical result.

Root-end applications for the three symmetric cases, free/free, fixed/fixed, and simply supported, where modelled with treatment applied in equal length segments from either end and application length measured toward the center and summed over the two segments. For the cantilever case, root-end application was modelled from the fixed end to the free end with one segment. This was approach was taken to assure consistency between these tests, NASTRAN tests, and experimentation.

With the first mode results, refer to Figure 39, the same trends as the NASTRAN results (refer Figure 23) basically hold as previously discussed, but because the mass effects are not considered the graphs always have positive slope. The cantilever is still the most dissipative condition for the root-end, while the fixed is still superior to the free case. The simply supported boundary condition, which is symmetric with end conditions that are less 'stiff' than clamped but much more than the free case, has behavior correspondingly falling between the two. The damping potential for the fixed case shows significant increase for the low application percentage and a plateau similar to the NASTRAN results for the mid-range (zero moment) and then a second rise over the region where the magnitude of the moment is higher. The free case shows a slow gain over the low application (and low moment) area until the application reaches near the center where the moment is a maximum. The simply supported case, as its moment curve is a pure half cycle of a sine wave and has peak moment at the center, had slightly higher damping potential than the free case.

For the second mode the curves again followed the same basic trends as the NASTRAN results (Figure 23) with the addition of the case of simply supported boundary conditions. The asymmetric case of cantilever has levels off in the region of low moment (15-25%) and a second rise area follows till 80% and then it levels off again. The fixed/fixed case has a flat region also in an area of low moment (20-35%) where the corresponding node of the complementary free/free displacement mode shape exists (recall this is equivalent to the moment of fixed/fixed boundary conditions). As with the first mode the free/free and simply supported boundary conditions show consistent increases once an initial dead region is passed (0-15%), this is interesting in the moment has a peak around 50% for both cases, which corresponds to the highest slope of the curves. Also, as with the previous mode, the fixed mode damping is greater than the free and simply supported cases up till about 70% where they are nearly equivalent. It should noted that for a limited region (15-30%) the fixed case is greater than the cantilever as the nodes for the fixed case moment is farther out and takes effect later.

For the first mode of vibration, the center application of the free/free beam was the most efficient over the whole range since its moment is sharply peaked at the center (Figure 40). Simply supported is next in treatment efficiency with its moment peaked at the center also but more mildly. The fixed case is the least effective in a normalized sense over the range since it has three peaks (one at each end and one at the middle) in its moment function and is therefore more linear, though a plateau is observed at the 50-70% range where the moment is a minimum.

For the second mode of the center application scheme the free/free is still the most effective but it has a dead region again from 0 - 10% and is fairly linear 20 - 80% range. The simply supported is again slightly less efficient free but follows the same trends. The fixed case is more effective than the simply supported case for the range of 0 - 60% as the moment higher for the initial 20 % from either end for the that case.

When evaluating treatment design from these curves it is important to note two main concerns, first there is no adjustment made for treatment stiffness and mass. Secondly, these can only readily be compared with normalized added treatment effectiveness and not with an absolute measure since this damping effectiveness is based on the mode's damping potential being divided into the composite damping. From initial results it appears that a good scale facto,r α, to compare similar modes that occur at different frequencies (free/free and simply supported first mode) is the ratio of the square of natural frequencies of the modes, though this is strictly an empirical observation. For the fixed and free cases these results compare very well with NASTRAN results illustrating that weight penalty for tape applications is not severe. The cantilever had a larger discrepancy for the first mode from the FEA results than the second mode as the region at the end experienced lower stress, hence less effective. An excellent use of this model is the application of damping material in more complex structures where experimentation and other closed form theories can not be readily applied.

6.3 Experimental Results

Experimental results are presented for the first and second bending modes of fixed/fixed and cantilever beams. The effect of treatment application length versus composite effective structural damping is analyzed for the conditions root-end application only. The variability of different damping extraction methods are compared and evaluated. The isotropic beam dimensions for both cantilever and fixed/fixed boundary conditions where; (Figure 1, Figure 9, and Figure 8) length (L) = 9.00 in., width=.875 in., base layer thickness (h_1) = .125 in., core thickness (h_2) = .005 in., and constraining layer thickness (h_3) = .010 in.. For all test points of the aluminum beams an ensemble of 3 tests consisting of 5 averages was performed to reduce experimental error as much as feasible. For the composite beams the beams where tested at several locations and the most noise free cases where utilized.

6.3.1 Cantilever Bending

For the cantilever beam, treatment was applied in one segment from the clamped or root-end. The application percentage is the treatment length, l_t, divided by the beam length, L.

For the first mode, all methods of extraction showed a maximum loss factor at about 50 percent application length (varying between .026 and .030) . (Figure 42) The two direct Frequency Response Function (FRF) methods, noted as Real and Imaginary Function, use the two components of the FRF respectively to determine damping. These two estimation methods agree quite well with each other throughout the experimental analysis. Han and Wick's curve fit procedure [30], agrees quite well with the direct FRF methods though it varies from an upper to a lower bound. The circle fit method [28] appears erratic for this case indicating that data transfer may have been corrupted. (This is probably a predominant reason

since it worked satisfactorily on other applications.) The log decrement method agrees well, with the frequency domain techniques, for this case and has a slightly higher peak (.0305 vs. .030). .

In the second mode bending analysis, the response of damping per added treatment has a plateau, $\eta \approx .016$, in the 30 to 50 percent range where the magnitude of bending moment is low. Outside this plateau, the response is fairly linear with a somewhat higher slope in the lower application region reaching $\eta \approx .044$ at 100 percent coverage. All four methods used in this case agreed well in estimation of damping up to 75 percent. At the case of complete coverage the Real FRF method is significantly below the others (.35 versus .44).

NASTRAN results follow the same trends as experimental results for the first mode, refer to Figure 43, but have less damping at low application percentage cases. This is probably due joint compliance resulting in unaccounted for dissipation. NASTRAN also overestimates for higher application cases indicating possible error in viscoelastic material property estimation. For the second mode, again the trends agree with plateaus and high slope regions in the same ranges. It seems likely that joint compliance again corrupted the experimental estimation of damping in the low application regions. The finite element model is slightly lower for all cases, except zero coverage, indicating that a moderate underestimate of dissipation characteristics of the viscoelastic.

6.3.2 Fixed/Fixed Bending

For the fixed/fixed beam, treatment was applied in two equal length segments $l/2$ from the clamped ends. The application percentage is the total treatment length divided by the beam length L.

For the first mode of fixed/fixed bending, the different estimation methods agree reasonably well. (Figure 44) They show a nearly linear behavior up to 50 percent application length (η_{50} = .022), with a degradation of return, lower slope, from 50 to 100 percent (η_{100} = .030).

The second mode shows no significant change in damping from 0 to 25 percent. From 25 to 100 percent behavior is roughly linear (η_{25} = .005, η_{100} = .036). There is significant discrepancy between the two fitting algorithms at 50 percent application where circle fit is approximately half the curve fit method (.009 to.017). These methods in general have been less consistent than the direct FRF methods and appear to bound the estimate of damping.

The first mode with NASTRAN generated results illustrate similar characteristics as the cantilever second mode, (Figure 45) Specifically, the experimental trends similar with the finite element results, which moderately (approximately 30 percent) underestimates the damping.

The second mode of NASTRAN appears to be a poor representation of the experimental specimen. This is partly due to an underestimate of the viscoelastic beam properties and joint compliance. Recall the same shear modulus and loss factor was used in all NASTRAN models, as earlier analysis showed was appropriate. The factors where consistently less than the manufacture specifications but were the best estimate based on comparison between initial experimental and finite element work. This correlation may have been in error, but since trends in general agree it appears that analysis was in a near-linear region of the loss factor to central layer properties. This near-linearity may not be valid for the high frequency case of fixed second bending mode. It should be noted that if a analytical model has damping estimates error of approximately 50 percent it is often considered acceptable, and if the error is less than 20 percent it is considered the model is considered very good.

6.3.3 Laminate Beams

In the experimental analysis of laminated composite beams, a graphite/epoxy 3-ply (90/0/90 stack-up) laminate was employed as the primary or 'base' beam structure. All beams tested were 10.25 inches long, 1.00 inches wide, and all graphite/epoxy plies were 6 mils thick and were tested in a cantilever configuration. The mechanical properties of the graphite/epoxy laminae are in Appendix B. The beams where tested using an eddy current probe and analyzed with the log decrement method (refer Chapter 4). The first test beam, Beam 1 (Figure 46), was the base 3-ply laminate. This test quantified the inherent loss factor and bending stiffness of the 'base' structure. The recorded loss factor, η_c, was .020 and the resonant first mode frequency ω_r was 2.78 Hz (Hz = cycles/s).

The second test beam, Beam 2 (Figure 46), was constructed by sandwiching a polypropylene core (10 mils thick (.0254 cm)) with two of the 3-ply laminates. This test was designed to determine the change in bending stiffness and loss factor for the seven layer construction to follow. The theory was that the polypropylene function as a spacer without adding significant damping and offsetting the outer layers. This test resulted in recorded loss factor, η_c, of .009 and resonant first mode frequency, ω_r, of 15.4 Hz.

The next test beam, Beam 3 (Figure 47), consisted of two 3-ply laminates sandwiching a viscoelastic core (10 mils thick (.0254 cm)). This test showed dramatic increase in the loss factor, η_c, from the polypropylene case (.009 to .300) and a significant decrease in resonant frequency, ω_r, (15.4 Hz to 10.4 Hz). This shift in loss factor and frequency indicated that there was a de-coupling of the two layers stiffness's and a large amount of relative slip in the core layer.

The last beam studied, Beam 4 (Figure 47), was constructed to model a more complex aerospace member. This laminate had a 15-ply stack up as follows;

[90/0/90]
10 mils ISD-112
[90/0/90]
10 mils polypropylene
[90/0/90]
10 mils ISD-112
[90/0/90]

with a total thickness of .174 inches. This specimen illustrates the application of viscoelastic in a more sophisticated design by sandwiching two of Beam 3 stack-ups around a polypropylene core. The resulting structure which had a loss factor, η_c, of .274 and first mode resonant frequency, ω_r, of 20.79 Hz.

These tests of laminate beams indicate that incorporation of a viscoelastic layer, possibly replacing one of the plies, can be employed to significantly increase the damping present. The major penalty is not weight but bending stiffness, the viscoelastic layer decouples the stiffness of the adjoining plies dramatically.

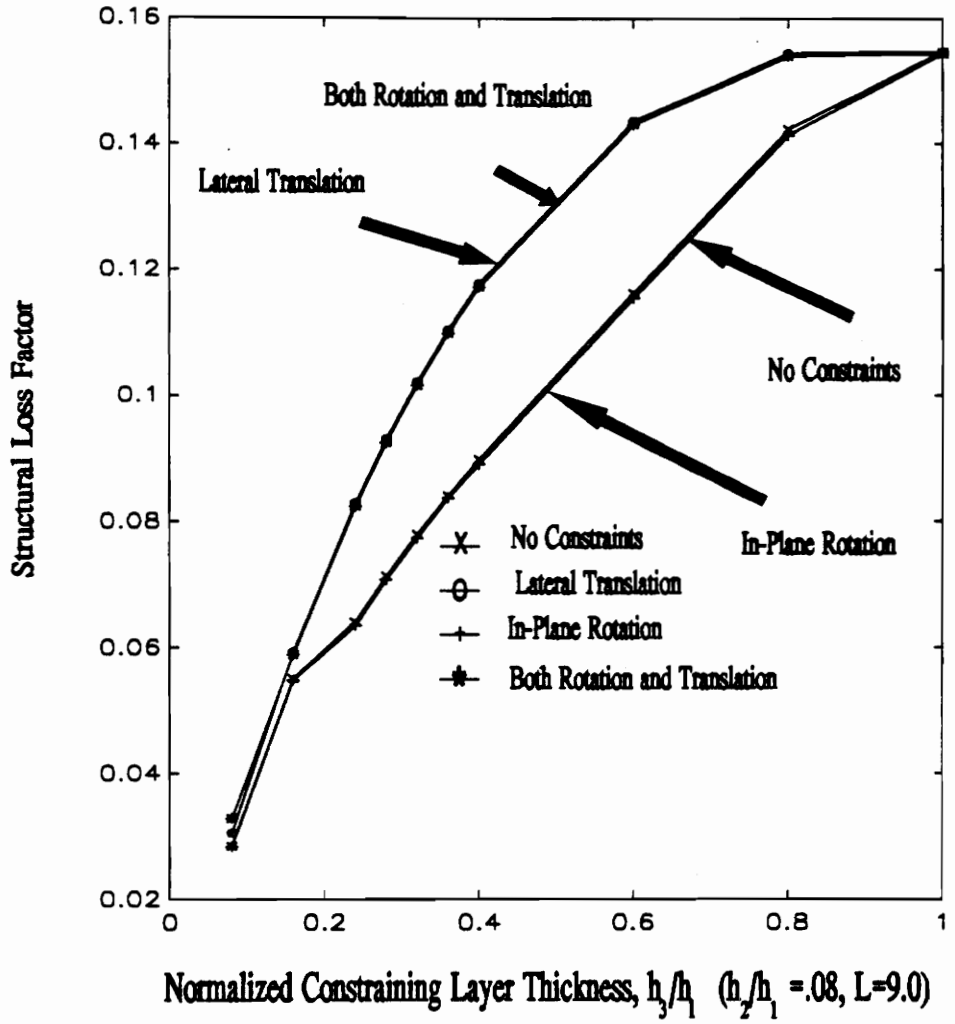

Figure 20. Effect of Multi-point Constraints in Estimation of Loss Factor: MSC/NASTRAN Translational and Rotational Constraints

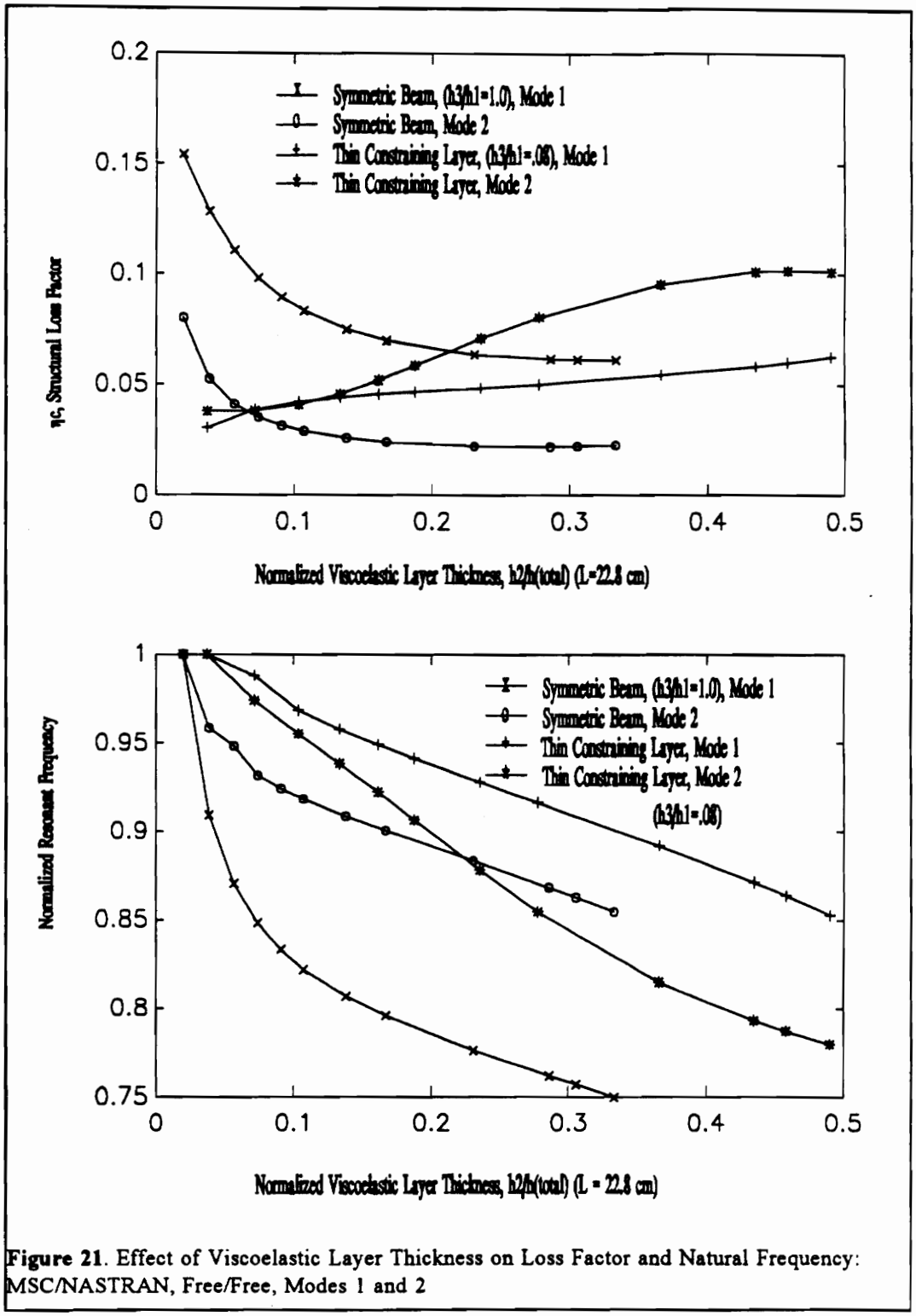

Figure 21. Effect of Viscoelastic Layer Thickness on Loss Factor and Natural Frequency: MSC/NASTRAN, Free/Free, Modes 1 and 2

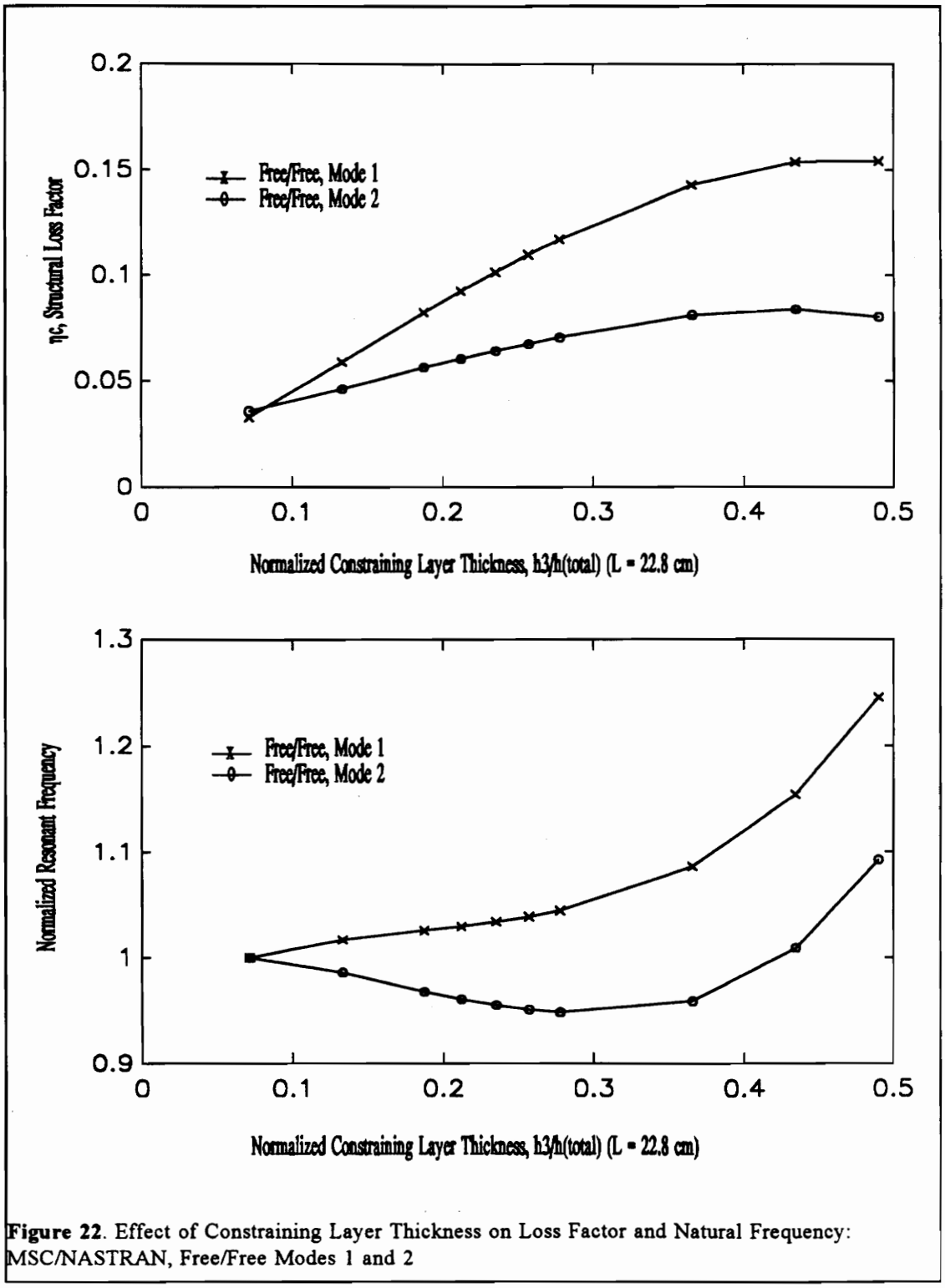

Figure 22. Effect of Constraining Layer Thickness on Loss Factor and Natural Frequency: MSC/NASTRAN, Free/Free Modes 1 and 2

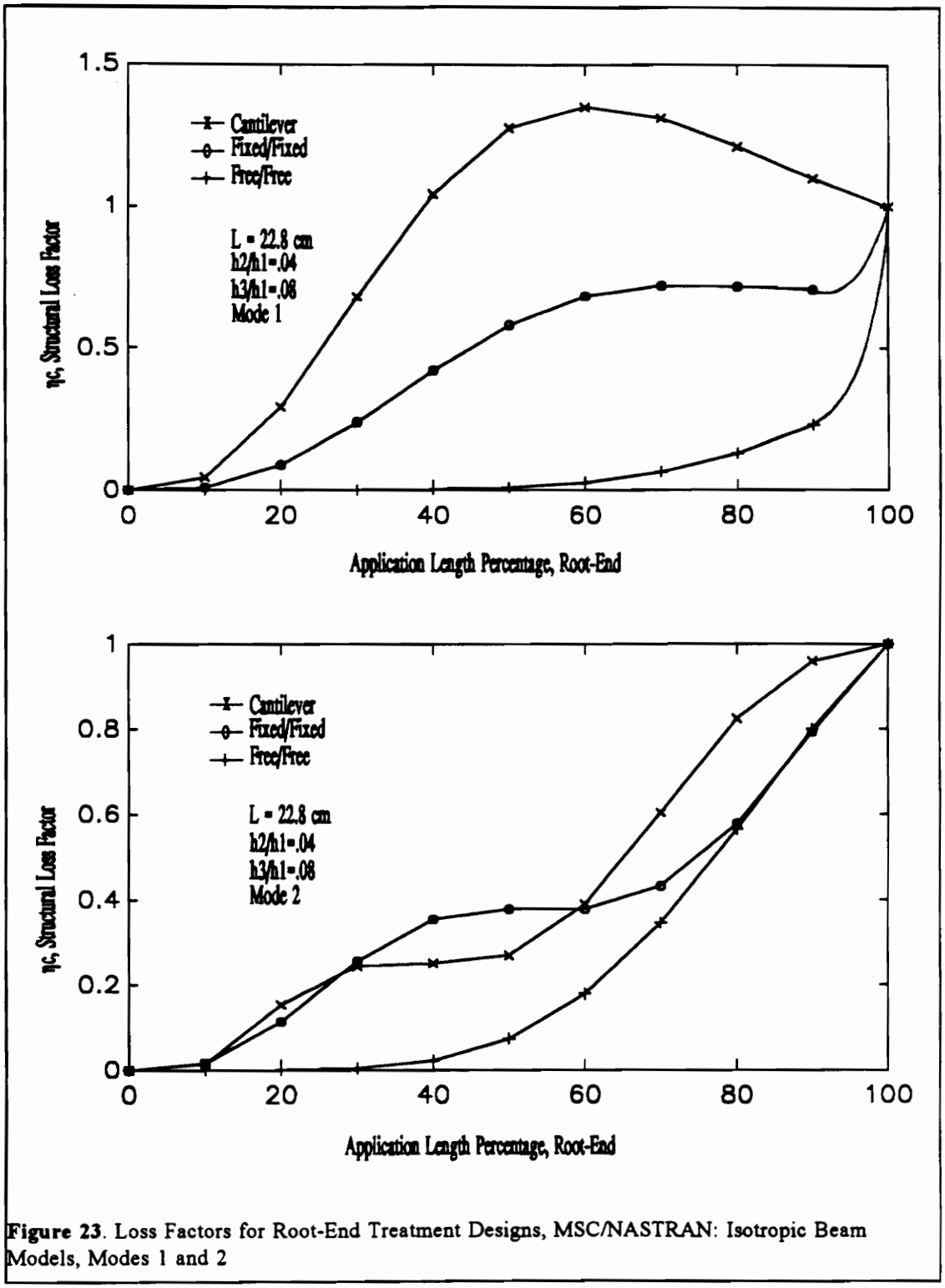

Figure 23. Loss Factors for Root-End Treatment Designs, MSC/NASTRAN: Isotropic Beam Models, Modes 1 and 2

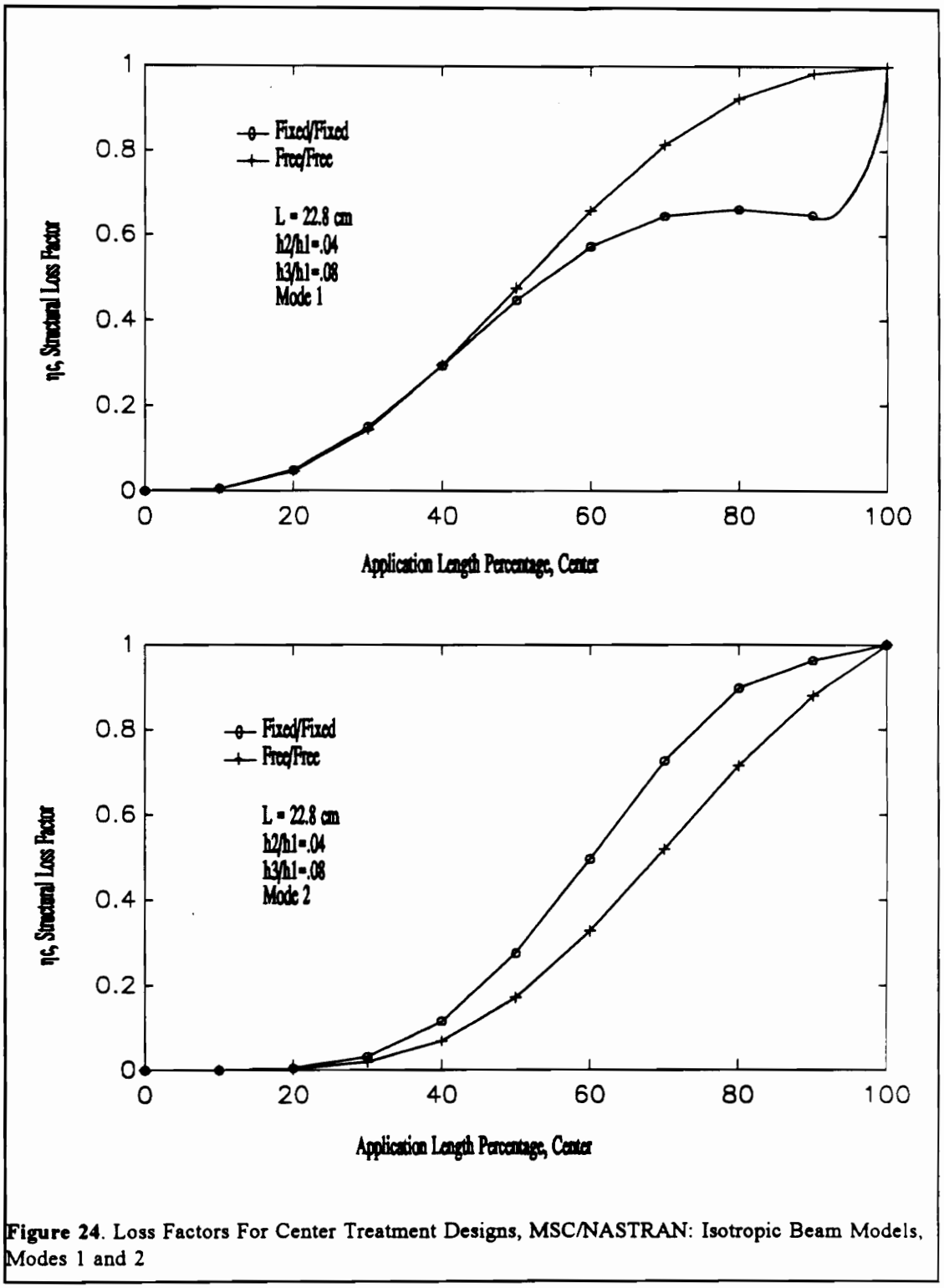

Figure 24. Loss Factors For Center Treatment Designs, MSC/NASTRAN: Isotropic Beam Models, Modes 1 and 2

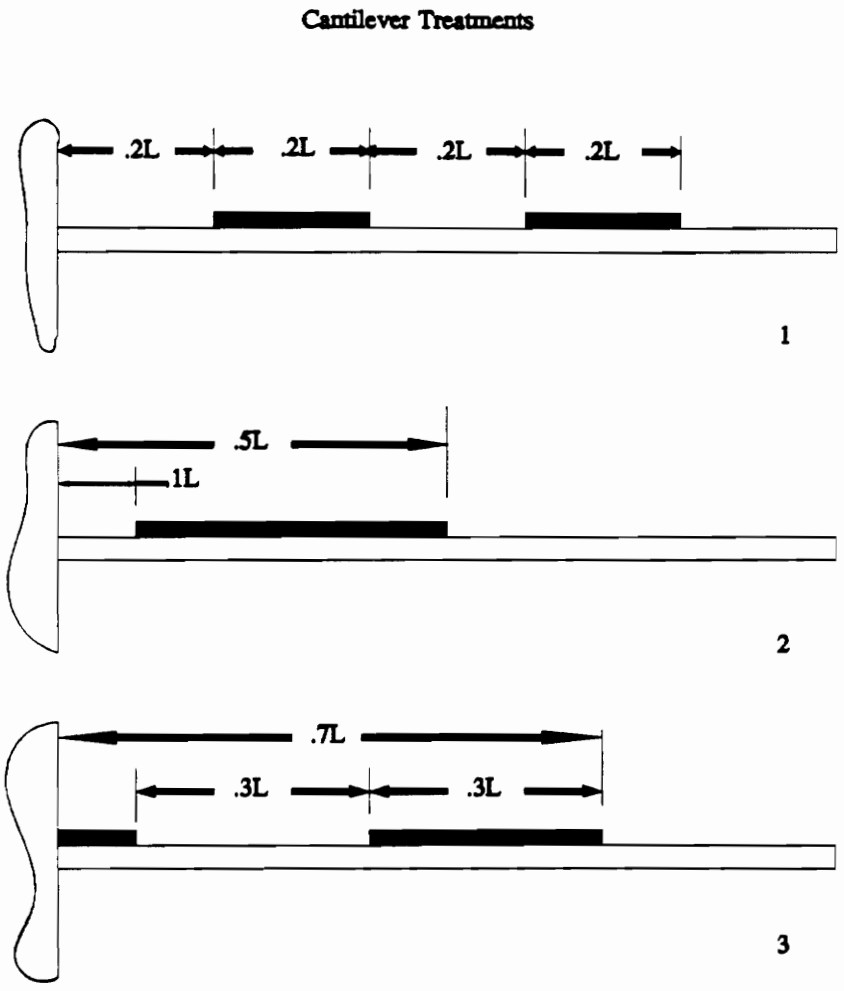

Figure 25. Cantilever Beam Segmented Treatment Designs

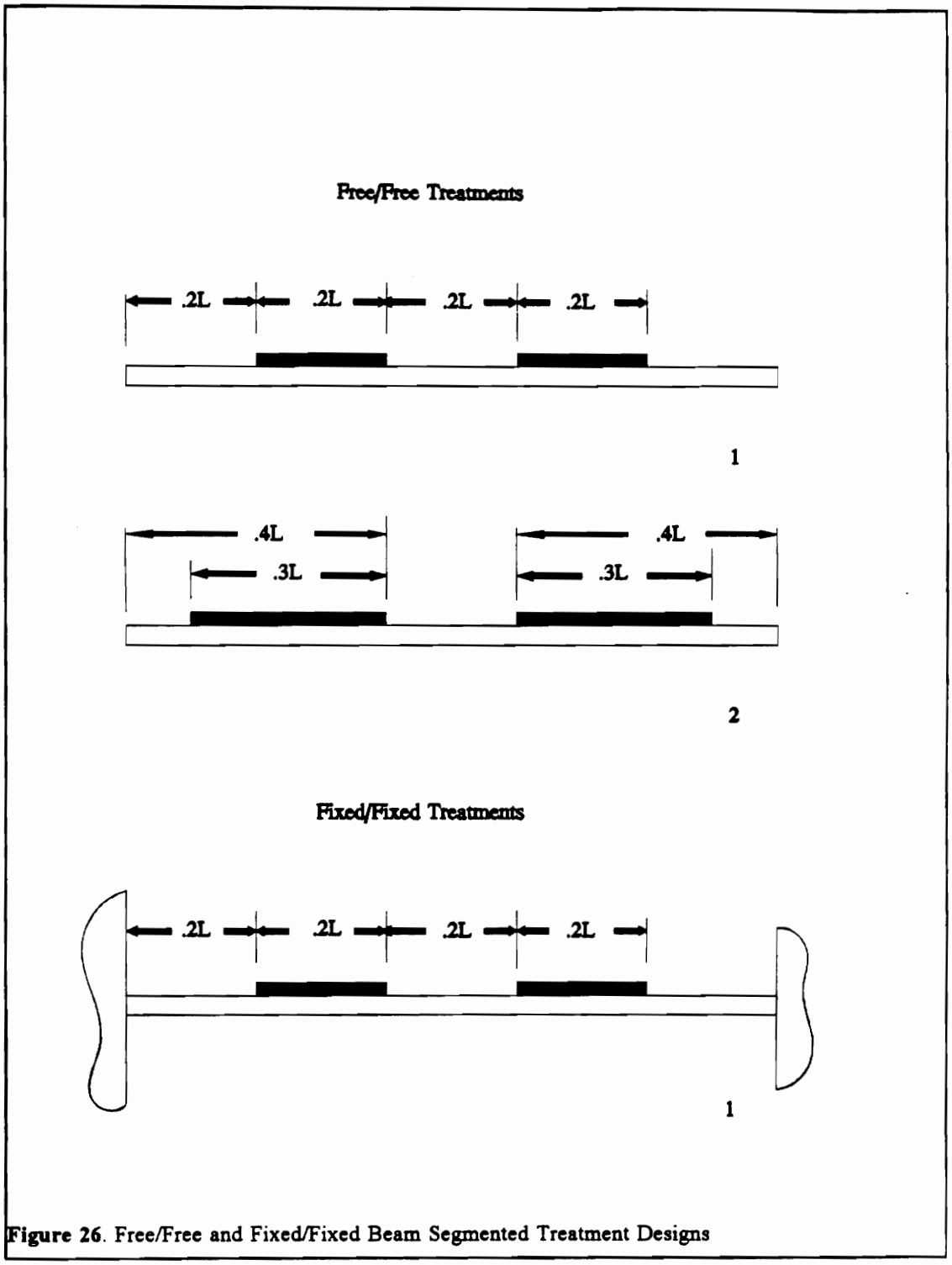

Figure 26. Free/Free and Fixed/Fixed Beam Segmented Treatment Designs

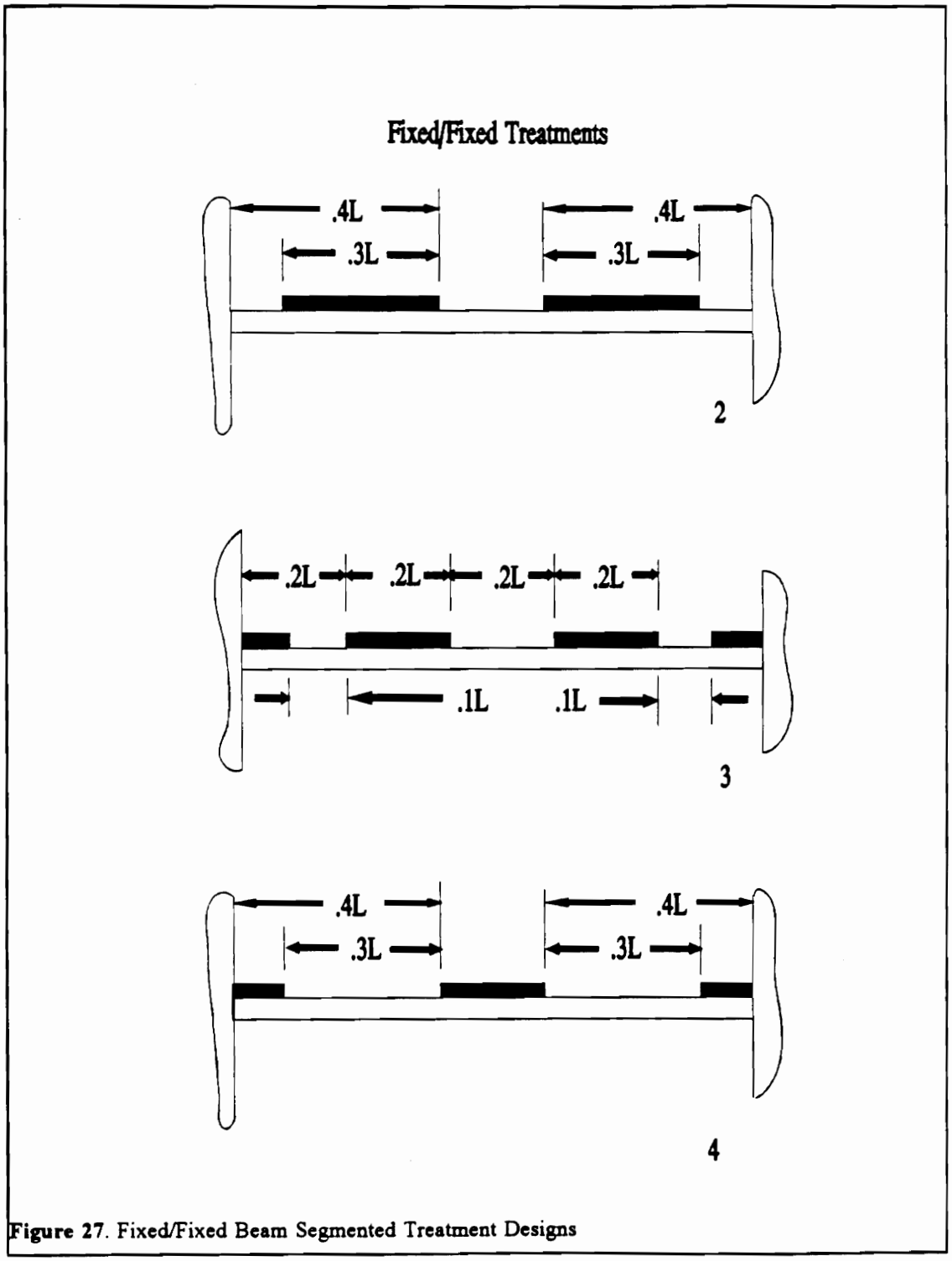

Figure 27. Fixed/Fixed Beam Segmented Treatment Designs

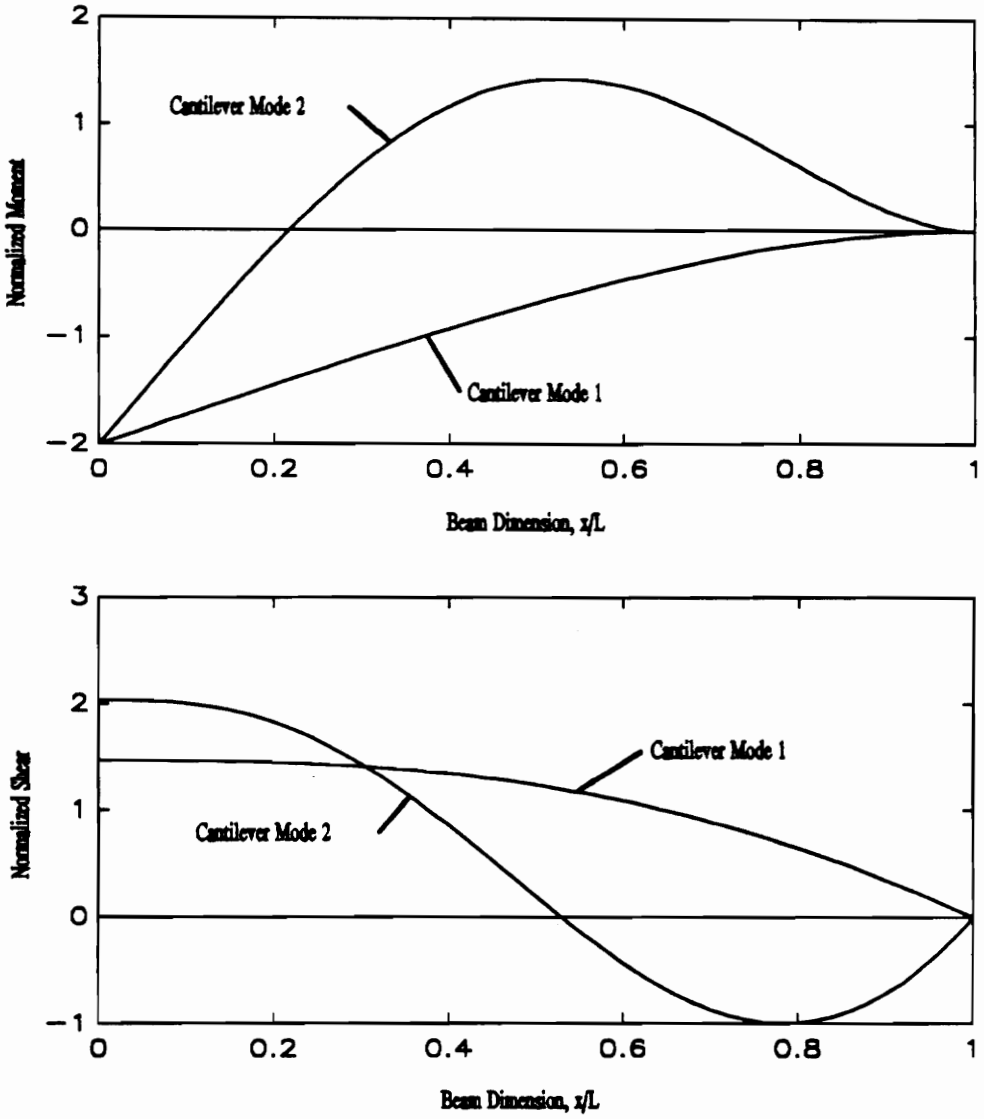

Figure 28. Cantilever Beam Moment and Shear Diagrams, Modes 1 and 2

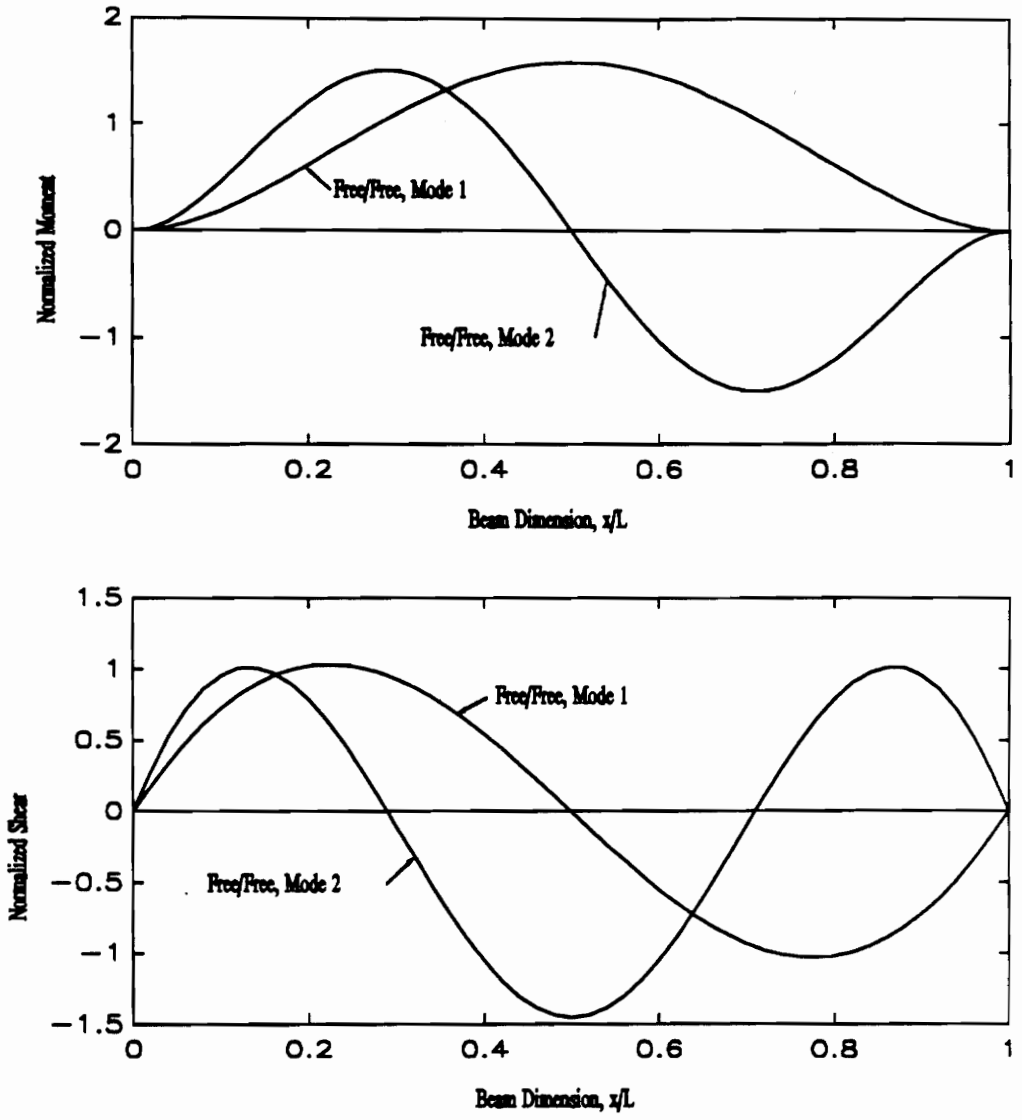

Figure 29. Free/Free Beam Moment and Shear Diagrams, Modes 1 and 2

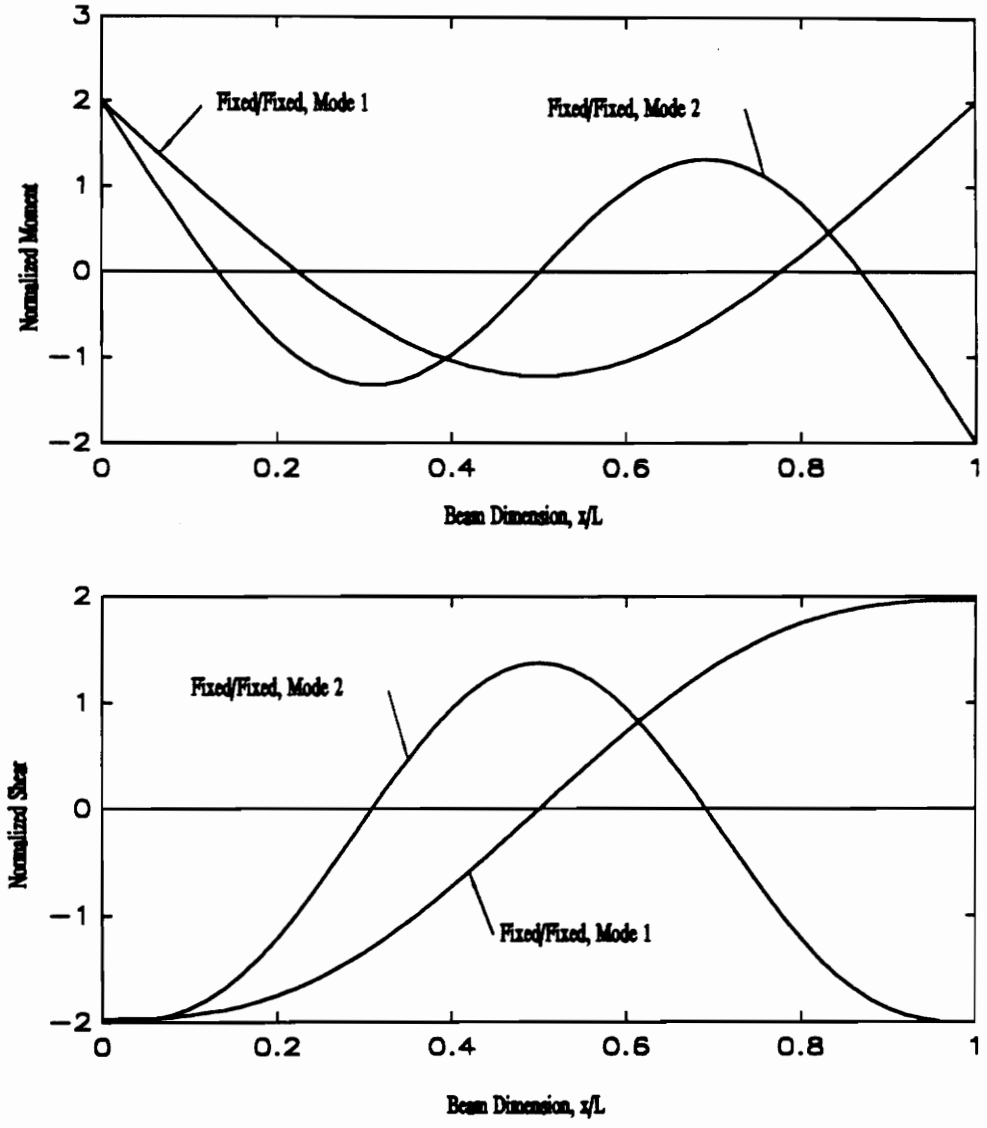

Figure 30. Fixed/Fixed Beam Moment and Shear Diagrams, Modes 1 and 2

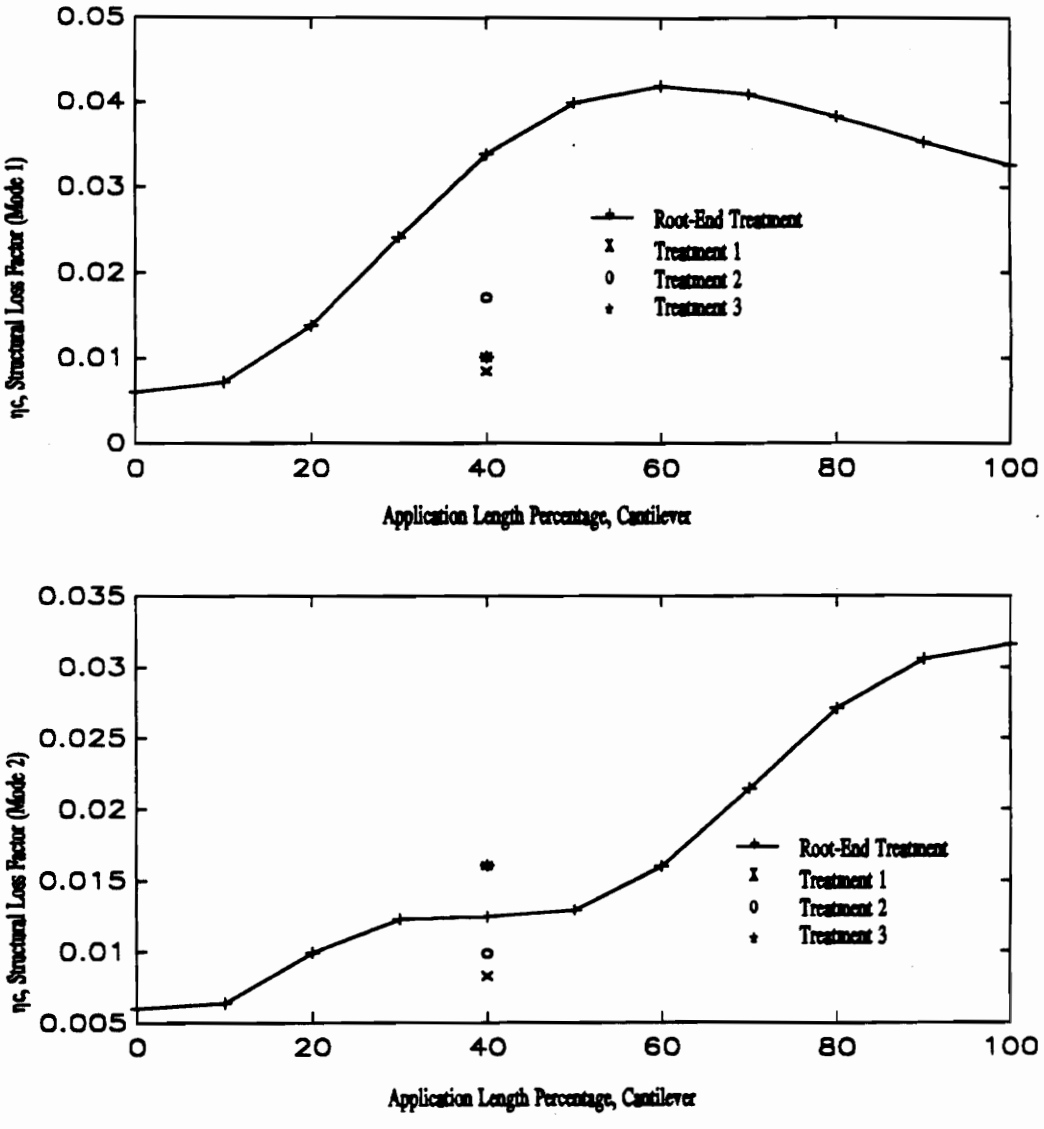

Figure 31. Comparison of Designed Treatments versus Root-End Application, Cantilever Modes 1 and 2, MSC/NASTRAN

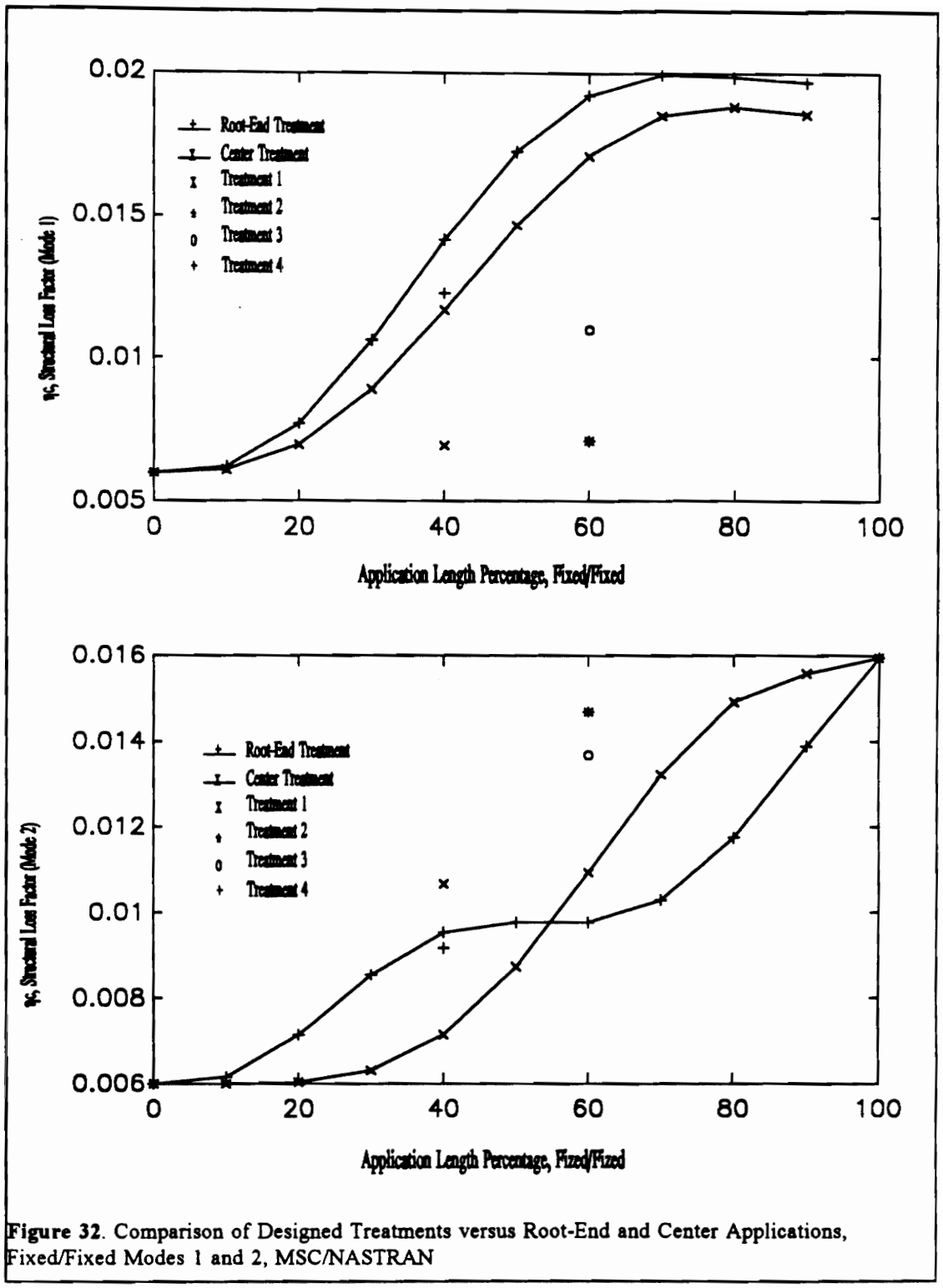

Figure 32. Comparison of Designed Treatments versus Root-End and Center Applications, Fixed/Fixed Modes 1 and 2, MSC/NASTRAN

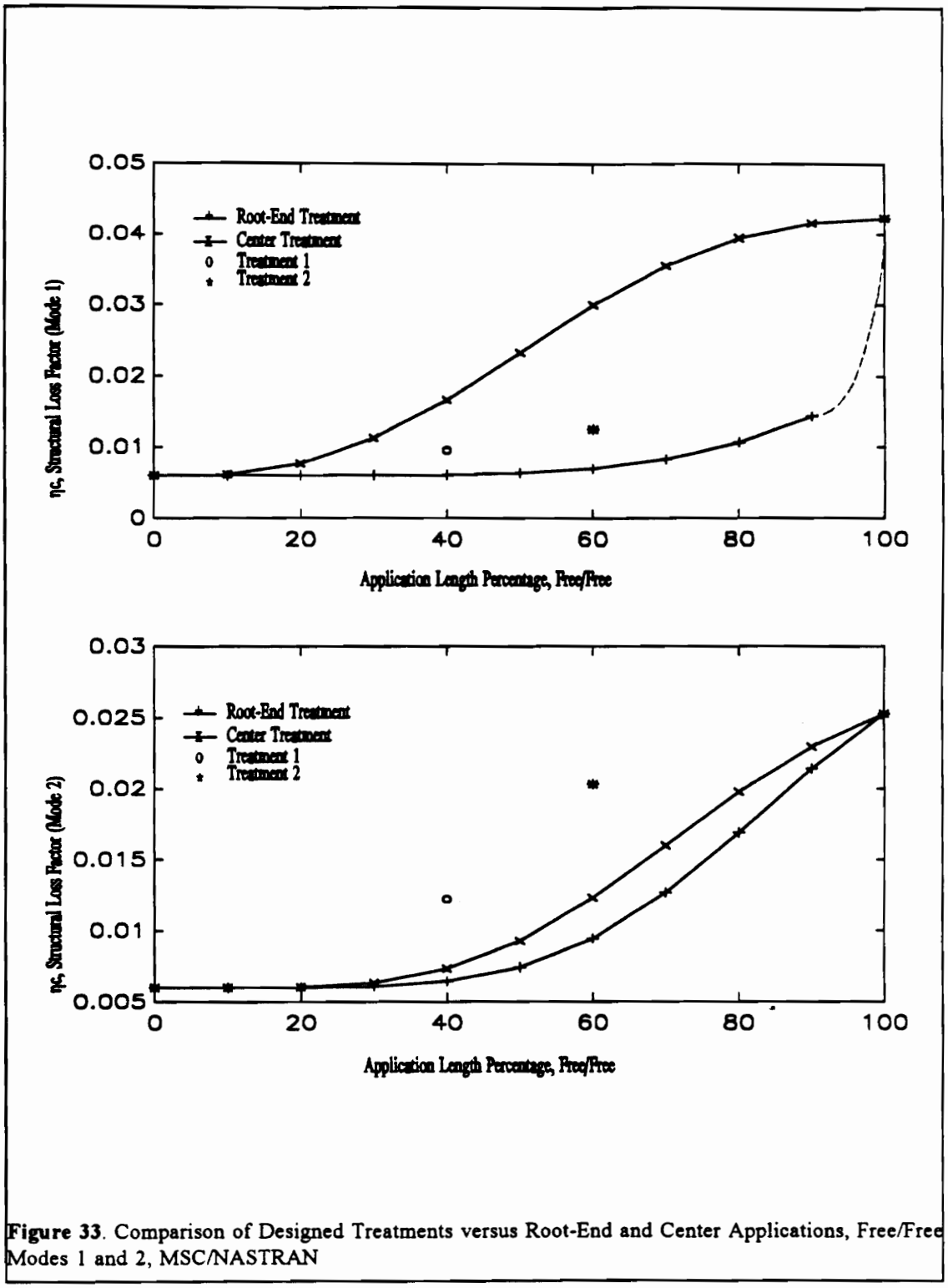

Figure 33. Comparison of Designed Treatments versus Root-End and Center Applications, Free/Free Modes 1 and 2, MSC/NASTRAN

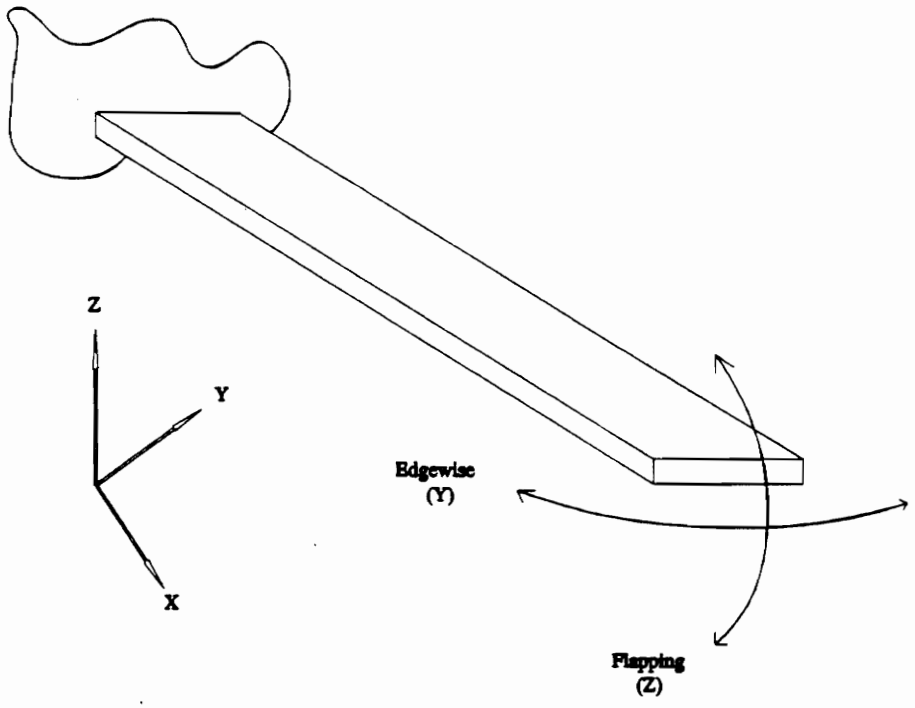

Figure 34. Flexural Motion of a Cantilever Beam

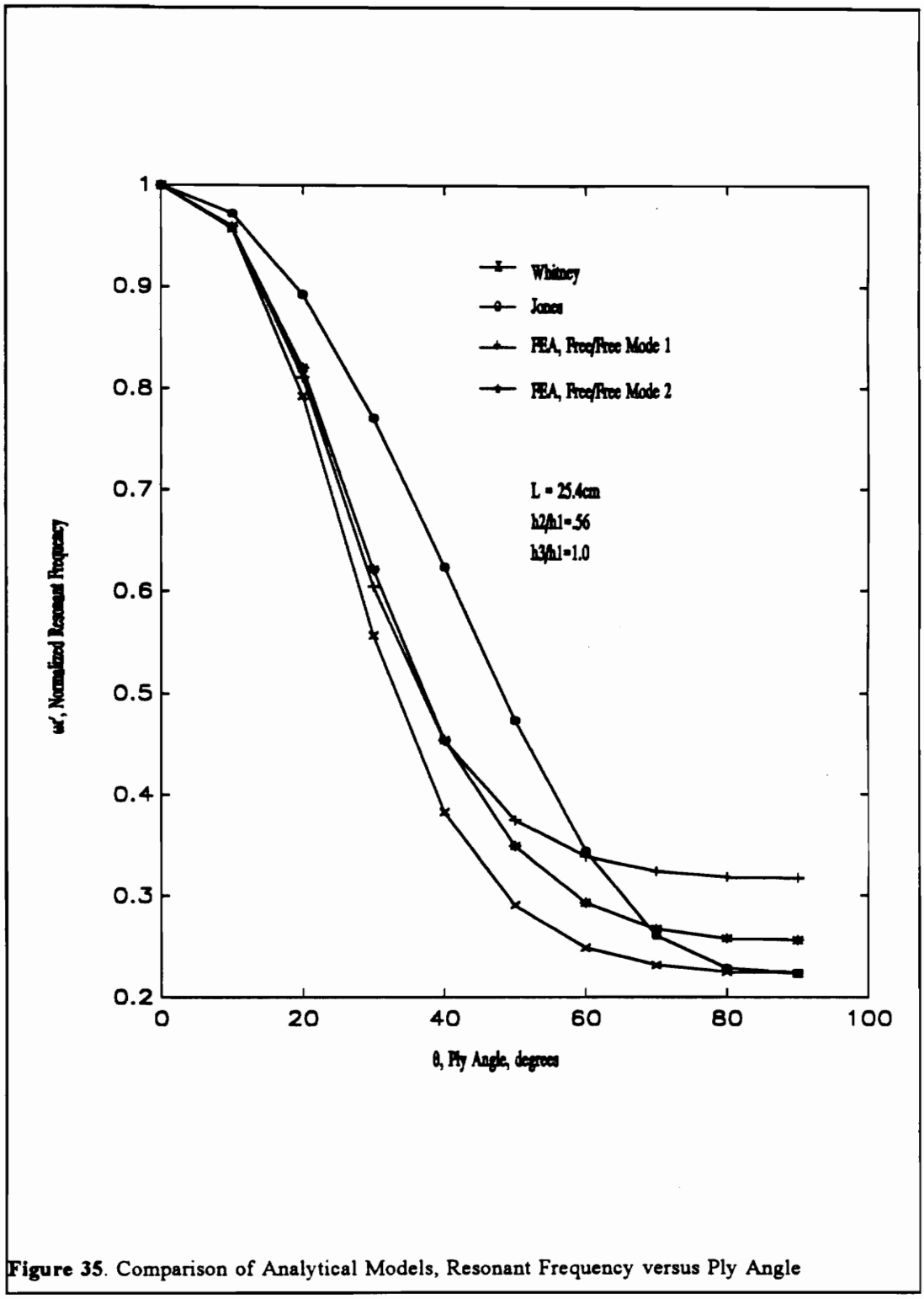

Figure 35. Comparison of Analytical Models, Resonant Frequency versus Ply Angle

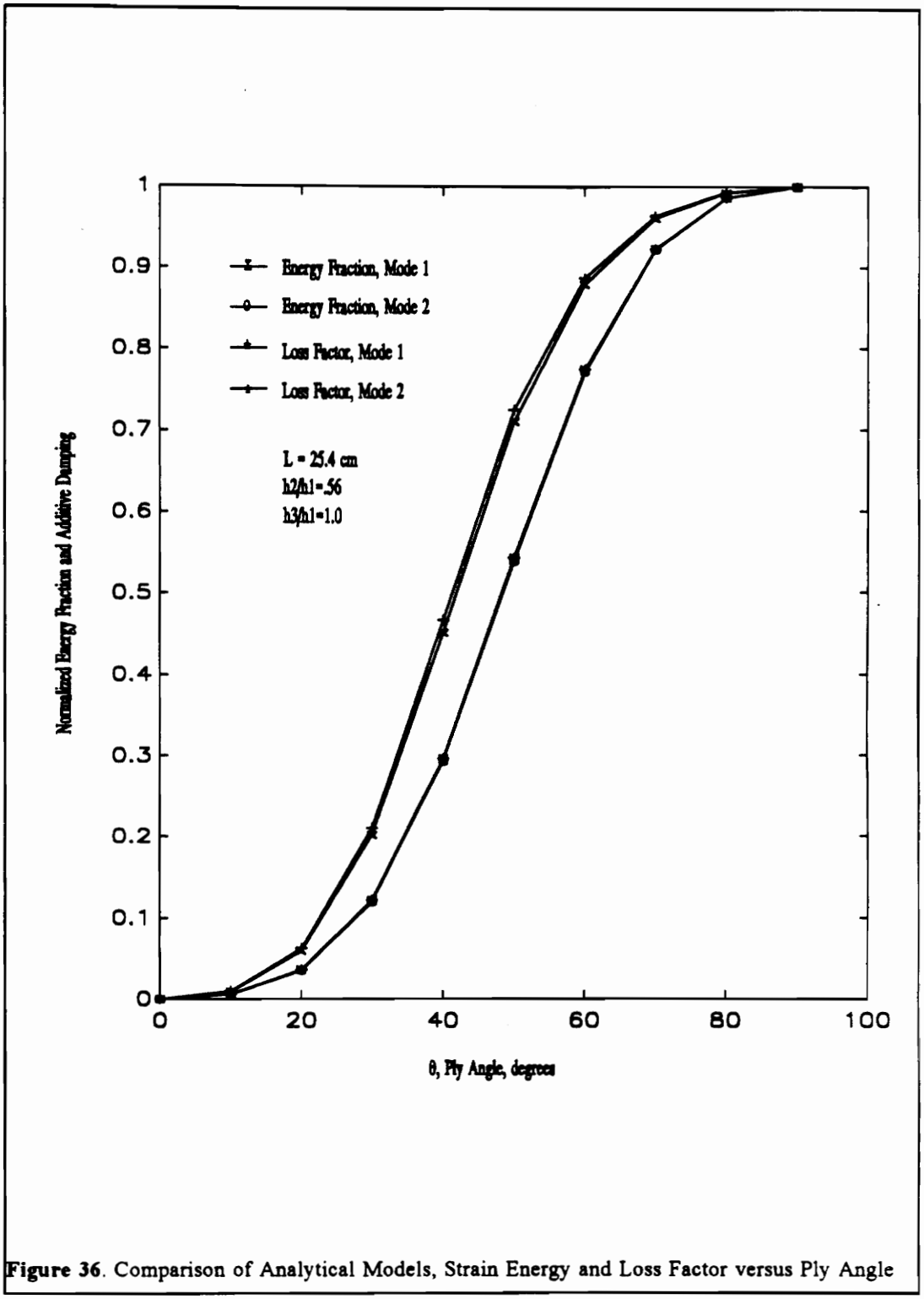

Figure 36. Comparison of Analytical Models, Strain Energy and Loss Factor versus Ply Angle

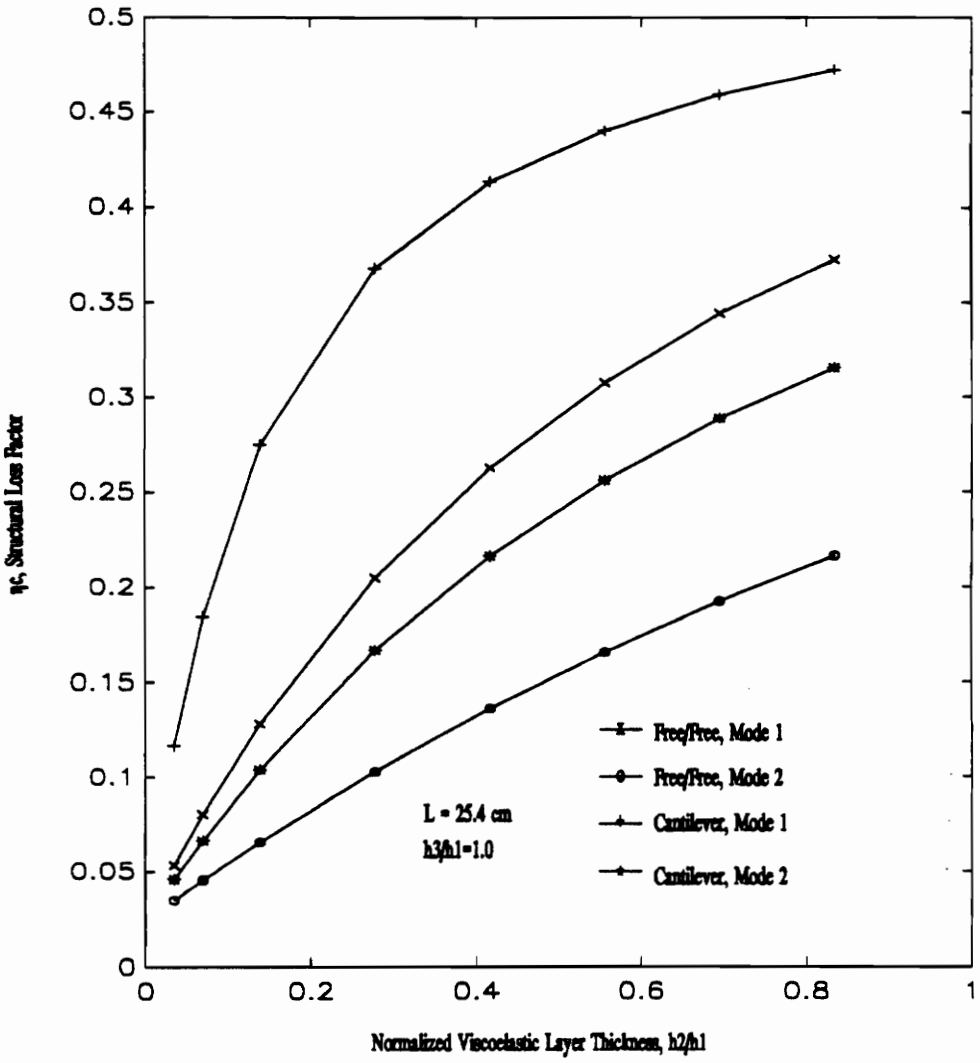

Figure 37. Loss Factor versus Viscoelastic Thickness, Cantilever and Free/Free, Laminate Beams, MSC/NASTRAN

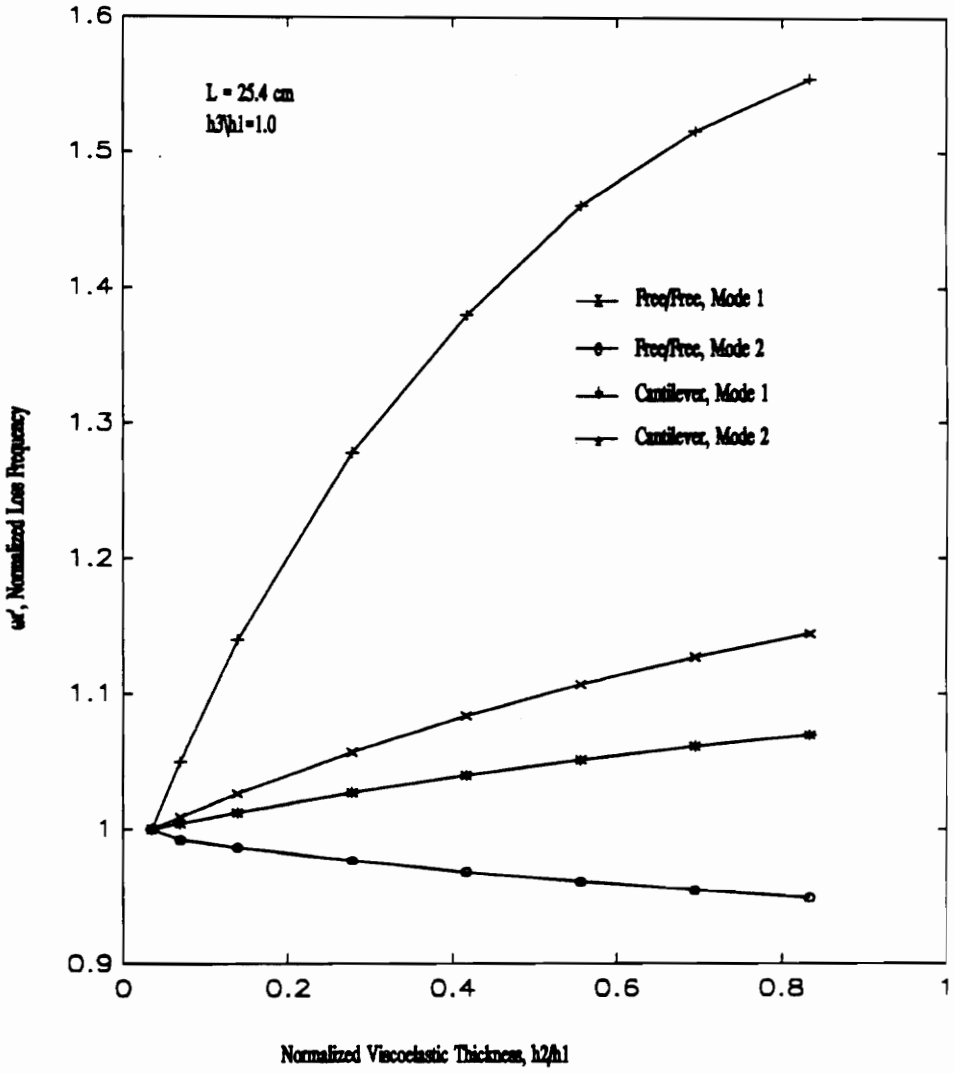

Figure 38. Resonant Frequency versus Viscoelastic Thickness, Cantilever and Free/Free, Laminate Beams, MSC/NASTRAN

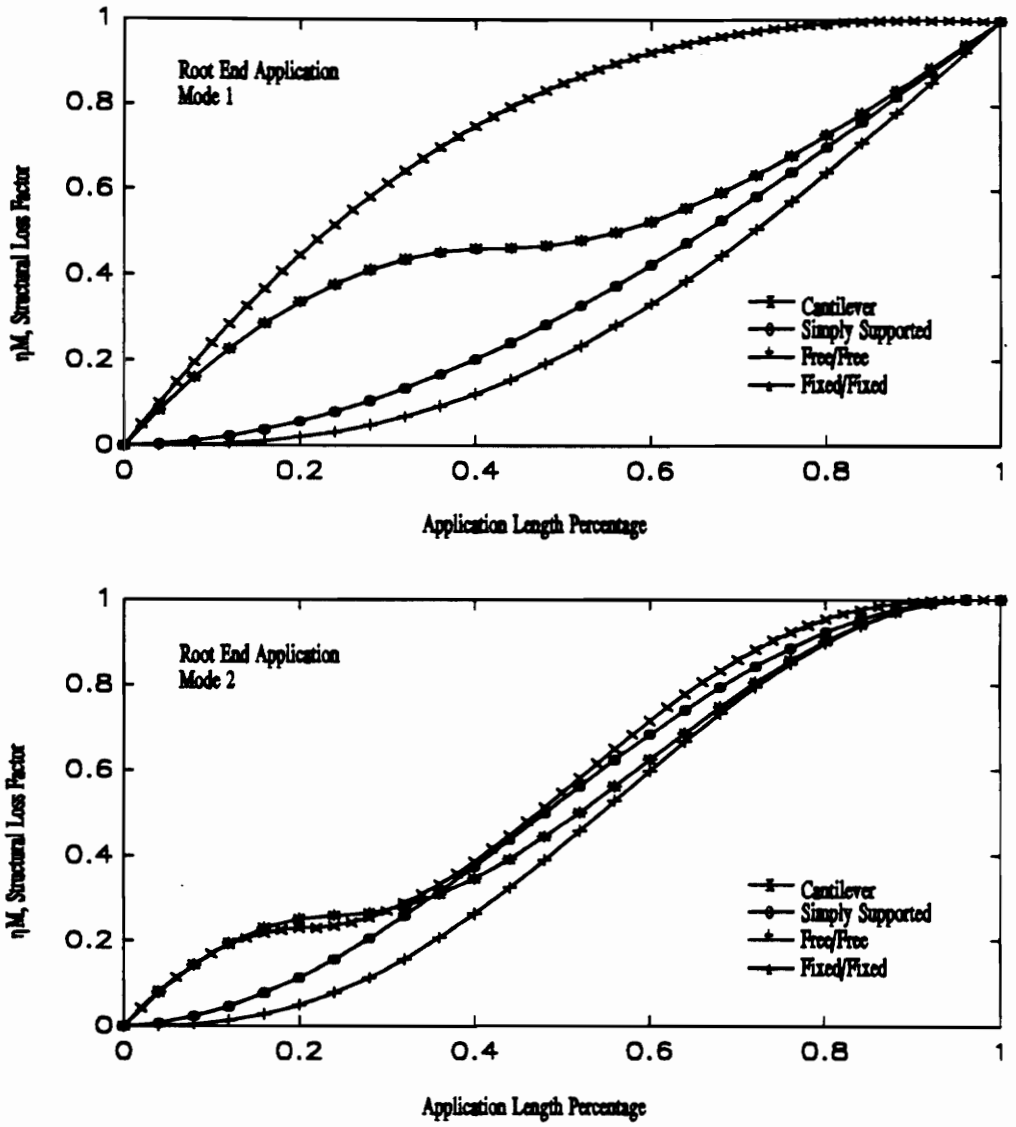

Figure 39. Moment Predicted Loss Factors, Root-End Treatments, Modes 1 and 2

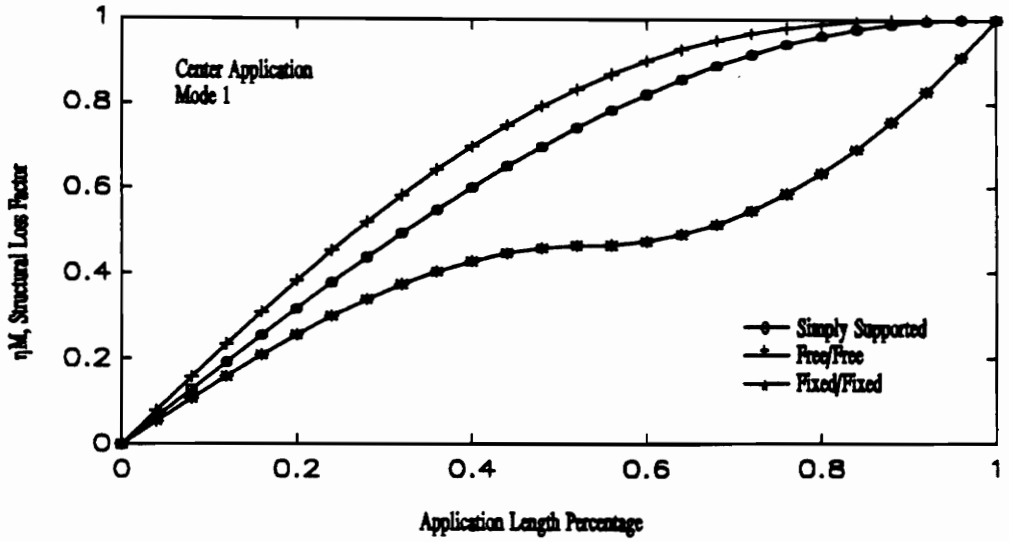

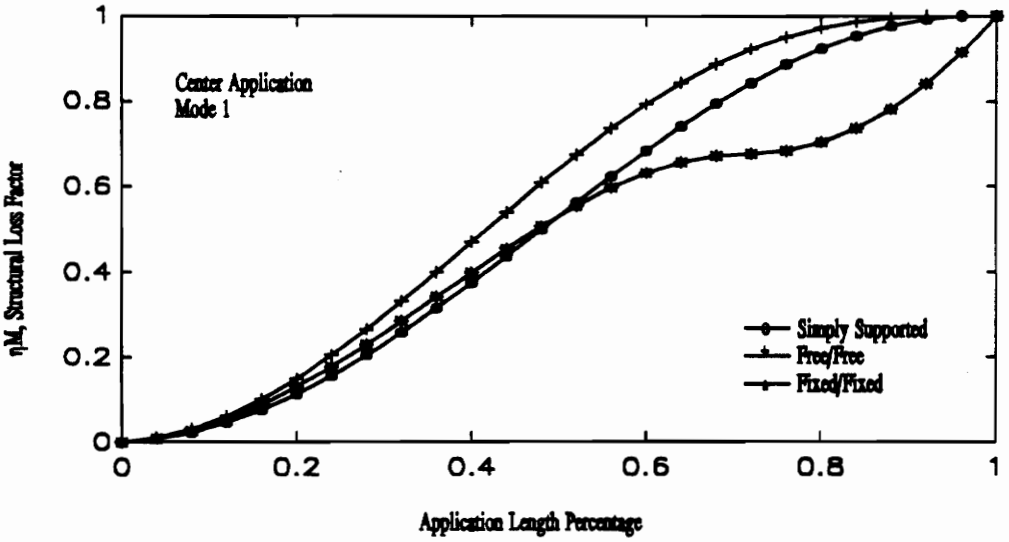

Figure 40. Moment Predicted Loss Factors, Center Treatments, Modes 1 and 2

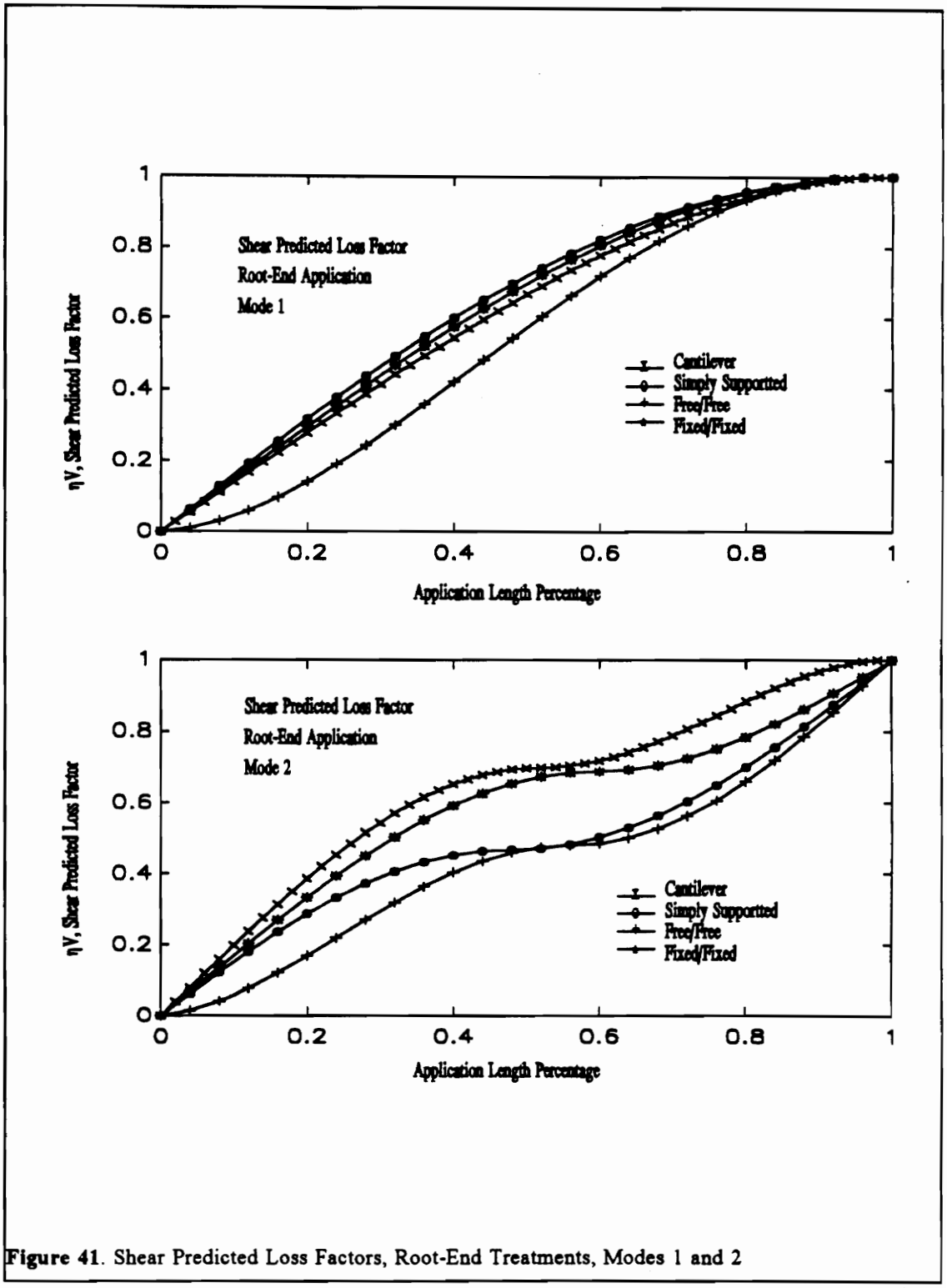

Figure 41. Shear Predicted Loss Factors, Root-End Treatments, Modes 1 and 2

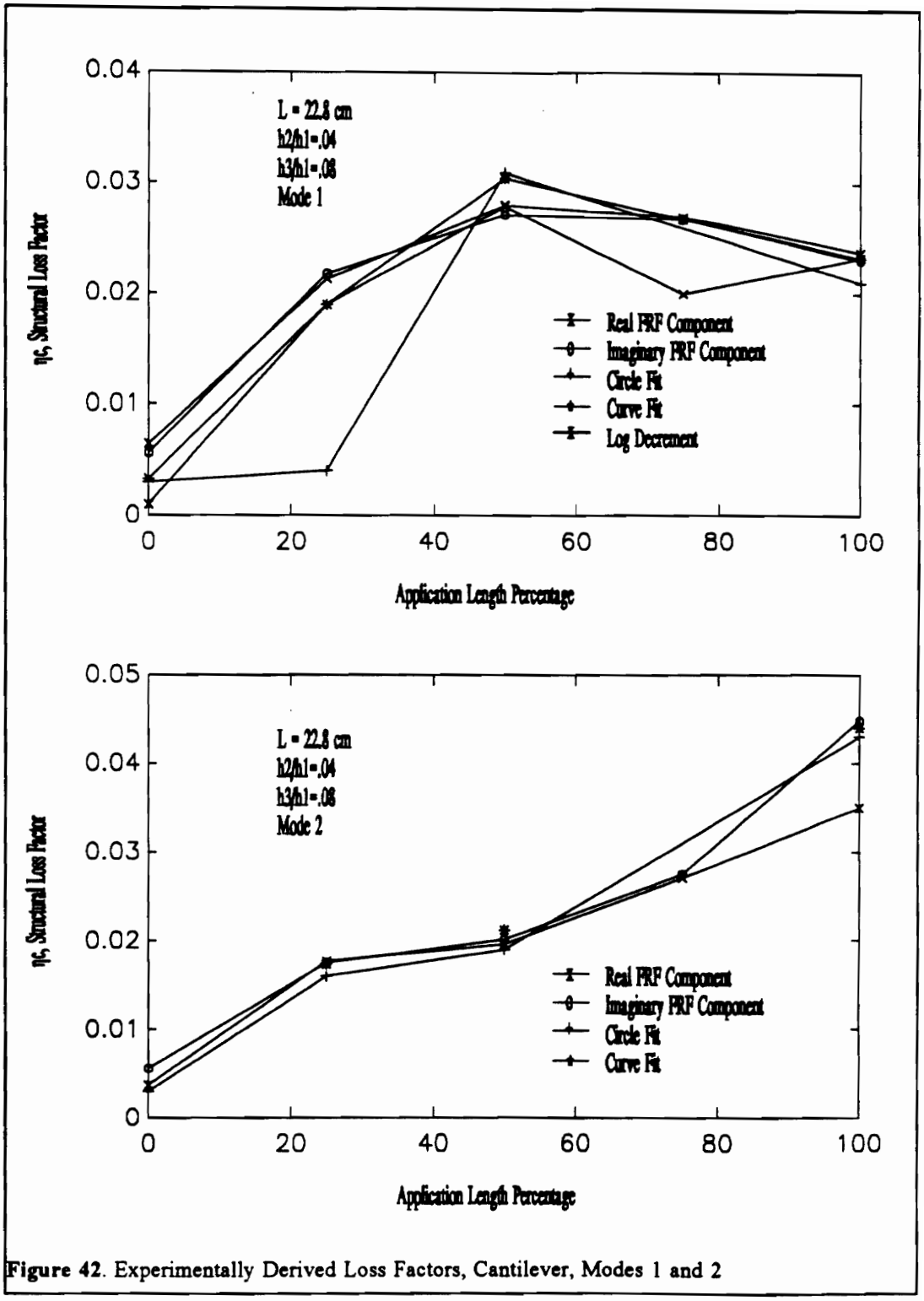

Figure 42. Experimentally Derived Loss Factors, Cantilever, Modes 1 and 2

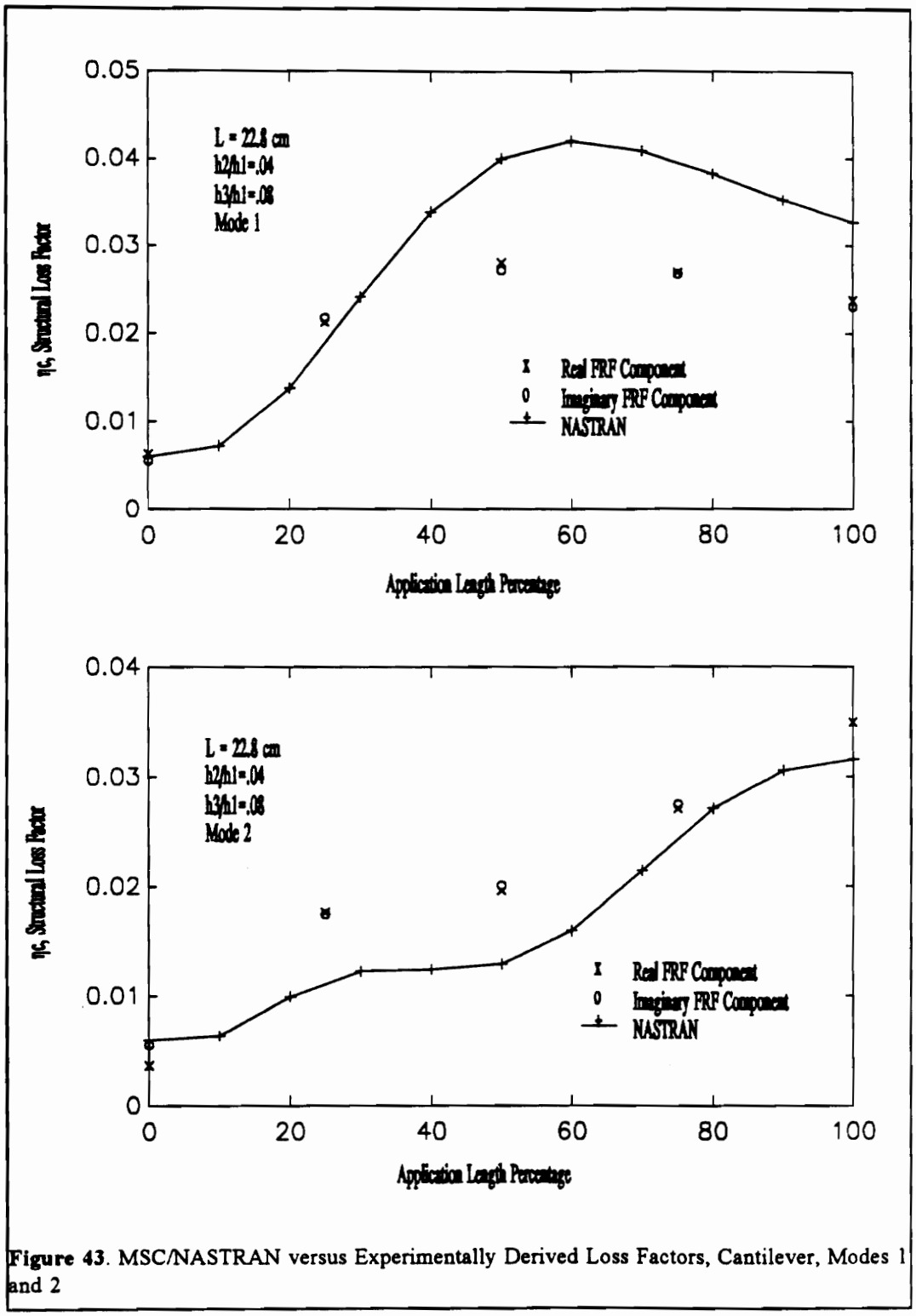

Figure 43. MSC/NASTRAN versus Experimentally Derived Loss Factors, Cantilever, Modes 1 and 2

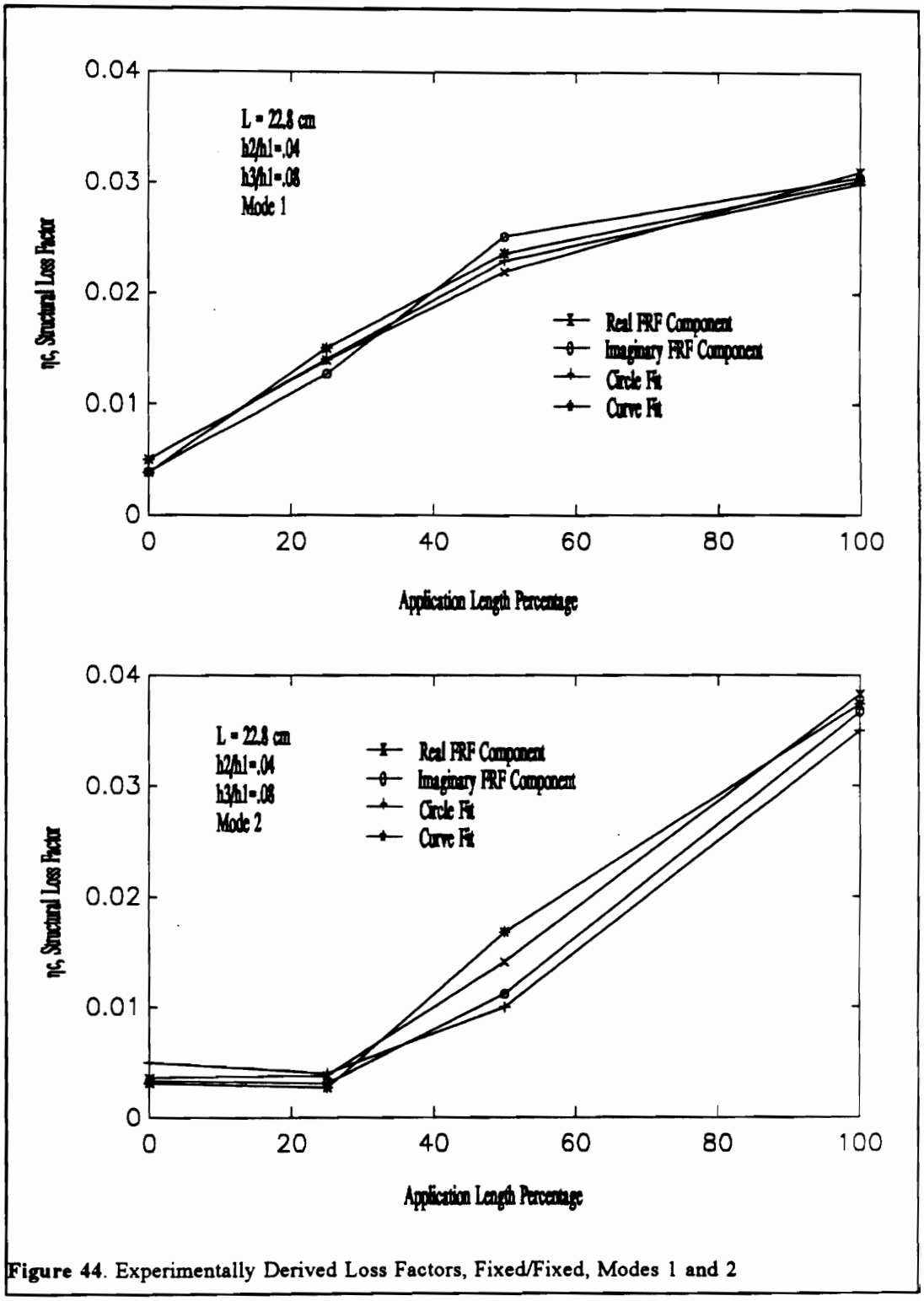

Figure 44. Experimentally Derived Loss Factors, Fixed/Fixed, Modes 1 and 2

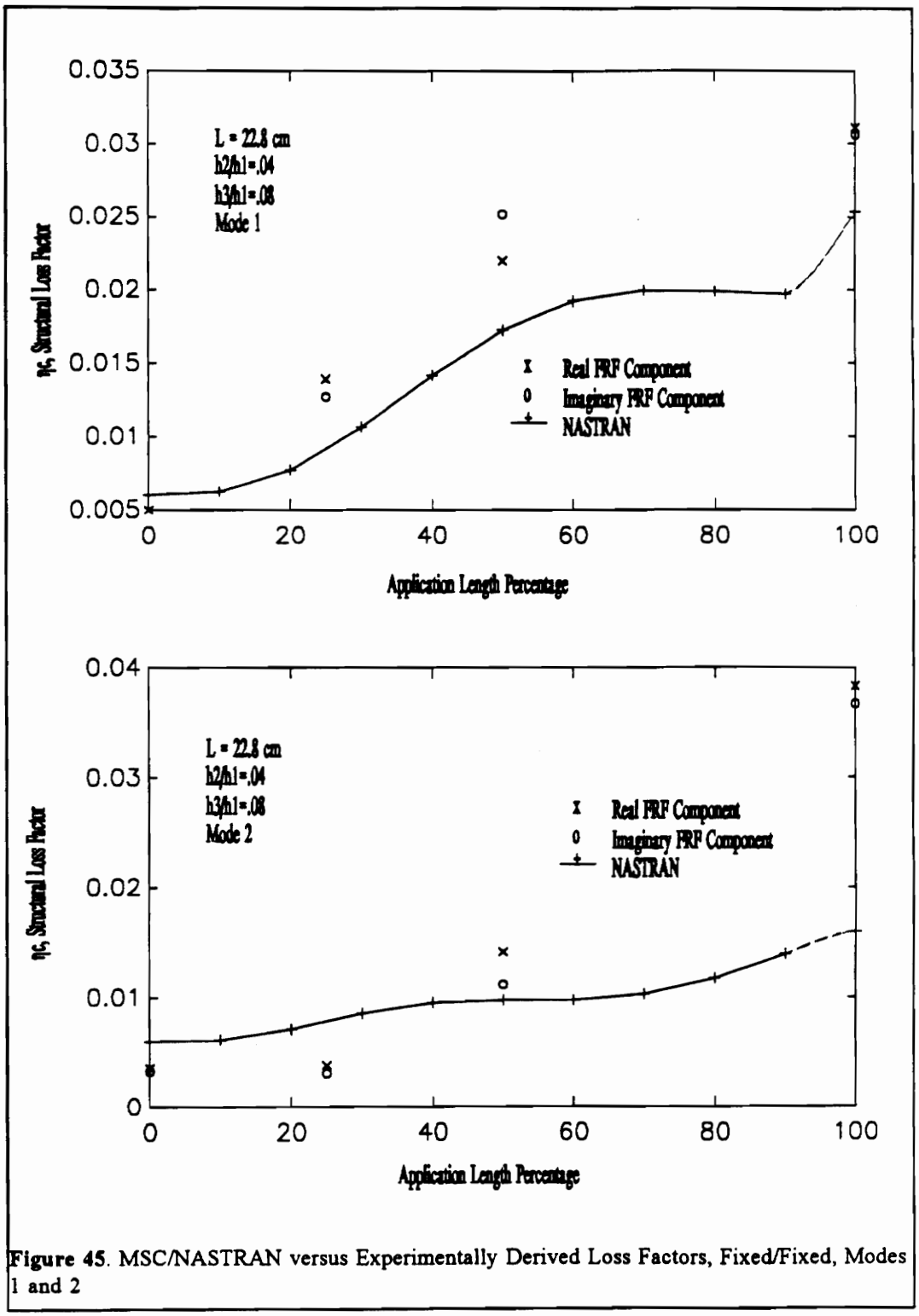

Figure 45. MSC/NASTRAN versus Experimentally Derived Loss Factors, Fixed/Fixed, Modes 1 and 2

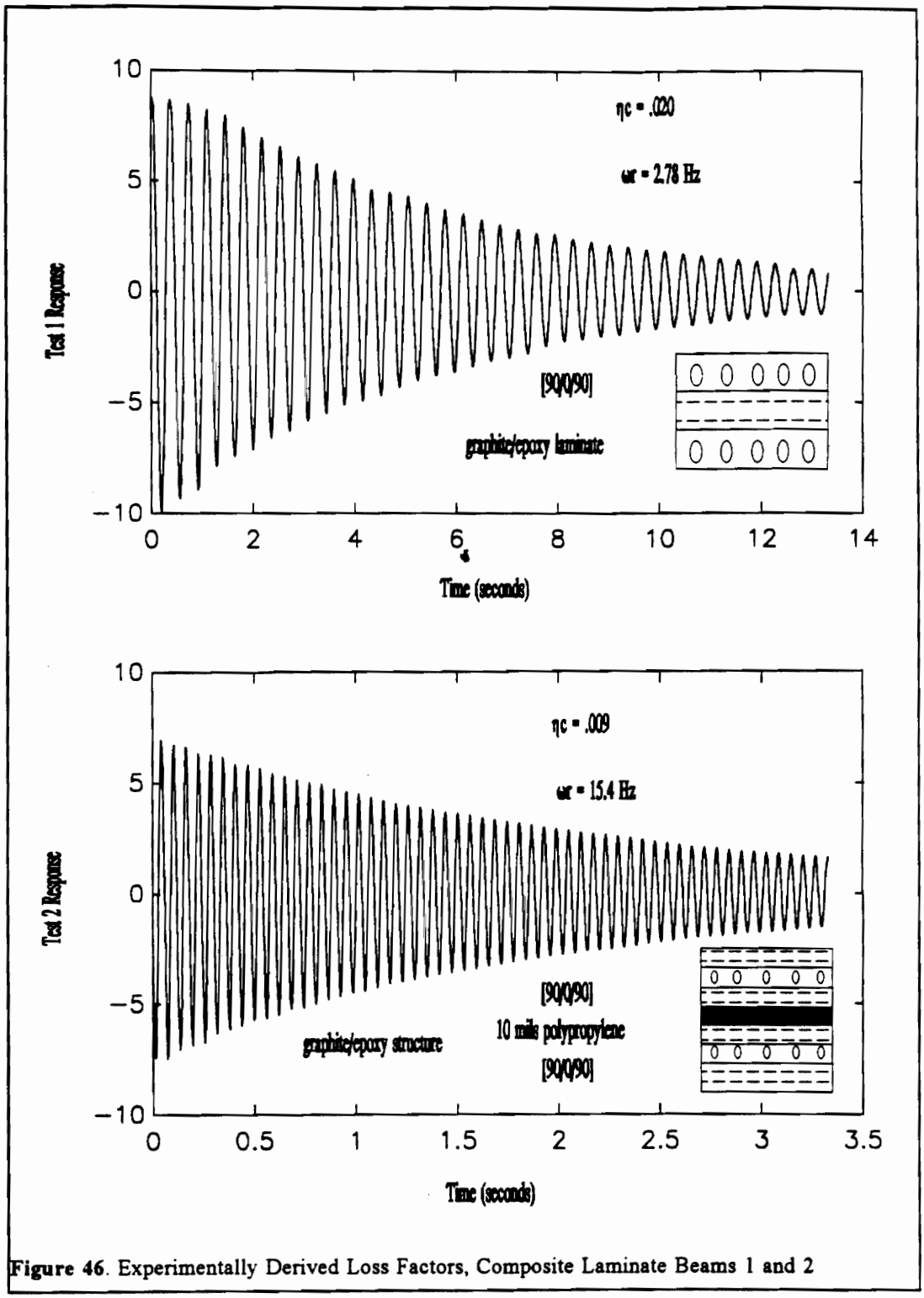

Figure 46. Experimentally Derived Loss Factors, Composite Laminate Beams 1 and 2

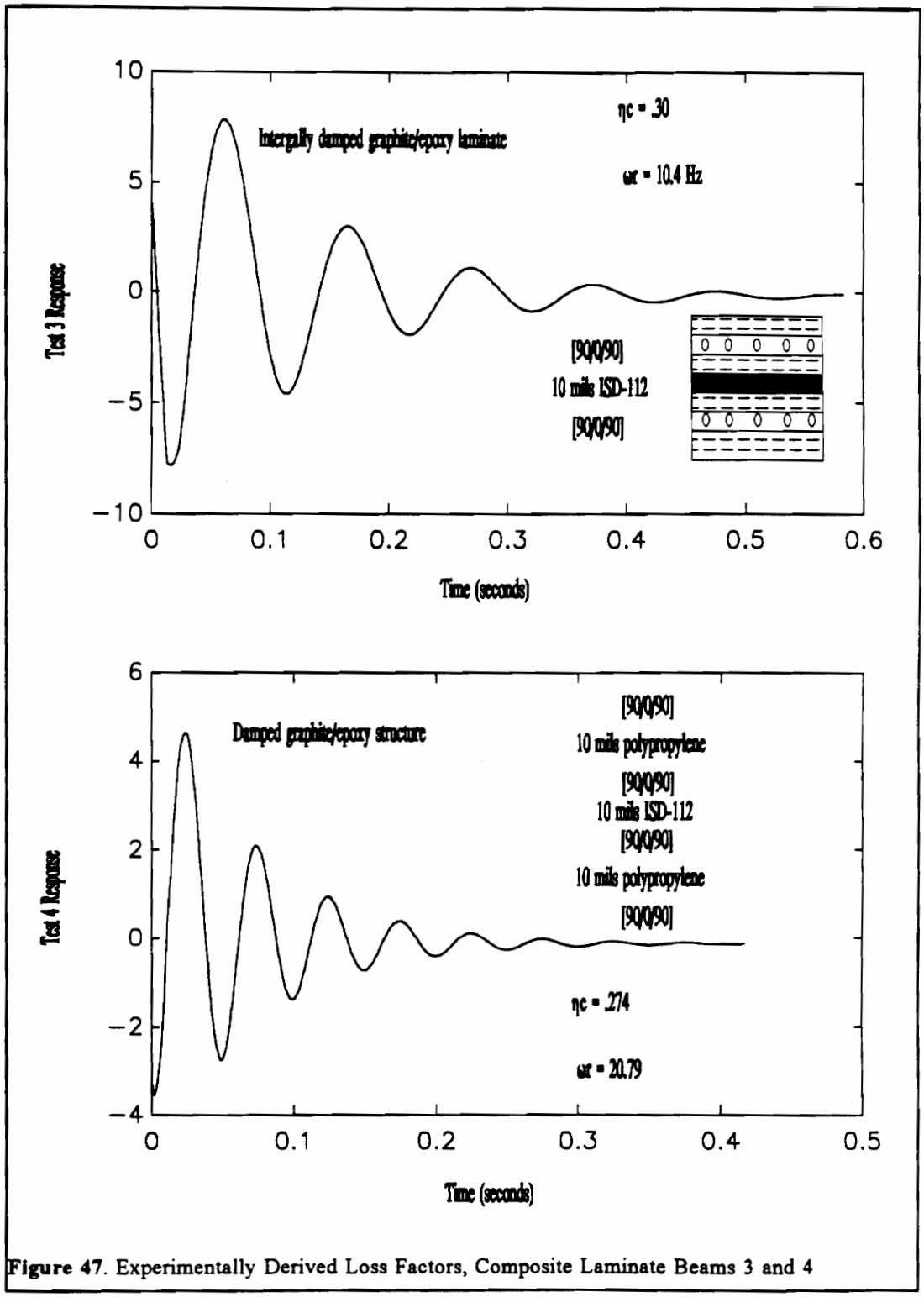

Figure 47. Experimentally Derived Loss Factors, Composite Laminate Beams 3 and 4

7 Conclusions

Analytical methods, closed form and approximate, have good trend prediction of loss factor sensitivity to the design parameters of component layer thickness and boundary conditions. Experimental verification was moderately successful for the finite element models (damping with 50 percent for most cases). The developed moment predicted loss factor estimates treatment effectiveness well. Partial coverage analysis illustrated the significance of treatment placement on a structure and its superiority to full and single segment treatments.

Finite element analysis of Constrained Layer Damping is relatively straight forward once some treatment properties (loss factor and shear modulus) and model specific issues (use of MPC's, etc.) are resolved. First, characterization of true viscoelastic properties is very difficult, the published nomograms vary considerably between each other and test specimens, and quantification of the source of error is laborious. Second, care must be taken to assure element compatibility, specifically at the viscoelastic interface. Third, when using thin viscoelastic treatment, the elements representing the viscoelastic material must be checked for convergence related to aspect ratio. If convergence has been verified, as has been documented (ref 21), aspect ratios as high as a 1000 have been used with good results. Convergence verification was used here to validate high aspect ratio elements (200-300 to 1 in some cases). Finally results must be checked to assure realistic mode shapes. In some analyses derived shapes can have elements erroneously passing through one another. If this is the case multi-point constraints may be required to assure a physically valid solution. The finite element analysis should give good trend indication in response but the model here had difficulty with absolute damping estimates, (Figure 43 and Figure 45). It also provided for a check of the Modal Strain Energy theorems for the case of laminate composite beams with viscoelastic core, (Figure 36).

Experimental damping estimation methods appeared to agree reasonably well, though there were point discrepancies and problems applying the circle fit method (Figure 42 and Figure 44). The simple direct FRF methods (Real and Imaginary FRF function) appeared to be the most consistent in this research. Both these methods used three points each at critical points on the FRF where the damping influence was dominant. (Figure 11) Both the direct FRF methods could be readily extended to a least squares approach with further investigation, which should improve estimates. The circle fit method, which fits a circle to the data whose diameter is inversely proportional to the loss factor, is more reliable with light damping. The curve fit method, which also employs a least square approach, has difficulty in properly estimating damping with noisy data, though it is better than the circle fit approach. The only practical consideration to improve any of these methods is to try to improve experimental conditions and procedure as all method work perfectly with theoretical data. The algorithm's ability to estimate loss factors is deteriorated by noise on data, joint compliance, and nonlinear response.

The RKU parameter study is a useful design tool to determine appropriate treatment for some relatively simple structures. The loss factor was shown to have optimal values over a fairly wide range of shear parameter, g.

Partial coverage treatments are the most efficient method of treatment application, as well as the easiest to retrofit. When well-thought-out, these treatments can be 3 to 4 times greater than equivalent continuous treatments. Conversely, when poorly placed, they can be 2 to 3 times less effective. (Figure 31 and Figure 33). There is also strong correlation between local moment and treatment effectiveness, which must be considered when designing treatment. Though this index does not give an absolute measure it is an excellent indicator of specific regions of the structure that are most receptive to treatment.

Ply angle stack-up of symmetric laminate beams, hence the central layer shear, has a strong influence (roughly $\sin^2\theta$ of the laminate studied here, where θ is the ply angle) on composite damping factor. Finite element analysis showed almost direct correlation between central layer shear strain energy (Modal Strain Energy theory) and composite damping factor. The effect of ply angle on resonant frequency was well predicted by Whitney's theory and fairly well by a Jones-based model when compared with finite element analysis (Figure 35). Results from laminate analysis for the effect of varying viscoelastic core thickness on composite loss factor agreed well with RKU trend prediction.

The moment predicted loss factor developed here extends partial treatment and boundary condition analysis with a simple model that estimated treatment effectiveness based on local moment. This model is an upper bound for treatment effectiveness as it does not compensate for mass and stiffness effects of the treatment. It is useful as a first approximation and design guide but cannot be compared in absolute terms since it lacks the dynamic information (mass, stiffness and damping) about the specimen. This method, while only used for beam analysis here, could readily be extended to plates and with further investigation could be able to correct for mass, stiffness, and determine an absolute estimate of composite damping.

In summary, analytical methods have good trend characterization but none, investigated here, have complete analysis ability and all must be supplemented with experimental results. Finite element analysis agrees well with experimental results and applicable closed form analytical models, but model verification is critical, as viscoelastic properties are difficult to quantify because of their nonlinear characteristics. Experimental estimation techniques appear well suited to model verification and trend indication. The simple experimental techniques (Real and Imaginary FRF component based methods) appear to work best. The moment based loss factor appears to be an excellent design tool for predicting damping treatment potential. Finally and most importantly, partial coverage is the best way to incorporate additive damping; it is simple, light, and application design is straightforward.

8 References

1. Mar, J. W., "Some Musings on How to Make Damping a Creative Force in Design," Vibration Damping 1984 Workshop Proceedings, Wright-Patterson Air Force Base, November, 1984.

2. Drake, M. L., "A Different Approach to 'Designed In' Passive Damping," *Shock and Vibration Bulletin* No. 55, June, 1985, pp. 109-117

3. Hogan, Brian J., "Damped Secondary Aircraft Structure Resists Vibro-Acoustically Induce Damage," *Design News*, June 17, 1985, pp. 112-114.

4. McCarty, Lyle H., "Damper converts Shock Loads to Heat," *Design News* May 2, 1988, pp. 80-81.

5. Hagood, N. W. IV, "Development and Experimental Verification of Damping Enhancement Methodologies for Space Structures." Massachusetts Institute of Technology, **Master's Thesis,** Sept, 1988.

6. Bland D.R., *The Theory Linear of Viscoelasticity,* Pergamon Press, New York, 1960.

7. Nashif, A. D., Jones, D.I.G., and J. P. Henderson, *Vibration Damping,* John Wiley & Sons Inc., New York, 1985.

8. Oberst, H. "ueber die Dampfung der Biegeschwingungen dunner Bleche durrch fest haftendeBelage," Acustica, Vol.2, Akustische Beihefte No.4, 1952, pp.181-194. (Translation by H.L. Blackford, Inc., 24 Commerce St., Newark, N.J.)

9. Ross, D., Ungar, E.E., and Kerwin, Jr., E.M., "Damping of Flexural Vibrations by Means of Viscoelastic Laminae," Section III *Structural Damping,* ASME, New York, NY, 1959.

10. DiTaranto, R. A., "Theory of Vibratory Bending for Elastic and Viscoelastic Layered Finite-Length Beams," *Journal of Applied Mechanics,* December, 1966, pp. 881-886.

11. DiTaranto, R. A. and W. Blasingame, "Effect of End Constraints on the Damping of Laminated Beams," *The Journal of the Acoustical Society of America,* Vol. 39, No. 2, 1966, pp. 405-407.

12. DiTaranto, R. A. and W. Blasingame, "Composite Damping of Sandwich Beams" *Journal of Engineering for Industry,* November, 1967, pp. 633-638.

13. Mead, D.J., and Markus, S., "The Forced Vibration of Three-Layer, Damped Sandwich Beamswiv Arbitrary Boundary Conditions," *Journal of Sound and Vibration,* Vol. 10, No. 2, 1969, pp. 163-175.

14. Mead, D.J., and Markus, S., "Loss Factors and Resonant Frequencies of Encastre' Damped Sandwich Beams," *Journal of Sound and Vibration,* Vol. 12, No. 1, 1970, pp. 99-112.

15. Mead, D.J., "Governing Equations for Vibrating Constrained-Layer Damping Plates and Beams," *Journal of Applied Mechanics,* June, 1973, pp. 639-640.

16. Abdulhadi, F., "Transverse Vibration of Laminated Plates with Viscoelastic Layer Damping,"*Shock and Vibration Bulletin,* Vol. 40, No. 5, Dec. 1969, pp. 93-104.

17. Kerwin, E. M. Jr., "Damping of Flexural Waves by a Constrain Viscoelastic Layer," *The Journal of the Acoustical Society of America,* Vol. 31, ,No. 7, 1959, pp. 952-962.

18. Plunkett, R., Lee, C.T., "Length Optimization for Constrained Viscoelastic Layer Damping," *The Journal of the Acoustical Society of America,* Vol. 48, No. 1 (Part 2), March 1970, pp. 150-161.

19. Rao, D. K., "Frequency and Loss Factors of Sandwich Beams Under Various Boundary Conditions," *Journal of Mechanical Engineering Science,* Vol. 20, ,No. 5, 1978, pp. 271-282.

20. Carne, T., "Constrained Layer Damping Examined By Finite Element Analysis," Society of Engineering Science 12th Annual Meeting, Austin, Texas, 20-22 October 1975, Proceedings of the University of Texas, 1975, pp. 567-576.

21. Holman, R.E. and Tanner, J.M., "Finite Element Modeling Techniques for Constrained Layer Damping," *AIAA Paper 81-0485,* April 1981.

22. Roussos, L.A., M.W. Hyer and E.A. Thornton "Finite Element Model with Nonviscous Damping" *AIAA Journal* Vol. 20, No. 6, June 1982, pp. 831-838.

23. Kluesener, M.F. "Results of Finite Element Analysis of Damped Structures", Vibration Damping 1984 Workshop Proceedings, Wright-Patterson Air Force Base, November, 1984.

24. Liguore, S. L., "Evaluation of Analytical Methods to Predict Constrain-Layer Damping Behavior" Virginia Polytechnic Institute and State University, **Master's Thesis,** May, 1988.

25. Vierck, Robert K., *Vibration Analysis, Second Edition,* Harper & Row, Publishers, New York, New York, 1986.

26. Thompson, William T., *Theory of Vibration With Applications, Second Edition,* Prentice-Hall, Inc., Englewood Cliffs, New Jersey, 1981.

27. Plunkett, R. "Measurement of Damping," Section V *Structural Damping,* ASME, New York, NY, 1959.

28. Luk, Y. W. and L. D. Mitchell, "System Identification of Via Modal Analysis" *Modal Testing and Refinement,* AMD-59, Ed: D. F. H. Chu, ASME, Nov. 13-18, 1983, pp. 31-49.

29. Hyer, M.W., W.J. Anderson and R. A. Scott "Non-Linear Vibrations of Three Layer Beams with Viscoelastic Cores, II: Experiment" *Journal of Sound and Vibration,* Vol. 61, No. 1, 1978, pp. 25-30.

30. Han, M.-C., and A.L. Wicks, "On the Application of Forsythe Orthogonal Polynomials for Global Modal Parameter Estimation", Proceedings of the 7th International Modal Analysis Conference, Las Vegas, Nevada, pp. 625-630, 1989.

31. Han, M.-C., and A.L. Wicks, "Improved Modal Parameter Estimation with Variance Weighting", Proceedings of the 8th International Modal Analysis Conference, Orlando, Florida, pp. 984-987, 1990.

32. Gersch, W. and D. Sharpe, "Estimation of Power-Spectra with Finite-Order Autoregressive Models", *IEEE Transactions on Automatic Control*, August, 1973, pp. 367-369.

33. Meirovitch, Leonard, *Elements of Vibration Analysis: International Student Edition*, McGraw Hill-Kogakusha, LTD., Tokyo, Japan, 1975.

34. Meirovitch, Leonard, *Analytical Methods in Vibrations*, The MacMillan Company, London, England, 1967.

35. Cook, Robert D., *Concepts and Applications of Finite Element Analysis, Second Edition* John Wiley & Sons, Inc., New York, New York, 1984.

36. MacNeal, Richard H., *The NASTRAN Theoretical Manual (level 15.5)*, MSC/NASTRAN, The MacNeal-Schwendler Corp., Los Angeles, California, 1972.

37. Bendat, Julius S. and Allan G. Piersol, *Random Data: Analysis and Measurement Procedures* John Wiley & Son, Inc., New York, New York, 1971.

38. Whitney, James M., *Structural Mechanics of Laminated Anisotropic Plates*, Technomic Publishing Co.,Inc., Lancaster, PA, 1975.

39. Jones, Robert M., *Mechanics of Composite Materials*, Hemisphere Publishing Group, New York, New York, 1975.

40. Blevins, James M., *Formulas for the Natural Frequency and Modeshape*, Van Nostrand Reinhold Co., New York, New York, 1979.

Appendix A

Euler-Bernoulli Beam Theory

The fundamental theory for slender isotropic beam vibrations is that of Euler-Bernoulli. The basic assumptions of this theory are; linear vibration, long and slender (high length to equivalent diameter ratios), plane sections remain plane, centroid and elastic axis aligned, transverse shear stress and rotary inertia can be neglected, and isotropic homogeneous beams. Referring to Figure 48 a summation of the forces and moments about the right face result in the following relations;

$$\left(\frac{dV}{dx}-p(x)\right)dx=0\ ,\quad \left(\frac{dM}{dx}-V-\frac{p(x)}{2dx}\right)dx=0 \qquad \textbf{(A.1.a,.b)}$$

where M, V, $p(x)$ are moment on the cross-section, shear force on the element and incremental loading respectively. By ignoring second order terms in eq. A.1.b and evaluating the pair (eq. A.1.a,.b) it is shown;

$$\frac{dV}{dx}=p(x)\ ,\quad \frac{dM}{dx}=V \qquad \textbf{(A.2.a,.b)}$$

or,

$$\frac{d^2M}{dx^2}=\frac{dV}{dx}=p(x) \qquad \textbf{(A.3)}$$

This final relation is true for composite (3-layer) beams since actual beam properties have not been introduced (as long as shear strains are negligible and plane sections remain plane). By restricting analysis to single layer or determining an equivalent bending stiffness, the fundamental relation from Statics is;

$$M=EI\frac{d^2y}{dx^2} \qquad \textbf{(A.4)}$$

where EI is the bending stiffness and assumed constant, thus the development is only valid for prismatic beams (no partial coverage beams). Using this relation in expression of moment response to loading it can be formulated;

$$\frac{d^2}{dx^2}\left(EI\frac{d^2y}{dx^2}\right)+m\ddot{y}=0 \tag{A.5}$$

where m is the mass density per unit length of the beam. For the special case of EI and m constant along length, and assuming harmonic the previous equation becomes;

$$EI\frac{d^4y}{dx^4}=m\omega^2y \tag{A.6}$$

The general solution of the forth order equation is;

$$y=A\cosh(\lambda x)+B\sinh(\lambda x)+C\cos(\lambda x)+D\sin(\lambda x) \tag{A.7}$$

where,

$$\lambda^4=m\frac{\omega^2}{EI} \tag{A.8}$$

The general form of the free vibration frequencies is defined from A.8 as;

$$\omega_n=\lambda_n^2\sqrt{\frac{EI}{m}}=(\lambda_n l)^2\sqrt{\frac{EI}{ml^4}} \tag{A.9}$$

where the values of λ_n are dependent of the boundary conditions at x = 0 and x = l. Many tables exist for commonly found boundary conditions [41].

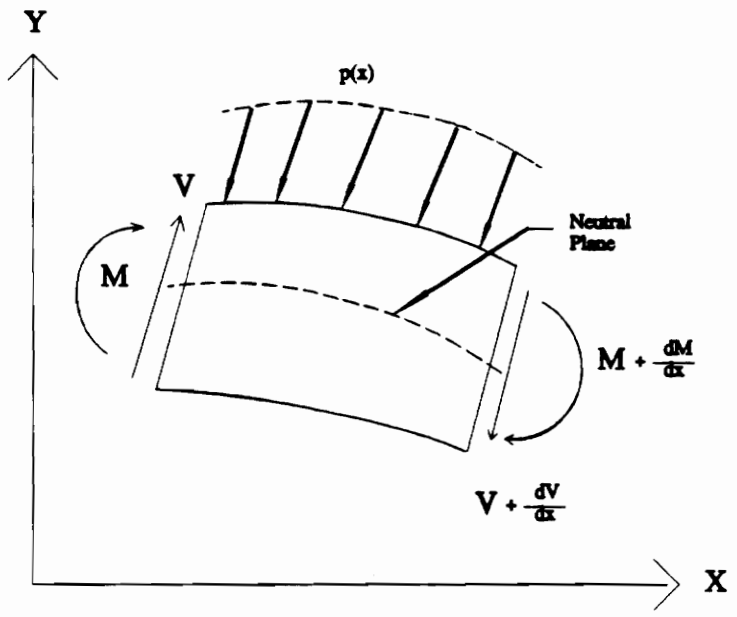

Figure 48 Euler-Bernoulli Beam Element

Appendix B

Experimental Equipment and Material Properties

Table I. Experimental Equipment

Hardware	Model, Maker	Test Domain Time/Frequency
Modal Analyzer	6080, Zonic	Frequency & Time
Mechanical Shaker	200 series, Ling Dymanic Systems	Frequency
Octave Filter	Bruel and Kjaer	Time
Force Transducer	208A03, PCB Electronics	Frequency
Acceleration Transducer	303A02, PCB Electronics	Frequency & Time
Impulse Tuned Hammer	PCB Electronics	Frequency & Time
Power Unit (DC)	480D09,D06,C06, PCB Electronics	Frequency & Time

Table II. Material Properties, Isotropic Beam Tests

Layer	Base	Viscoelastic	Constraining
Thickness	.317 cm	.013 cm	.013-.327 cm
Material	Al 6061-T6	3M ISD-112	Al 6061-T6
E	69 (GPa)	1400 (kPa)	69 (GPa)
G	27 (GPa)	450 (kPa)	27 (GPa)
ν	.30	.49	.30
ρ (kg/m^3)	2700	970	2700

Table III. Material Properites, Composite Beam Tests

Layer	Base	Viscoelastic	Constraining
Thickness	.015 cm/ply	.025 cm	.015 cm/ply
Plys	3	1	3
Material	Graphite- Epoxy	3M ISD-112	Graphite-Epoxy
E_1	400 GPa	1400 kPa	400 GPa
E_2	70 GPa	1400 kPa	70 GPa
G_{12}	42 GPa	450 kPa	42 GPa
ν_{12}	.30	.49	.30
ρ (kg/m^3)	1600	970	1600
η	.024	see 3M graph	.024

Vita

John Francis Schultze was born on September 24, 1963 in Washington, District of Columbia. He lived in the Maryland suburbs of Washington until graduation from Winston Churchill High School in 1981. After attending Montgomery College and Florida Institute of Technology he entered to the University of Maryland at College Park in 1982. He graduated from there with a Bachelor of Science degree in Mechanical Engineering in May, 1985. In August of that year, after spending the summer in the South Pacific, he started with Martin Marietta Aerospace of Orlando, Florida. While working as a design engineer and analyst there, he began graduate studies at the University of Central Florida. After Two and one half years there he enrolled at the Virginia Polytechnic Institute and State University. He completed his Masters of Science degree in Mechanical Engineering in December, 1992. He is a PhD candidate at the University of Cincinnati in the areas of modal analysis and structural control.